2015

Development of clinically relevant in vitro performance tests for powder inhalers

Xiangyin Wei
Virginia Commonwealth University

DEVELOPMENT OF CLINICALLY RELEVANT IN VITRO PERFORMANCE TESTS FOR POWDER INHALERS

A dissertation submitted in partial fulfillment of the requirements for the degree of Doctor of Philosophy at Virginia Commonwealth University.

by

Xiangyin Wei

Master of Science, Shanghai Institute of Pharmaceutical Industry, China, 2011

Director: Peter R. Byron, Ph.D.

Professor, Department of Pharmaceutics

Virginia Commonwealth University

Richmond, Virginia

October, 2015

ACKNOWLEDGEMENTS

This dissertation would not have been possible without the tremendous help and support from the following people:

First and foremost, I would like to express my deepest gratitude to my main advisor Dr. Peter R. Byron, for giving me the best training possible in the past four and a half years. He was a great academic advisor and mentor, and was always supportive and encouraging. He walked me through every difficulty I have encountered, cheered me up whenever I felt upset, and celebrated even the small achievements I have made. He understood my needs and helped me develop the professional skills required to become an independent scientist. He created great opportunities for me and helped me build self-confidence over the past years. I would not be the person I am today without his help and guidance.

I am also very grateful for the help and support from my other dissertation committee members, Dr. Michael Hindle, Dr. P. Worth Longest, Dr. Masahiro Sakagami and Dr. Aron H. Lichtman. I really appreciate their valuable time and insightful comments on my PhD work. In addition, I would like to thank Dr. Michael Hindle for giving me enormous help in the lab; he spent a lot of time helping me with the instrument setup and troubleshooting, and making sure everything worked properly in the lab. I could not have

finished my work by now without his help. I would also like to thank Dr. P. Worth Longest for giving me advice on the engineering part of my PhD work and offering me access to his lab, without which I could not do the computational fluid dynamic (CFD) simulation work for this dissertation.

I received huge help and support from my current and former colleagues in the Aerosol Research Group: Dr. Joanne Peart, Dr. Renishkumar Delvadia, Dr. Megha Mohan, Dr. Min Li, Dr. Ruba Darweesh, Dr. Yoen-Ju Son, Dr. Srinivas Behara, Dr. Laleh Golshahi, Dr. Anubhav Kaviratna, Dr. Soundos Saleh, Mandana Azimi, Susan Boc, Tien Truong, Sneha Dhapare, Anuja Raut, Bao K. Huynh, Katharina Bormann, Hua Li, and Xiang Li. These are amazing people and it has been a great pleasure working with them. Some of them I would like to give my special thanks to: Dr. Joanne Peart and Dr. Soundos Saleh, who offered me great help with my presentations; Dr. Renishkumar Delvadia, who established the foundation work of collecting human inhalation profile data used in this dissertation and provided important initial analyses; Bao K. Huynh and Katharina Bormann, who greatly assisted my work at VCU and I am really grateful for that. Members from Dr. Longest's group at Department of Mechanical and Nuclear Engineering also provided enormous help with my PhD project: Dr. Geng Tian, Dr. Ross Walenga, Dr. Landon Holbrook, and Dale Farkas. Specially, I would like to thank Dr. Geng Tian for giving me CFD training and offering me consultancy whenever I had questions. Dale Farkas has also been very helpful in providing the VCU models and mouthpiece adapters for my PhD work. Besides these, Dr. Jurgen Venitz from Department of Pharmaceutics gave me great help on statistical analyses, Bishoy Hanna from Department of Pharmaceutics helped with my understanding about pharmacokinetics, Dr. Pan Wu from

Nanjing University in China helped me with MATLAB® coding, Dr. Chi Pan from Zhejiang University in China broadened my knowledge in clinical practice, and Quan Xi from Shanghai Institute of Pharmaceutical Industry in China helped with my questions about formulation.

Many people at School of Pharmacy gave me practical help during the past few years, especially Laura S. Georgiadis, Keyetta Tate and Shakim Jackson. I would like to give my special thanks to Dr. Susanna Wu-Pong for providing the VCU BEST program, through which I received another type of training and learned a lot more about myself.

I would like to thank my “families” and friends in Richmond for their great help and support in my life in America: Elaine and Robert Metcalf, Kate and Lex Strickland, Dr. Meng Wang, Dr. Kai Liu, Mengyao Li, Fang Yuan, Dr. Yu Xu, Qianwen Qin, and Dongwei Wang. I would also like to thank Dr. Sian Byron for her time and efforts in making the best cookie bars ever. And Dr. Fang Jin for connecting me to VCU five years ago.

Last but not least, I would like to thank my beloved families for their endless support: my husband Dr. Haifeng Sun, my parents Qiuzhen Chen and Zhengzhong Li, and my parents-in-law Huzhen Hou and Xiaodong Sun.

TABLE OF CONTENTS

LIST OF FIGURES

LIST OF TABLES

LIST OF GLOSSARY

A	cross sectional area
ACT	Air Classifier Technology
AIT	Alberta Idealized Throat
ANOVA	analysis of variance
API	active pharmaceutical ingredients
APSD	aerodynamic particle size distribution
AUC	area under the curve
B	respiratory bifurcation
C	central lung region
CAD	computer-aided design
CDF	cumulative distribution function
CF	cystic fibrosis
CF_j	conversion factor
CFC	chlorofluorocarbon
CFD	computational fluid dynamics
CI	confidence intervals
cm	centimeter
COPD	chronic obstructive pulmonary disease

CT	computed tomography
CV	coefficient of variation
d	geometric diameter
d_{ae}	aerodynamic diameter
D_{50}	NGI's stage cutoff diameter
$D_{50, Q}$	cutoff diameter of NGI's stage at a specific flow rate Q
$D_{50, Qn}$	cutoff diameter of NGI's stage at the nominal flow rate Qn
DF	deposition fraction
DPI	dry powder inhaler
F	filter
F	female
FDA	U.S. Food and Drug Administration
FEF 25-75%	forced expiratory flow between 25-75%
FET	forced expiratory time
FEV1	forced expiratory volume in the first second
FIR	flow increase rate
FPF	fine particle fraction
FR	flow rate
FVC	forced vital capacity
GI	gastrointestinal
GSD	geometric standard deviation
HFA	hydrofluoroalkane
HPLC	high performance liquid chromatography

I	intermediate lung region
ICRP	International Commission on Radiological Protection
IFC	inhalation flow cell
IP	inhalation profile [small, medium and large in Chapters 3 and 4 were simulated to represent 10, 50 and 90 percentile flow rate vs. time curves in a normal adult, mixed-gender population; small, medium and large in Chapters 5 and 6 were simulated to cover the 95% confidence intervals of the profiles reported by Newman et al. (2000)].
IVIVC	*in vitro–in vivo* correlation
kPa	kilopascal
L	liter
LLN	lower limit of normal
LOQ	limit of quantification
LRN	low-Reynolds number
M	male
m_j	mass of a single particle
M_j	drug mass depositing on a NGI stage j
MDI	metered dose inhaler
MI	mixing inlet
min	minute
MIP	mouth inspiratory pressure
mm	millimeter
msec	millisecond

MMAD	mass median aerodynamic diameter
MOC	micro-orifice collector
MP	inhaler mouthpiece
MRI	magnetic resonance imaging
MT	mouth-throat model (small, medium and large)
NGI	Next Generation Impactor
n	number
NMI	Nephele Mixing Inlet
OPC	Oropharyngeal Consortium
P	peripheral lung region
P/C	aerosol deposition in the peripheral lung to the central lung ratio
PEF	peak expiratory flow
PFT	pulmonary function test
PI	penetration index
PIFR	peak inhalation flow rate
PK	pharmacokinetic
Q	flow rate
QC	quality control
QD	“quick and deep” inhalation
Qn	nominal flow rate
R	airflow resistance
r^2	coefficient of determination
RLD	reference listed drug

RMSE	root mean square error
ROI	regions of interest
RSD	relative standard deviation
S	stage
SD	standard deviation
sec	second
SIP	stochastic individual pathway
SPECT	single photon emission computed tomography
t	time
T	total inhalation time
TLD	total lung dose
$TLD_{in\ vitro}$	total lung dose *in vitro*
T_{PIFR}	time to reach peak inhalation flow rate
T_{hold}	time to maintain peak inhalation flow rate
T	total inhalation time
USA	United States of America
USP	United States Pharmacopeia
uv	ultraviolet
V	inhaled volume
VCU	Virginia Commonwealth University
W7	Westech 7 Stage Impactor
2D	two dimensional
3D	three dimensional

μg	microgram
μm	micrometer
ρ	particle density

ABSTRACT

DEVELOPMENT OF CLINICALLY RELEVANT IN VITRO PERFORMANCE TESTS FOR POWDER INHALERS

By Xiangyin Wei, M.S.

A dissertation submitted in partial fulfillment of the requirements for the degree of Doctor of Philosophy at Virginia Commonwealth University.

Virginia Commonwealth University, 2015

Major Director: Peter R. Byron, Ph.D.
Professor, Department of Pharmaceutics

While realistic *in vitro* testing of dry powder inhalers (DPIs) can be used to establish *in vitro–in vivo* correlations (IVIVCs) and predict *in vivo* lung doses, the aerodynamic particle size distributions (APSDs) of those doses and their regional lung deposition remains unclear. Four studies were designed to improve testing centered on the behavior of Novolizer®. Different oropharyngeal geometries were assessed by testing different mouth-throat (MT) models across a realistic range of inhalation profiles (IPs) with Salbulin® Novolizer®. Small and large Virginia Commonwealth University (VCU) and Oropharyngeal Consortium (OPC) models produced similar ranges for total lung dose *in vitro* ($TLD_{in\ vitro}$), while results for medium models differed significantly. While either group

may be selected to represent variations in oropharyngeal geometry, OPC models were more difficult to use, indicating that VCU models were preferable. To facilitate simulation of human IPs through DPIs, inhalation profile data from a VCU clinical trial were analyzed. Equations were developed to represent the range of flow rate vs. time curves for use with DPIs of known airflow resistance. A new method was developed to couple testing using VCU MT models and simulated IPs with cascade impaction to assess the APSDs of $TLD_{in\ vitro}$ for Budelin® Novolizer®. This method produced IVIVCs for Budelin's total lung dose, *TLD*, and was sufficiently precise to distinguish between values of $TLD_{in\ vitro}$ and their APSDs, resulting from tests using appropriately selected MT models and IPs. For example, for *slow inhalation*, TLD values were comparable *in vivo* and *in vitro*; $TLD_{in\ vitro}$ ranged from 12.2±2.9 to 66.8±1.7 mcg aerosolized budesonide while APSDs *in vitro* had mass median aerodynamic diameters of 3.26±0.27 and 2.17±0.03 μm, respectively. To explore the clinical importance of these variations, a published computational fluid dynamic (CFD) model was modified and coupled to accept the output of realistic *in vitro* tests as initial conditions at the tracheal inlet. While simplified aerosol size metrics and flow conditions used to shorten CFD simulations produced small differences in theoretical predictions of regional lung deposition, the results broadly agreed with the literature and were generally consistent with the median values reported clinically for Budelin.

CHAPTER 1

INTRODUCTION

1.1 BACKGROUND

The history of inhalation therapy can be traced back some 4,000 years, when ancient Indian herbal smoke preparations with bronchodilating properties were used to treat asthma and other respiratory conditions (Anderson, 2005). But it was not until 1956, and the launch of the first pressurized metered dose inhaler (pMDI), that the modern era of pulmonary drug delivery began (Sanders, 2007). In the last 60 years we have seen great advances in aerosol delivery technology, and the emergence of safer and more effective drugs to treat pulmonary diseases like asthma and chronic obstructive pulmonary disease (COPD). At the time of this thesis, there are 32 branded orally inhaled drug products covering 19 active pharmaceutical ingredients (APIs) approved by the U.S. Food and Drug Administration (FDA) for treatment of asthma and COPD (U.S. Food and Drug Administration, 2015a). With the exception of some nebulizer solutions however, none of these products have generic competitors in the USA. Patients are forced to pay for branded inhalers and unless they have top-notch insurance or high income, disease treatment can be difficult to maintain due to the high cost of these combination products that combine a drug formulation with a device to deliver it as an aerosol (Rosenthal, 2013).

Ideally, as products come off patent, the launch for cheaper generic equivalents should alleviate the problem. Unfortunately, even though a number of patents for inhaled drugs are expiring [e.g. Advair® Diskus®, U.S. patent 5,873,360 expires on Feb 23, 2016; (U.S. Food and Drug Administration, 2015b)], product development scientists and the regulators experience problems proving that a new inhaler delivers drug in the same way as the “innovator”.

1.2 DRY POWDER INHALER

Dry powder inhalers (DPIs) are a major developing platform for aerosol drug delivery that has been replacing propellant based devices in recent years, in part because of the environmental effects of chlorofluorocarbon (CFC) and hydrofluoroalkane (HFA) propellants. Most commercial DPIs are passive DPIs that require the patient’s inhalation power to generate the drug aerosol cloud. Passive DPIs can be classified into three categories: (a) unit dose, where the drug formulation is stored in a single capsule, blister or cartridge (e.g. Foradil® Aerolizer®); (b) multiple unit dose, where the drug formulation is stored in blisters fixed on strips or disks (e.g. Advair® Diskus®); (c) multi-dose, where the drug formulation is stored in a reservoir (e.g. Budelin® Novolizer®) and the powder metered by the device itself.

A typical powder formulation contains micronized drugs milled to a respirable particle size (usually 1–5 μm), blended with larger carriers (e.g. α-lactose monohydrate) to facilitate flow and reduce the aggregation of micronized drug powders (Telko & Hickey, 2005). When a patient activates a DPI and inhales, air is introduced into the device that causes the drug-carrier blend to be dispersed and to deaggregate due to air turbulence

and mechanical impaction with the device (Telko & Hickey, 2005). The extent of powder dispersion and the efficiency in generating small particles for pulmonary delivery from a DPI is dependent on device design (which determines powder dispersion mechanism), drug formulation (which determines the cohesive and adhesive forces between particles), and the patient's inhalation maneuver (which determines the forces available for aerosolization). General principles of powder metering and dispersion from a typical DPI are illustrated in Figure 1.1.

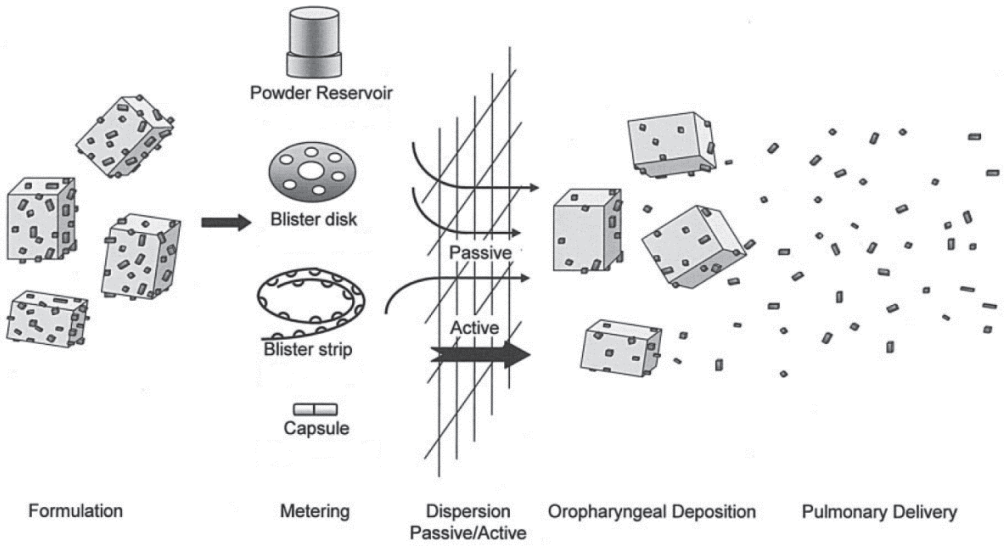

Figure 1.1. General principles of powder metering and dispersion from a DPI (Telko & Hickey, 2005). A typical powder formulation contains micronized drugs blended with much larger carrier particles that when inhaled, deaggregate to generate small respirable particles for pulmonary delivery.

Although different DPIs adopt similar principle for powder dispersion (Figure 1.1), their device design and powder dispersion mechanisms differ significantly. For example, Aerolizer® contains pre-metered drug in a single hard capsule. The patient activates the inhaler by piecing the capsule ends with eight pins at the device base (four pins on each side). Upon inhalation, the capsule spins in the capsule chamber and releases powder

into the airstream due to vibration and centrifugal forces; drug-carrier deaggregation occurs largely through particle-device collisions and air turbulence (Coates et al., 2005). Novolizer® contains drug formulations in a cartridge that may or may not be replaceable and may deliver up to 200 metered doses (Fenton et al., 2003). The device uses “Air Classifier Technology (ACT)” that enables collisions to occur within a “cyclone” inside the device so that during inhalation, tangential air is introduced at different point inside a multi-channel classifier which consequently, causes the drug-carrier agglomerates to deaggregate under centrifugal, collision and frictional forces (de Boer et al., 2003). The device is designed to favor the retention of large carrier particles within the classifier, while small drug particles are easily released from the device (de Boer et al., 2003). *In vitro* testing under compendial conditions (see section 1.4) showed that Novolizer delivers consistent doses in the early, middle, and late stages of cartridge emptying with a comparatively small relative standard deviation (RSD) of 5.56% (de Boer et al., 2004). More detailed reviews on this topic and recent advances can be found at (Chan et al., 2014; Son & McConville, 2008; Zhou et al., 2014).

Of the many variations in DPI design, airflow resistance across the device is an important factor that affects a patient’s inhalation maneuver. Clark and Hollingworth (1993) found that the mean peak inhalation flow rate (PIFR) generated by healthy volunteers at their maximum inhalation efforts reached over 150 L/min for a low resistance DPI device (Rotahaler®), while the value was only 50 L/min for a high resistance DPI device (Inhalator®). In the same study, the authors also found that PIFR dropped to 80 L/min and 30 L/min respectively for the two DPIs when subjects reduced their inhalation efforts to a “comfortable level” (Clark & Hollingworth, 1993). As passive DPIs rely upon a

patient's inhalation to disperse the formulation and deliver drug to the lung, changes in inhalation effort through a DPI can significantly affect drug deposition in the airways. Borgström et al. (1994) reported that total lung deposition of budesonide inhaled via Turbuhaler® reached 27.7% of the metered dose when subjects inhaled at a PIFR of 60 L/min, while the value decreased to 14.8% for a lower PIFR of 35 L/min. Similarly, Newman et al. evaluated budesonide deposition from "ASTA Medica", a prototype inhaler that became the commercially available Budelin® Novolizer®, and found on average, using gamma scintigraphy, that this inhaler delivered higher doses to the lung at a PIFR of 99 L/min (32.1% of the metered dose) than at 65 L/min or 54 L/min (25.0% and 19.9% of the metered dose, respectively) (Newman et al., 2000). To ensure optimal drug delivery, patients are usually instructed to inhale fast and deeply through a DPI, and training tools such as In-Check Dial™ (a peak flow meter integrated with different resistance orifices to mimic DPI resistances) may be used to help patients reach a desired PIFR for a given device (Chrystyn, 2003; Lavorini et al., 2010). Even with trained inhalation maneuvers however, large inter-subject variations are still observed in the clinical lung deposition studies (Borgström et al., 2006). Because of this variability, and because powder inhalers are likely to dominate the aerosol marketplace of the future, this thesis is focused on the development and application of realistic ("bio-relevant") testing of DPIs. Indeed, most of the work in this thesis seek to explain the variability seen in lung deposition for "ASTA Medica", the Budelin prototype. Newman et al. (2000) explained the wide variations in drug delivery to the lung based on variations in the way normal subjects inhaled. In this thesis, experiments and results are presented that offer insights both to the effects of

inhalation profiles and orphyaryngeal geometry on pulmonary drug deposition from the same inhaler.

1.3 INHALER BIOEQUIVALENCE: STATUS AND CHALLENGES

FDA approval of generic products requires that bioequivalence be demonstrated between the proposed drug product and the “innovator” or reference listed drug (RLD) (U.S. Food and Drug Administration, 2013). This requires comparative testing between the generic and the RLD, where the applicants must prove “no significant difference in the rate and extent to which the active ingredient or active moiety in pharmaceutical equivalents or pharmaceutical alternatives becomes available at the site of drug action when administered at the same molar dose under similar conditions in an appropriately designed study” ("Code of Federal Regulations," 2015). While pharmacokinetic (PK) studies alone are usually considered sufficient for establishing bioequivalence of orally administered drugs with systemic action (Saluja et al., 2014), situations are far more complex for pulmonary delivered drugs with local or “topical” activity. As illustrated in Figure 1.1, aerosolized drugs from an inhaler are designed to be delivered via oral inhalation. Because the mouth is the conduit, the drug deposits in both the oropharynx and lung. Drug depositing in the oropharyngeal region will be swallowed into the gastrointestinal (GI) tract, and only the dose entering the lung can induce local therapeutic effects. Furthermore, because local effects in the airways depend on regional dose and distribution (Anderson & Newman, 2009; Usmani, 2015; Usmani & Barnes, 2012; Usmani et al., 2005), the way in which an aerosol deposits in the lung can influence product and drug efficacy. Given that the aerosols produced from inhalers may vary in size depending

on drug formulation, device design and patient-related human factors, this “proof of similarity” or bioequivalence becomes quite a challenge, especially because some inhalers contain multiple drugs with different aerosol characteristics (Daley-Yates et al., 2014; Daley-Yates et al., 2009; Tarsin et al., 2006). Taken overall, because drug concentration at the “site of action” does not rely upon the systemic circulation (the plasma is “downstream” of drug absorption from either the GI tract or the lung; Figure 1.2), PK studies alone are not considered adequate to establish bioequivalence of orally inhaled drug products in the USA (Saluja et al., 2014). In practice, PK may assure equivalent systemic exposure but it fails to assure local exposure in the airways.

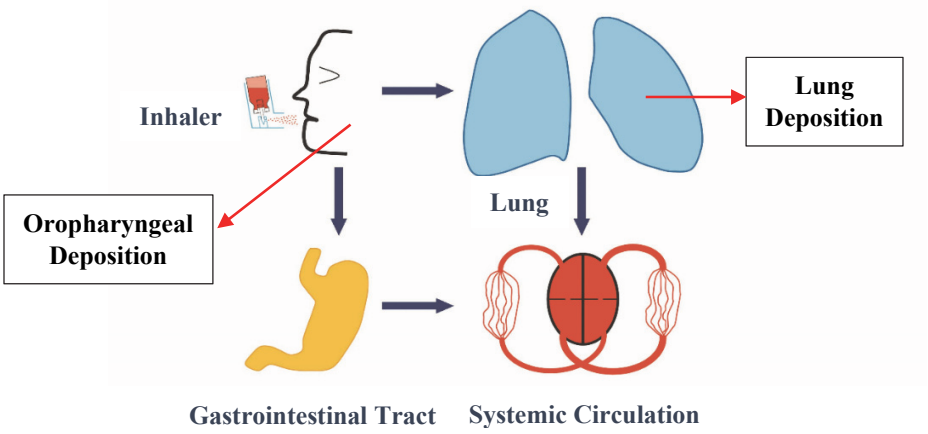

Figure 1.2. Schematic of drug deposition and disposition in the human body after delivery through the pulmonary route. Figure was redrawn from (Anderson & Newman, 2009).

FDA’s current thinking about inhaler bioequivalence is based on an aggregate “weight of evidence” approach (Lee et al., 2009; Saluja et al., 2014); for DPIs, this includes demonstration of comparative *in vitro* performance [single actuation content and aerodynamic particle size distribution (APSD) tests], comparative systemic exposure (PK studies), comparative local action (clinical end point studies), and comparative device and

formulation design (Figure 1.3). Product-specific draft guidance has also been released for DPIs containing fluticasone propionate and salmeterol xinafoate based on this approach (U.S. Food and Drug Admiistration, 2013).

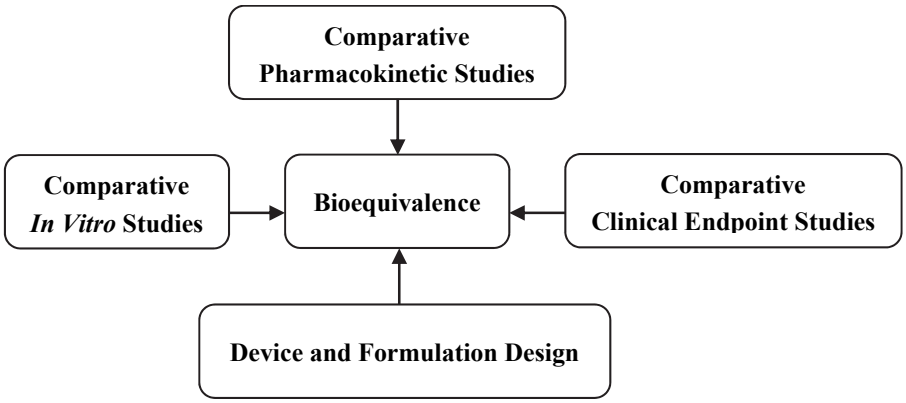

Figure 1.3. FDA's aggregate "weight of evidence" approach for establishing bioequivalence of dry powder inhalers. Figure was redrawn from (Lee et al., 2009).

Of the two major types of multi-dose inhalers, DPIs are arguably a greater challenge to regulators because they rely on the patient's inhalation to produce the aerosol, and aerosol properties can depend on the way the patient inhales (Tarsin et al., 2006). Even for low-variance inhalers [e.g. Novolizer®, (Delvadia et al., 2012)], it appears to be difficult to select individuals that even when trained, inhale in such a way that the lung dose *in vivo* is reproducible. In practice, topical delivery from DPIs is variable even in normal trained subjects (Newman et al., 2000), and this variability needs to be recognized when attempting to assess the equivalence of two inhalers. In addition to this, when comparing *in vitro* properties, a performance characteristic should be chosen that has a proven relationship to efficacy in the clinic. In short, it is necessary to show an *in vitro–in vivo* correlation (IVIVC) for example, between inhaler *in vitro* attributes (e.g. APSDs) and *in vivo* drug deposition in the lung (Newman & Chan, 2008), before using

the *in vitro* attribute to judge the similarity of two devices. This raises uncertainties for product development scientists and the regulators concerning the meaningful definition of *in vitro* equivalence between the test and reference products. In short, the answer to the question “If the two products show equivalence *in vitro*, will they have potentially equivalent *in vivo* performance?” is presently unknown. A good example to illustrate the complexity of this topic is the studies published by Daley-Yates et al. (2014; 2009), where test and reference DPIs showed comparable *in vitro* performance, but *in vivo* PK studies suggested significant differences in systemic exposure and lung absorption of fluticasone between the two inhalers. One possible reason for those discrepancies is that compendial (e.g. United States Pharmacopeia, or USP) *in vitro* test methods for measurement of APSDs (U.S. Pharmacopeial Convention, 2013) do not readily reflect the real situation of inhaler use in the clinic (see section 1.4), so that apparent “equivalence” *in vitro* does not necessarily relate to the clinical performance of the inhalers (Daley-Yates et al., 2014). As we enter an era where generic inhalers are needed, it will be necessary and beneficial for both drug developers and regulators if more predictive *in vitro* test methods are researched and established for orally inhaled drug products.

1.4 IN VITRO PREDICTION OF AEROSOL DEPOSITION IN THE HUMAN LUNG

The study of aerosol deposition in the human lung dates back to the 1950s, when the deposition of hazardous environmental aerosols in the lung were of major concerns to the public. Specifically, the dosimetry, proportion and position of aerosol deposition and how the human lung could remove certain aerosols, after deposition had occurred were studied for humans breathing tidally (Gerrity, 1989). In those studies, human

subjects were instructed to inhale radiolabeled, monodisperse, insoluble particles through a large mouthpiece using required breathing patterns. Subsequently, aerosol deposition and clearance in the lung were monitored externally using scintillation detectors. A large meta-analysis of these deposition studies was performed by Stahlhofen et al. (1989) in the late 1980s with the goal of reducing discrepancies in existing deposition data and providing reliable, less variable, empirical equations for predicting aerosol dosimetry in different regions of the respiratory tract. Factors including particle characteristics, subjects' breathing patterns and airway geometries were considered important determinants of aerosol deposition in the human lung.

Table 1.1. Aerosol deposition study characteristics: Environmental aerosols vs. drug aerosols delivered from DPIs.

Environmental Aerosols	Drug Aerosols from DPIs
a. Monodisperse dilute aerosols	a. Polydisperse concentrated aerosol clouds
b. Particles are insoluble	b. Particles are soluble and absorbable
c. Particle size do not change – aerosols are stable	c. Drug-carrier deaggregation and APSDs depends on patient-device interactions – aerosols are not stable; deagglomeration and/or hygroscopic effects may occur during administration
d. Subjects inhale tidally from a stable aerosol reservoir	d. Subjects inhale once only, fast and deeply through the inhaler; aerosols are created during this process

The semi-empirical models developed by Stahlhofen et al. (1989) and others [e.g. the ICRP model (International Commission on Radiological Protection (ICRP), 1994)] provided valuable information for pharmaceutical scientists wishing to study aerosol drug deposition in the human lung. However, caution should be applied when using these models to predict drug deposition from inhalers. Stahlhofen's work (Stahlhofen et al., 1989) generally employed insoluble dilute stable aerosols that did not change size during entry into the human subjects following or during tidal inhalation in each study. DPIs on the other hand involve single deep inspirations of powder mixtures; such concentrated aerosols are created and administered at the same time. That situation is far more complex than those involved in early lung deposition studies (Table 1.1).

The present compendial methods (U.S. Pharmacopeial Convention, 2013) determine the APSD of the drug leaving a powder inhaler under fixed conditions (airflow rate and volume are specified). Often the data is processed to yield the mass of drug exiting the inhaler with aerodynamic diameters smaller than about 5 μm because this is often construed as most likely to penetrate the lung. Indeed, the "fine particle fraction" (FPF, designated as drug fraction with particle size < ~5 μm) is usually considered to be an important *in vitro* parameter that predicts inhaler performance *in vivo*. The pharmacopeial methods were initially designed for quality control (QC) and batch release purposes, while offering an approximation of inhaler use in the clinic to capture key performance characteristics. For example, with DPIs, APSD is tested at a constant flow rate equivalent to the maintenance of a 4 kPa pressure drop across the inhaler (to approximate the inhalation effort that humans can potentially achieve), with 4 L air (to approximate the vital capacity of a human adult). The aerosol exiting the inhaler is then

passed through the 90° bent induction port into a standardized, calibrated cascade impactor (U.S. Pharmacopeial Convention, 2013) (Figure 1.4). While the methods are still far from realistic, as human oropharyngeal geometries are much more complex than the induction port (Swift, 1994), and the square wave profile during testing does not resemble a patients' breath profile, attempts have been made to correlate the particle size distribution data collected from DPIs with the human lung deposition results *in vivo*.

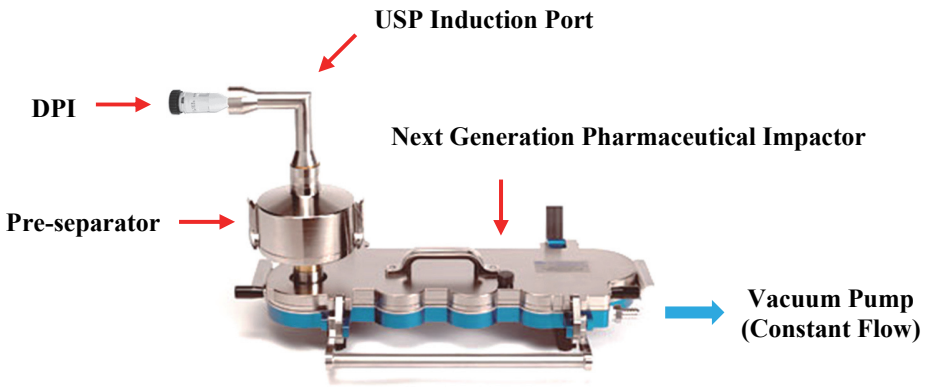

Figure 1.4. Illustration of compendial (pharmacopeial) methods to determine aerodynamic particle size distributions (APSDs) for DPIs at a fixed air flow rate and volume. Aerosol exiting the inhaler is passed through the 90° bent induction port into a standardized, calibrated Next Generation Pharmaceutical Impactor (NGI; a commonly used cascade impactor for testing pharmaceutical aerosols). A pre-separator is used to remove large particles in the aerosol cloud before it enters NGI.

Newman and Chan (2008) performed a meta-analysis of the literature data on this topic and found that in general, $FPF_{6.8\mu m}$ appeared to over-predict the fraction of the drug dose depositing in the lung tested using gamma scintigraphy, while $FPF_{3\mu m}$ appeared to produce a correlation with the mean *in vivo* lung deposition data (Figure 1.5). The study was a nice exploration of the use of convential APSD data (collected during QC testing) to predict the mean *in vivo* lung dose. In spite of those findings however, clinical variations in lung deposition, which may even exceed 100% coefficient of variation (CV) for low dose

DPIs (Borgström et al., 2006), shows that DPI deposition remains “patient specific” and unpredictable.

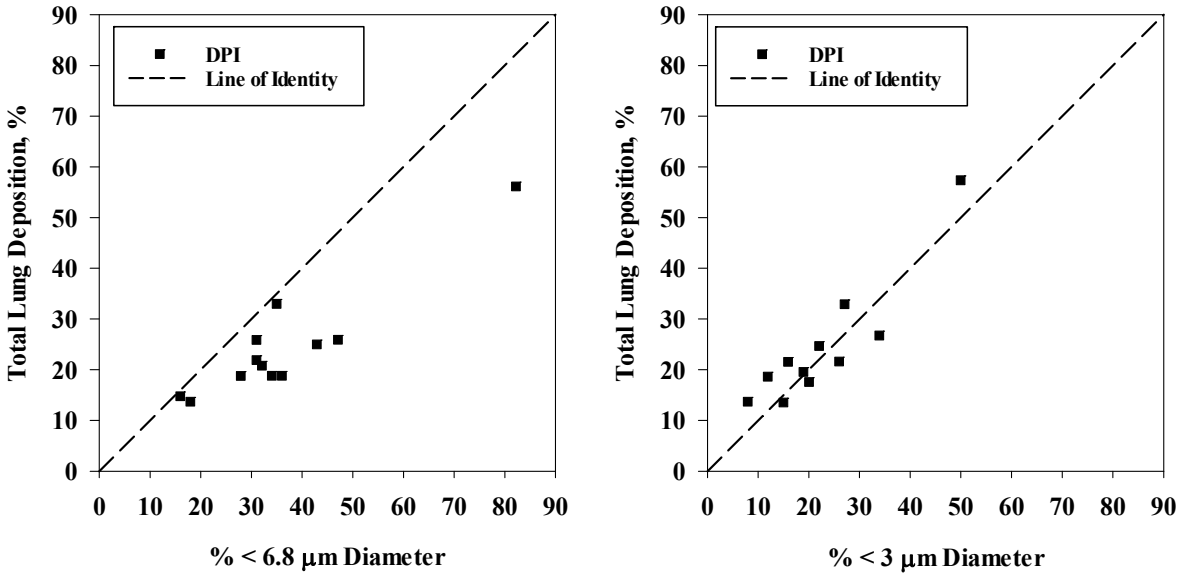

Figure 1.5. Correlations between mean total lung deposition (by gamma scintigraphy) and the mean drug fraction with aerodynamic diameters smaller than 6.8 µm (left panel) and 3 µm (right panel), respectively. Figures were redrawn from Newman and Chan (2008). Only data for DPIs were included. Individual variations between subjects were not shown.

Other than trying to correlate particle size distribution with total lung deposition, a lot of efforts have been devoted to developing more realistic *in vitro* test methods and improve our ability to predict inhaler *in vivo* performance. These studies have been mainly focused on developing realistic human mouth-throat (MT) models and inhalation profiles (IP) to mimic inhaler use in the clinic, with the ultimate goal of achieving better *in vitro–in vivo* correlations (IVIVCs). Recent advances relevant to DPI testing in this area are summarized below.

Realistic Mouth-Throat Models

The human upper airway has long been recognized as a barrier to sucessful pulmonary drug delivery, where aerosolized drugs must bypass the right-angled oropharyngeal region in order to reach the lung (Swift, 1994). Borgström et al. (2006) found that throat deposition was the major source of inter-subject variations observed in clinical lung deposition studies. They suggested that upper airway geometries may significantly affect aerosol deposition in the lung. Three dimensional (3D) geometries of the oropharyngeal region can be obtained from cadaver casts or medical imaging like computed tomography (CT) using scans from x-ray or magnetic resonance imaging (MRI); the latter has become the major tool for studying airway geometries because cadaver casts usually suffer from distortion from postmortem tissue shrinkage (Byron et al., 2010). While individual upper airway geometries have been studied and used to improve IVIVCs (Olsson et al., 1996), more “representative” human oropharyngeal geometries and the corresponding physical models remain uncertain. Questions like, “What is the most representative geometry?” and “Can the model(s) cover inter-subject variations?”, remain difficult to answer and controversial. Different approaches have been proposed regarding this topic (Burnell et al., 2007; Delvadia et al., 2012; Olsson et al., 2013; Stapleton et al., 2000; Xi & Longest, 2007; Zhang et al., 2007) and three main types of realistic MT models developed based on oropharyngeal geometry studies of healthy human adults (Figure 1.6). MT models for children and infants have also been developed (Carrigy et al., 2014; Ruzycki et al., 2014), but the topic of pediatric models is beyond the scope of this thesis and will not be discussed.

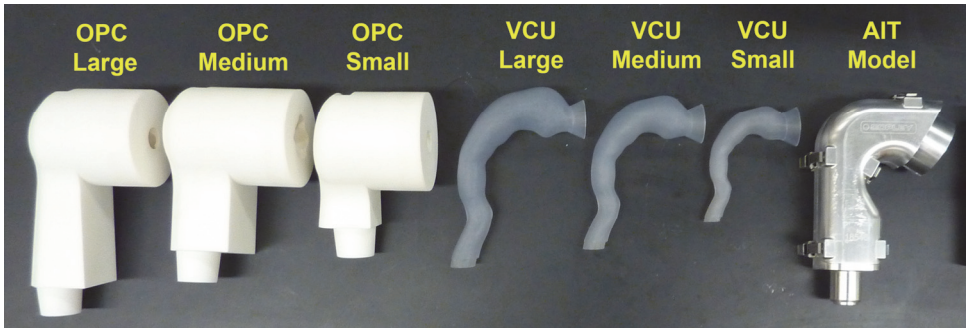

(a) Side View

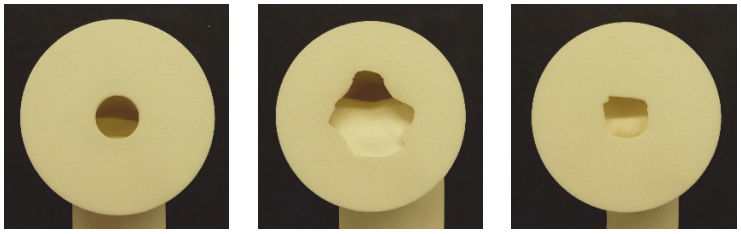

OPC_L OPC_M OPC_S

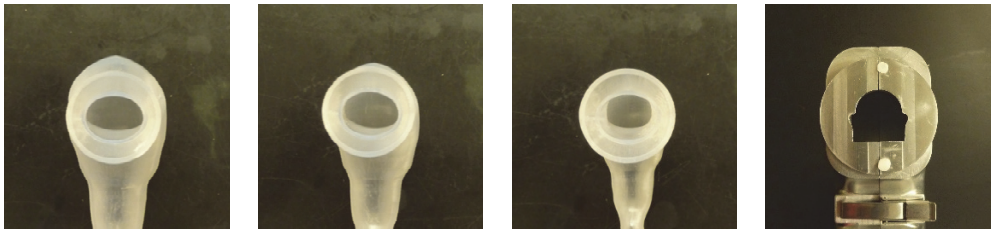

VCU_L VCU_M VCU_S AIT

(b) View from the Mouth Entry

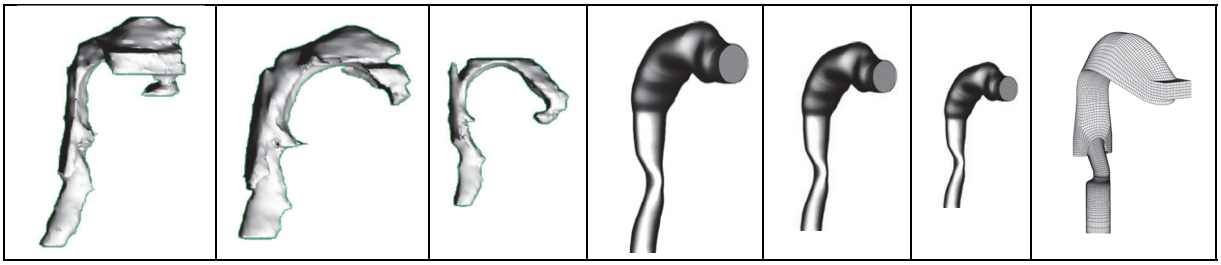

OPC_L OPC_M OPC_S VCU_L VCU_M VCU_S AIT

(c) Internal Geometry or Diagram

OPC_L*	OPC_M*	OPC_S*	VCU_L	VCU_M	VCU_S	AIT*
84.4	91.7	27.6	96.1	61.6	26.6	75.4

*Determined experimentally using water

(d) Internal Volume (cm^3)

Figure 1.6. Realistic mouth-throat (MT) models developed for inhaler *in vitro* testing: Oropharyngeal Consortium (OPC) Large (OPC_L), OPC Medium (OPC_M), OPC Small (OPC_S) (Burnell et al., 2007; Oropharyngeal Consortium, 2013), Virginia Commonwealth University (VCU) Large (VCU_L), VCU Medium (VCU_M), VCU Small (VCU_S) (Delvadia et al., 2012; Longest, 2012), Alberta Idealized Throat (AIT; Medium) (Stapleton et al., 2000).

Small, medium and large Virginia Commonwealth University (VCU) MT models (Longest, 2012) were designed and built in our laboratories using well-documented anatomical data from the literature. In brief, the VCU medium MT model (Figure 1.6) is a geometrically realistic physical model of the mouth-throat that was constructed by rapid prototyping (Byron et al., 2010). The model is derived from CT imaging of a male human oropharynx as described by Xi and Longest (2007) and Xi et al. (2008). The imaging data was processed and simplified by computer-aided design (CAD) to preserve important anatomical details but enable reliable prototyping. VCU small and VCU large MT models (Figure 1.6) were scaled by volume to cover approximately 95% of the volumetric variations seen in mixed gender healthy human adults as described in Delvadia et al. (2012). The internal MT volumes for the VCU small, medium and large models of 26.6, 61.6, and 96.1 cm^3, respectively, were consistent with 95% confidence intervals (CI) derived from Burnell et al.'s values for mean±2SD (Burnell et al., 2007).

Small, medium and large Oropharyngeal Consortium (OPC) MT models (Oropharyngeal Consortium, 2013) were also developed by an industry consortium (AstraZeneca, GlaxoSmithKline and sanofi-aventis) to represent the medium and extremes for *in vitro* aerosol drug capture in mixed gender human subjects inhaling through different mouthpieces (Burnell et al., 2007). OPC models were constructed using real human oropharyngeal geometries produced from MRI imaging, with slight modifications of the mouth opening of each geometry to facilitate *in vitro* testing (Oropharyngeal Consortium, 2013). Notably, the selection of the small, medium and large OPC models was based on the Consortium's assessment of aerosol deposition, not on measurements of the internal geometries of the models themselves (Burnell et al., 2007).

The Alberta Idealized Throat (AIT) is an idealized model developed (a) to represent the "average geometry" of the human mouth-throat and its major fluid dynamic properties (with respect to aerosol capture) and (b) enable ease of manufacturing in metal (Stapleton et al., 2000). The 3D geometry of AIT was designed based on dimensions from MRI images, CT images, and visual observations to mimic those features in a real human mouth-throat that cause aerosol deposition (Warren H Finlay et al., 2010). Currently only a medium AIT model is available, although a ±30% scaling factor was proposed to cover inter-subject variability in aerosol deposition (Warren H Finlay et al., 2010). All models shown in Figure 1.6 are geometrically different and tailored in different ways to enable their manufacture and use. One feature in common, however, is that the interior surfaces of all models are unrealistically smooth, and they also neglect the entry of the nasopharyngeal airways into the back of the throat. Additionally, these models require an airtight adapter to locate and to angle an inhaler "correctly" into the mouth opening of the model.

Inhalation Profiles

The commercially available DPIs for treatment of asthma and COPD are all breath actuated, which requires a patient's inhalation to disperse powdered drug formulations. These formulations usually contain micronized drugs blended with lactose as the carrier. Different types of lactose are employed that result in different lactose and drug aerosols for lung delivery. The extent of drug-carrier de-aggregation, and thereafter the size distribution of drug aerosols, depends on the combined effects of inhaler design, powder formulation, and patient's inhalation maneuver (Telko & Hickey, 2005). While inhaler design is important however, it is likely that the patient's inhalation profile (IP) is the most

significant feature defining pulmonary drug delivery from DPIs. Aerosol dispersion and release from a selected DPI is known to be affected by many factors like a patient's peak inhalation flow rate (PIFR), flow increase rate (FIR; the rate at which the air flow accelerates to PIFR) and inhaled volume (V) (Chavan & Dalby, 2002; de Boer et al., 1997). Realistic IPs therefore, if appropriately collected and chosen, are likely to enable studies that provide more complete information on DPI performance than we presently see from compendial tests alone (Burnell et al., 1998a).

The general method to collect IPs from a group of healthy subjects or patients is to use an "inhalation flow rate recorder", where a flow meter and/or flow-calibrated pressure transducer is attached to a placebo DPI or an orifice plate with equivalent resistance to the test inhaler (Azouz et al., 2015b; Harris & Willoughby, 2010; Tiddens et al., 2006; Weers et al., 2013). Each subject's inhalation can then be recorded, after instruction, as flow rate vs. time or pressure drop vs. time profiles using methods described by Clark and Hollingworth (1993). While the methods for collecting inhalation profiles are generally similar across different research groups, variable approaches have been used to select "representative" IPs from each group's database for inhaler *in vitro* testing. Weers et al. (2013) chose four individual IPs with peak pressure drop representing the ranges of patients' inhalation efforts in their study. A similar approach was applied by Casaro et al. (2014) where five individual IPs were selected to cover the medium and ranges of PIFRs in the database. Olsson et al. (2013) proposed select IPs representative of the medium and 95 percentile variations for both PIFR and PIF; this method was adopted by Chrystyn et al. (2015) in a recent study. Besides using individual IPs, well simulated IPs based on measured key inhalation parameters also show great

potential for use *in vitro* tests to predict lung deposition (Delvadia et al., 2013a; Delvadia et al., 2012).

1.5 CURRENT STATUS AND CHALLENGES

Realistic *in vitro* testing of DPIs can be performed essentially by coupling well-designed MT models to selected IPs that mimic inhaler use in the clinic or in practice. The approach has already been found helpful while building IVIVCs for inhaled drug products. The system most typically employed is shown in Figure 1.7.

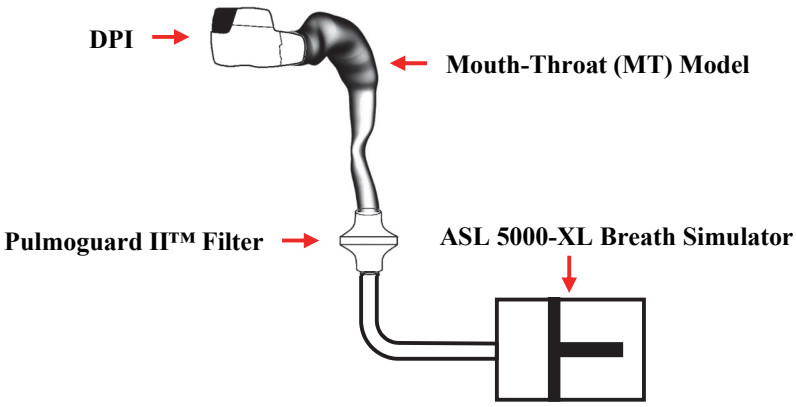

Figure 1.7. Experimental setup for realistic *in vitro* testing. A DPI is primed and inserted into a realistic mouth-throat (MT) model. Internal surface of the MT is coated to retain powder particles. A breath simulator with sufficient capacity is programmed to withdraw realistic inhalation profiles (IPs) through a low resistance filter. The mass of drug that reaches the filter, $TLD_{in\ vitro}$, depends on the product, and the MT-IP combinations.

The *in vitro* predicted lung dose ($TLD_{in\ vitro}$; designated as the drug dose exiting the MT model; Figure 1.7) can be compared with the *in vivo* lung deposition data for the same inhaler obtained either from gamma scintigraphy studies (Delvadia et al., 2013a; Delvadia et al., 2012; Zhang et al., 2007), or from PK studies performed using a charcoal block

technique to prevent drug absorption from the GI tract (Olsson et al., 2013; Weers et al., 2014). The test methods have also been used as predictive tools to estimate the drug dose likely to penetrate patients' lungs as part of the product development process (Chrystyn et al., 2015; Pitcairn et al., 2012; Weers et al., 2013). Although such methods are more clinically relevant and shown to produce better IVIVCs than the standard compendial methods, their application remains challenging. At this stage, industry scientists and regulators are left to debate which MT models to select and how to choose representative IPs. No effort has yet been made to standardize the approach.

Another question relates to the importance of regional drug distribution in the lung; this may well be relevant to the therapeutic effects of certain inhaled drugs (Anderson & Newman, 2009; Usmani et al., 2005), but *in vitro* methods have yet to be developed that are predictive of regional drug deposition from DPIs *in vivo*. Recent advances on the topic have been to couple realistic *in vitro* testing with compendial cascade impactor methods to measure the size distribution of aerosol drugs leaving the MT model. These require the use of flow-balancing devices like the Nephele Mixing Inlet (NMI) or Electronic Lung™ to enable particle size distributions for drugs exiting the MT model to be measured at constant cascade impactor flow rates, following aerosol dispersion and release from an inhaler under realistic (variable flow) inhalation conditions (Casaro et al., 2014; Chrystyn et al., 2015; Olsson et al., 2013; Tarsin et al., 2006). But it remains unclear (a) how to measure APSDs under all inhalation conditions and (b) how even "realistic" size distribution data could be used to predict regional drug deposition in the lung. Overall, methods need to be developed, validated, standardized and improved to better evaluate DPI performance under realistic conditions. Emergent modeling approaches like CFD

simulations (Longest & Holbrook, 2012; Wong et al., 2012), that allow the motion of air flow and inhaled particles in human airways to be predicted based on principles of fluid mechanics, have been shown to be promising for aerosol deposition predictions in the lung. If these methods are to be used in bridging lung doses and particle size distribution data with *in vivo* regional lung deposition data, considerable method development and improved lung modeling is needed.

1.6 PROJECT AIM

This thesis is designed to further our understanding of DPI performance *in vitro* and *in vivo*. It describes efforts to improve realistic *in vitro* test methods for DPIs to explore the truth about the ranges of total lung dose and the particle size distributions of drugs that are likely to enter the lung from a marketed DPI. Methods have been developed to: (a) compare and select MT models for realistic *in vitro* testing (Chapter 3); (b) choose appropriate IPs for realistic testing of a wide range of DPIs (Chapter 4); (c) measure APSDs for DPIs across a range of IPs that extends beyond the currently permitted maximum flow rate for compendial cascade impactors (Chapter 5); (d) evaluate one proposed CFD method for its ability to predict regional lung depositions for a single inhaler based both on realistic APSD data for the inhaler and the *in vivo* data for regional drug distribution in the lung taken from the literature (Chapter 6).

CHAPTER 2

HYPOTHESES AND SPECIFIC AIMS

The goal of this research was to develop clinically relevant *in vitro* performance test methods for powder inhalers that enable variations in aerodynamic particle size distributions (APSDs) of drug aerosols to be characterized at the exit of selected mouth-throat (MT) models, across the range of breath profiles likely to be used by healthy human adults. To accomplish this objective, the project was subdivided into a series of hypotheses and specific aims:

Hypothesis I. Representative MT models with human oropharyngeal geometries can be selected from the literature, manufactured and evaluated experimentally for use in realistic *in vitro* performance tests for DPIs.

Specific Aim I. Different types of MT models and the USP cascade impactor induction port will be compared for ease of use and drug retention when tested across a realistic range of inhalation profiles (IPs) with Salbulin® Novolizer®. Values for total lung dose *in vitro* ($TLD_{in\ vitro}$, or the dose exiting each internally-coated MT model) will be compared statistically across MTs, and the practical advantages and disadvantages of different models will be explored.

Hypothesis II. A general method for simulating a range of representative IPs for use with any powder inhaler of known air flow resistance can be derived from existing Virginia Commonwealth University (VCU) clinical trial data for healthy adults, provided the general instructions for inhalation from the chosen device during use are consistent with those that normally accompany passive powder inhalers.

Specific Aim II. VCU clinical trial data collected from healthy adults by Delvadia (2012) will be analyzed further. A statistically valid range of IPs and associated algorithms will be tested for their ability to adequately fit the experimentally generated IP data across a population of mixed gender normal human adult volunteers inhaling through a range of air flow resistances typical of those in marketed DPIs.

Hypothesis III. When realistic IPs are used to generate aerosol drugs from a typical DPI, Budelin® Novolizer® (budesonide 200 mcg/dose), reliable methods can be developed to determine the APSD of $TLD_{in\ vitro}$, the dose exiting the MT model.

Specific Aim III. The Pharmacopeial Next Generation Pharmaceutical Impactor (NGI) will be modified and recalibrated to enable its use at high air flow rates consistent with the measurement of the budesonide APSD exiting MT models in excess of 100 L/min. The modified, recalibrated NGI will be used to characterize the drug clouds from Budelin® Novolizer® exiting each MT model across a range of realistic IPs, by using an aerosol mixing inlet supplied with dilution air to maintain constant air flow through the impactor.

Hypothesis IV. Computational fluid dynamic (CFD) modeling can be employed with initial conditions that describe the APSD of drug aerosols exiting MT to predict regional lung deposition of budesonide aerosols from Budelin® Novolizer® and the results can be compared with clinical data.

Specific Aim IV. The stochastic individual pathway (SIP) lung model and associated CFD methods, as developed by Tian et al. (2015a) for use with realistic IPs, will be evaluated for its ability to predict regional budesonide deposition in the lung from Budelin® Novolizer® following (a) experimental APSD characterization of $TLD_{in\ vitro}$ and (b) assumed entry of the APSD to the trachea of Tian et al.'s model at the chosen IPs. The predicted regional deposition results from CFD will be compared with those reported in the literature for the same inhaler following its collection based on two dimensional (2D) gamma scintigraphy (Newman et al., 2000).

CHAPTER 3

SELECTING REPRESENTATIVE HUMAN MOUTH-THROAT MODELS FOR REALISTIC DPI TESTING

3.1 INTRODUCTION

Realistic *in vitro* testing methods that are able to discriminate between inhalers and inhaler formulations and predict drug doses likely to deposit in the human lung (total lung dose; TLD) should offer significant benefits to personnel involved in clinical planning for inhaled product development. Such predictions can be made by collecting and analyzing the aerosol drug escaping a realistic mouth-throat (MT) model following delivery from an inhaler using inhaled flow rate vs. time profiles (IPs) likely to be used by the relevant patient population. At this time, three main types of MT models have been developed and all have shown promising *in vitro–in vivo* correlations (IVIVCs) (Delvadia et al., 2013a; Delvadia et al., 2012; Olsson et al., 2013; Weers et al., 2014; Zhang et al., 2007). However, there are significant differences in their development philosophies, geometries and manufacture. Product developers wishing to predict TLD values in humans are left to select an MT model (perhaps in several sizes) and couple these to a range of IPs that are expected to span the likely inspiratory maneuvers to be used with their chosen inhaler.

This chapter is an attempt to describe the issues that are currently associated with these choices, with the ultimate view of rationalizing the selection of the Virginia Commonwealth University (VCU) MT models used in the remainder of this thesis to describe the further development of *in vitro* performance test methods for dry powder inhalers (DPIs). Salbulin® Novolizer® (Meda Pharmaceuticals, Hertfordshire, U.K.) was selected and used as the test inhaler in this chapter to compare drug retention across MT models with different geometries. Budelin® Novolizer® (Meda Pharmaceuticals, Hertfordshire, U.K.) was selected as the test inhaler in the remainder of the thesis to compare drug retention in VCU MT models.

3.2 MATERIALS AND METHODS

Mouth-Throat Models

Small, medium and large VCU models (Delvadia et al., 2012) were made from ultraviolet-laser-cured resin (Accura® 60, 3D System, Valencia, CA) using a rapid prototyping process of stereolithography (Viper si2™ SLA® system, 3D Systems, Valencia, CA), with vertical layer thickness of 0.1 mm. The three dimensional (3D) geometries of VCU models are available to download at www.rddonline.com (Longest, 2012). Small, medium and large Oropharyngeal Consortium (OPC) models (Burnell et al., 2007) were purchased from Emmace Consulting AB (Södra Sandby, Sweden). These models were designed by the Oropharyngeal Consortium (AstraZeneca, GlaxoSmithKline and sanofi aventis) and manufactured using polyamide, also by rapid prototyping. The 3D geometries of OPC models are available to download at www.isam.org (Oropharyngeal

Consortium, 2013). The medium Alberta Idealized Throat (AIT) (Warren H Finlay et al., 2010) and the USP inlet (U.S. Pharmacopeial Convention, 2013) were purchased from Copley Scientific (Nottingham, U.K.). Unlike VCU and OPC models that are constructed from plastic, AIT model and USP inlet are manufactured in aluminum. The three types of realistic MT models and the USP inlet are shown Figure 3.1; further detail and descriptions of these models was provided in Chapter 1 and Figure 1.6.

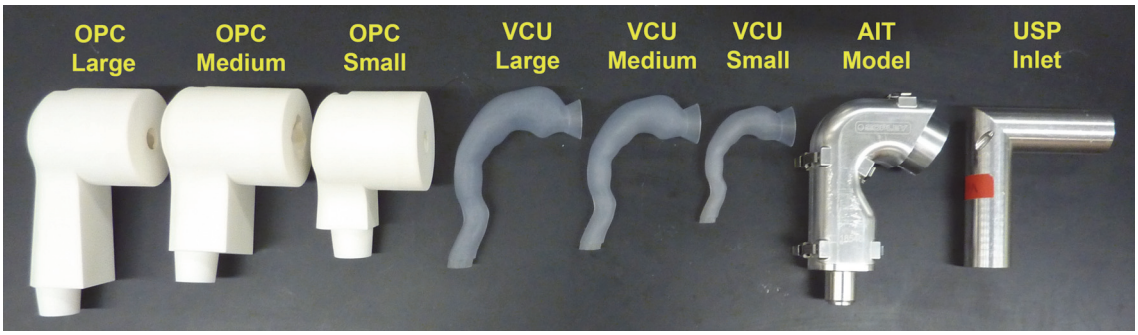

Figure 3.1. Realistic mouth-throat (MT) models developed for inhaler *in vitro* testing. From Left: Oropharyngeal Consortium (OPC) Large, OPC Medium, OPC Small (Burnell et al., 2007; Oropharyngeal Consortium, 2013), Virginia Commonwealth University (VCU) Large, VCU Medium, VCU Small (Delvadia et al., 2012; Longest, 2012), Alberta Idealized Throat (AIT; Medium) (Stapleton et al., 2000) and USP Inlet (U.S. Pharmacopeial Convention, 2013).

Inhalation Profiles

The clinical study data and methods described by Delvadia to simulate IPs for realistic DPI testing (Delvadia, 2012) was used to simulate IPs suitable for test of Salbulin Novolizer (airflow resistance = 0.0241 $kPa^{0.5}L^{-1}min$) as shown in Figure 3.2. Three IPs representing the typical range of these DPI-trained profiles were determined based on Delvadia's statistical treatment where individual flow rate (FR) profiles were ranked at

each time point, and the 10, 50 and 90 percentile values selected to produce the three red inhalation profiles (Figure 3.2).

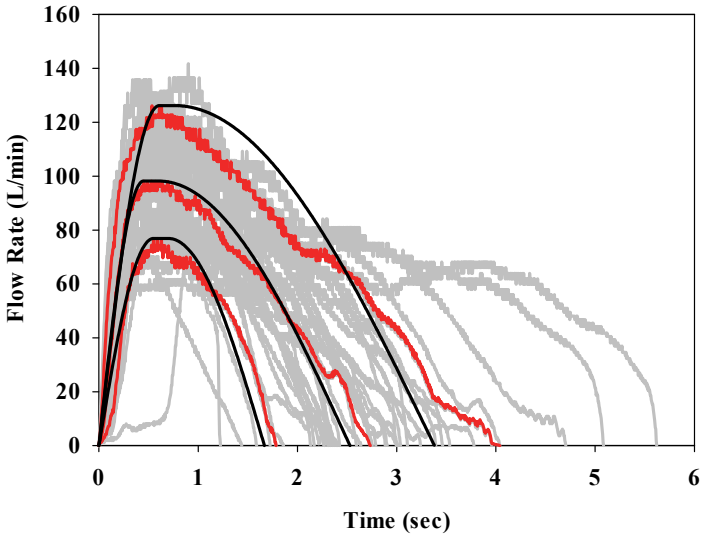

Figure 3.2. Individual flow profiles (gray; volumetric flow rates entering mouth vs. time) from DPI-trained normal adult volunteers inhaling through an inhalation flow recorder with an identical airflow resistance to Novolizer [data from (Delvadia, 2012)]. Red profiles are the 10, 50 and 90 percentile results that illustrate the range of profiles seen across this population. The smoothed profiles shown in black are the simulated profiles used to program the breath simulator for the *in vitro* MT model comparisons described below following simulation according to Delvadia using Equations 3.1 to 3.4 with parameters described in Table 3.1 (Delvadia, 2012; Delvadia et al., 2012).

The red FR vs. time, t, profiles were then simulated using Equations 3.1 to 3.3 below (Delvadia, 2012; Delvadia et al., 2012) to produce the black profiles shown in the figure. Values for the inhalation parameters used in the equations are shown in Table 3.1, where peak inhalation flow rate (PIFR), time at which PIFR occurs (T_{PIFR}), and total inhaled volume (V, area under the curve) were obtained directly from the red profiles, and duration of inhalation (T) was calculated from Equation 3.4. The three simulated IPs were used for the realistic *in vitro* testing of Salbulin with each of the MT models shown in Figure 3.1.

$$FR(t) = PIFR \times \sin\left(\frac{\pi}{2}\frac{t}{T_{PIFR}}\right) \qquad 0 \le t < T_{PIFR} \qquad \text{Equation 3.1}$$

$$FR(t) = PIFR \qquad T_{PIFR} \le t < \left(T_{PIFR} + 0.15\right) \qquad \text{Equation 3.2}$$

$$FR(t) = PIFR \times \cos\left(\frac{\pi}{2}\frac{\left(t - \left(T_{PIFR} + 0.15\right)\right)}{\left(T - \left(T_{PIFR} + 0.15\right)\right)}\right) \qquad \left(T_{PIFR} + 0.15\right) \le t \le T \qquad \text{Equation 3.3}$$

$$T = \frac{\pi}{2}\left(\frac{60V}{PIFR} - 0.15\right) + 0.15 \qquad \text{Equation 3.4}$$

Table 3.1. Peak inhalation flow rate, PIFR, time at which PIFR occurs, T_{PIFR}, total inhaled volume, V and duration of inhalation, T values for 10, 50 and 90 percentile simulated IPs according to the method described by Delvadia (Delvadia, 2012; Delvadia et al., 2012) and shown in Figure 3.2.

IP[a]	PIFR (L/min)	T_{PIFR} (sec)	V (L)	T (sec)
10 Percentile	76.9	0.550	1.43	1.667
50 Percentile	98.2	0.450	2.72	2.525
90 Percentile	126.2	0.610	4.64	3.380

[a]Figure 3.2, black profiles

Experimental Setup for Realistic In Vitro Testing

Figure 3.3 is a schematic of the experimental apparatus to evaluate aerosol drug deposition and the *in vitro* total lung dose ($TLD_{in\ vitro}$) for a powder inhaler under realistic conditions. Salbulin® Novolizer® (label claim: 120 mcg albuterol sulfate per delivered dose) was donated by Meda Pharmaceuticals (Hertfordshire, U.K.) and used to compare the eight MT models shown in Figure 3.1.

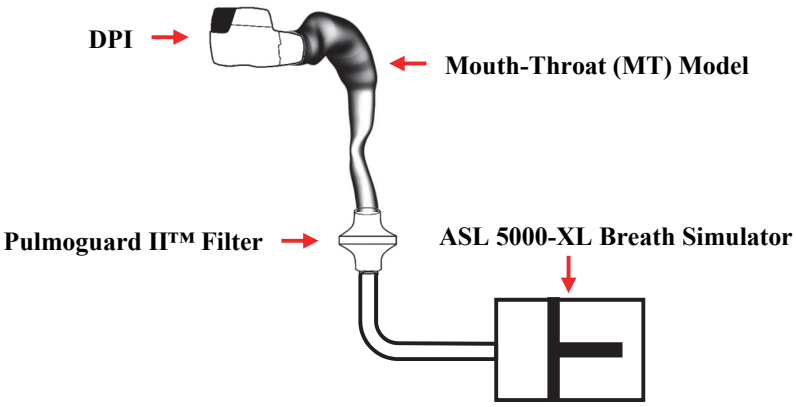

Figure 3.3. Schematic of experimental setup for measurement of total lung dose *in vitro* ($TLD_{in\ vitro}$), or the dose exiting the MT model, under simulated, realistic human inhalation conditions.

During testing, the inhaler was primed and inserted into an adapter manufactured to form an airtight junction between the inhaler mouthpiece and the MT model. Adapters for VCU MT models are described at www.rddonline.com (Longest, 2012), and were identical to those used previously (Delvadia et al., 2012). Adapters for OPC MT models were obtained from Emmace Consulting AB, while those for the AIT and USP inlet were manufactured in-house from Ten-to-One / High Tear Strength Mold Rubber (Micro-Mark, Berkeley Heights, NJ) positioned to site the inhaler exit at the center of the opening to the chosen MT model. During each simulated IP, air was drawn through the newly primed inhaler (single actuation) and MT model into a low resistance filter (Pulmoguard II™, Queset Medical, North Easton, MA) capable of retaining all of the aerosolized drug that passed through the model. The filter was connected to a programmable breath simulator (ASL 5000-XL, IngMar Medical, Pittsburgh, PA) to produce the standard IP at the mouth opening of the MT model. The internal surfaces of the VCU and OPC models were coated using two applications of 2% (w/v) Brij™ 35 (ACROS Organics™, Thermo Fisher

Scientific, Waltham, MA) in glycerol followed by allowing excess solution to drip and evaporate from the model for at least 2 h (Mitchell, 2003; Olsson et al., 2013). Because Brij solutions failed to adequately wet the metal surfaces of the AIT model and the USP inlet port, those models were coated instead using two spray applications of Molykote® 316 Silicone Release Spray (Dow Corning, Midland, MI) followed by solvent evaporation prior to each experiment (Hindle et al., 1996). A randomized experimental design was implemented to vary the MT models and recover the drug from the filter ($TLD_{in\ vitro}$; Figure 3.3) following withdrawal of individual actuations (doses) by triggering the breath simulator programmed for the black IPs shown in Figure 3.2. The apparatus was disassembled after each dose, and albuterol sulfate was recovered by rinsing the inhaler (with drug cartridge removed), MT and filter using known volumes of 65% methanol: 35% 20mM ammonium formate buffer (v/v) and analyzed using high-performance liquid chromatography (HPLC). Albuterol sulfate assay was performed using Allure® PFP Propyl column (5µm, 3.2×150mm, Restek Corporation, Bellefonte, PA), 65% methanol: 35% 20mM ammonium formate buffer (v/v) as mobile phase (flow rate: 0.75 mL/min), and UV detection at 276 nm (2998 Photodiode Array Detector, e2695 Seperation Module, Waters, Milford, MA). Injection volume was 100 µL and calibration curves were linear in the range of 0.2–10.0 mcg/mL ($r^2 > 0.999$). Each experiment was performed at least 9 times. Statistical analyses were performed for drug doses retained on and delivered from the inhaler, and $TLD_{in\ vitro}$ using one-way ANOVA and Tukey's HSD in JMP Pro 11 (SAS Institute Inc., Cary, NC). Further analyses to evaluate the effects of the MT models, IPs, and model sizes on values for mean $TLD_{in\ vitro}$ were performed by two-way ANOVA (MT models and IPs) and three-way ANOVA respectively.

3.3 RESULTS

Effects of IP Selection on Inhaler Performance

Drug doses retained on and delivered from the Novolizer device were analyzed for the 10, 50 and 90 percentile IPs. Data were pooled across the eight MT models for each IP (n≥72), and were presented as percent of manufacturer's label claim (120 mcg albuterol sulfate per delivered dose) in Figure 3.4.

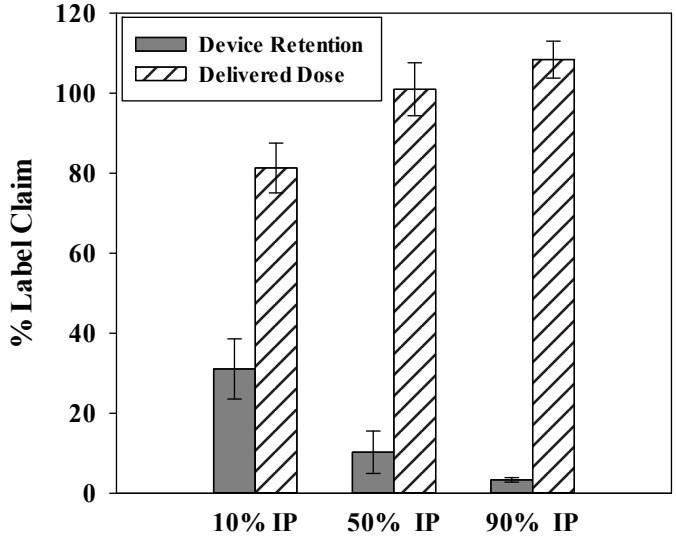

Figure 3.4. Percent of manufacturer's label claim (120 mcg albuterol sulfate per delivered dose) for drugs retained in the mouthpiece or delivered from the Novolizer device (device retention and delivered dose, respectively) for the 10, 50 and 90 percentile IPs. Data were pooled across eight MT models for each IP and presented as mean±SD (n≥72). Statistically significant differences were observed for both the mean device retention and mean delivered dose between different IPs in all cases (Student's t-test, $p<0.05$).

The 10 percentile IP produced the highest value for mean device retention (31.0% label claim), while this value reduced to 10.2% label claim for the 50 percentile IP and 3.4% label claim for the 90 percentile IP. Most notably, when tested with the 10 percentile IP, Salbulin only delivered a mean of 81.3% of label claim. Statistically significant

differences were observed for both the mean device retention and mean delivered dose between different IPs (one-way ANOVA, $p<0.05$), consistent with the literature reports for this device (Delvadia et al., 2012).

Effects of IP Selection on $TLD_{in\ vitro}$

Values for $TLD_{in\ vitro}$, designated as the drug dose escaping the MT model and collected on the filter from Salbulin, are shown in Figure 3.5 for each MT model tested using the 10, 50 and 90 percentile IPs typical of trained adults inhaling through a resistance equivalent to that of Novolizer.

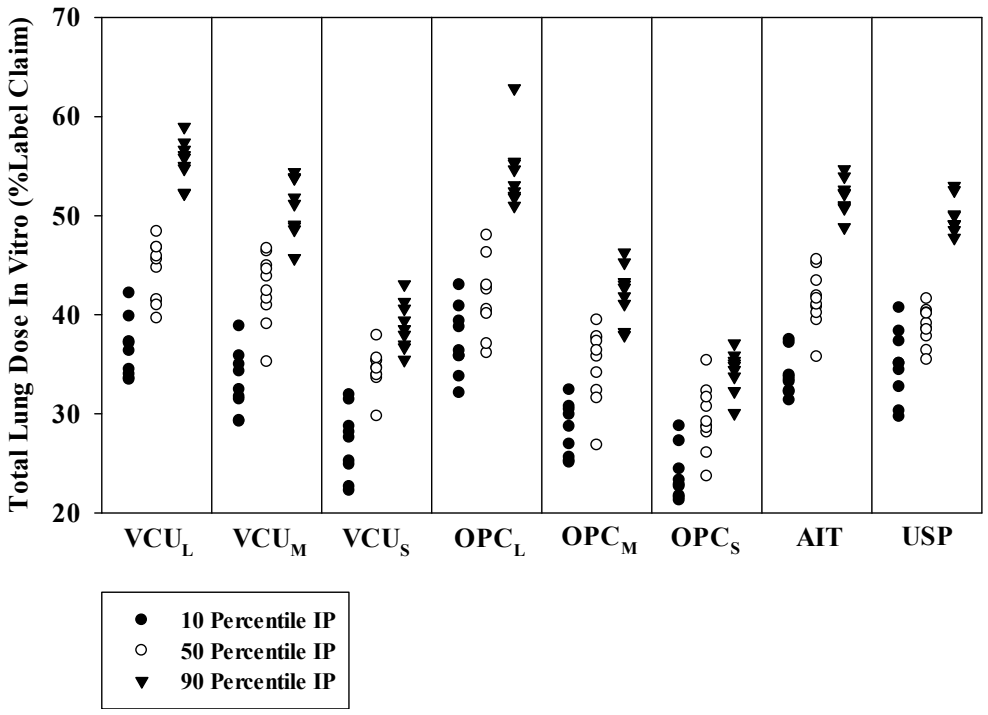

Figure 3.5. Percent of manufacturer's label claim (120 mcg albuterol sulfate) exiting the MT model ($TLD_{in\ Vitro}$) from Salbulin Novolizer after randomized testing using the 10, 50 and 90 percentile IPs. The subscripts L, M and S represent Large, Medium and Small MT models, respectively (Figure 3.1).

Notably, the change of test IPs produced large variations in $TLD_{in\ vitro}$ for each MT model, and the larger MTs generally produced a larger range of results for $TLD_{in\ vitro}$ than was seen for smaller MTs. For a selected MT model, the 90 percentile IP produced highest values for $TLD_{in\ vitro}$, while the 10 percentile IP produced the lowest values. The effects of IP variations on $TLD_{in\ vitro}$ indicate that more efficient drug-carrier deaggregation occurred when larger IPs were used for Salbulin testing; for this inhaler and others, the effects of improved powder deaggregation seen with larger flow rates may be expected to exceed the effects of the increased inertia of drug particles passing into the MTs (i.e. impacting and depositing in MT) due to the higher values of $TLD_{in\ vitro}$ seen with larger IPs.

While the approach used to generate the 10, 50 and 90 percentile flow rate vs. time curves in Figure 3.2 will be analyzed more thoroughly in Chapter 4 that describes an improved simulation technique for a spectrum of standard IPs for use with DPIs of different airflow resistances, the significant variations in $TLD_{in\ vitro}$ observed in this study suggested that it is important to include both the medium (the 50 percentile IP) and the extremes (the 10 and 90 percentile IPs) to fully evaluate the likely clinical performance of a powder inhaler like Salbulin Novolizer. Powder inhaler performance, even for a well-designed DPI like Salbulin Novolizer, was highly dependent on the selected IP. The ranges with which $TLD_{in\ vitro}$ could be determined when using a single IP in these models was of the order of 5–12% of label claim (Figure 3.5); this increased to 15–30% of label claim when Novolizer was tested at the extremes (the 10 or 90 percentile IP), even though these simulated IPs were based on the inhalation maneuvers recorded following Delvadia's study of trained adult subjects of both genders (Delvadia, 2012).

Effects of MT Model Selection on $TLD_{in\ vitro}$

This investigation showed that the choice of MT model clearly impacts the value of $TLD_{in\ vitro}$ and thus the anticipated values for TLD in the clinic (Figure 3.6). Statistical differences between the mean values are illustrated in Figure 3.6. Perhaps most surprising from Figure 3.6, was the finding of a statistical difference between the results shown among the three “medium” models (VCU medium, OPC medium and AIT). Notably, for all three IPs, the VCU medium and AIT models produced statistically comparable results while the OPC medium model produced a value for $TLD_{in\ vitro}$ that was significantly smaller than its counterparts. The USP inlet also produced statistically comparable results to VCU medium and AIT models in all three cases, illustrating that this pharmacopeial standard conduit (used to connect an inhaler to a cascade impactor) can sometimes produce comparable results with MT models that were designed with “realistic geometries”, provided its internal surfaces are coated to ensure impacted powder retention. The comparison of two “small” models also showed statistical differences for the 50 and 90 percentile IPs, where OPC small produced a significantly smaller value for $TLD_{in\ vitro}$ than VCU small. Notably however, these two models produced comparable results for the 10 percentile IP. The two “large” models, in contrast, showed statistically comparable results for all three IPs.

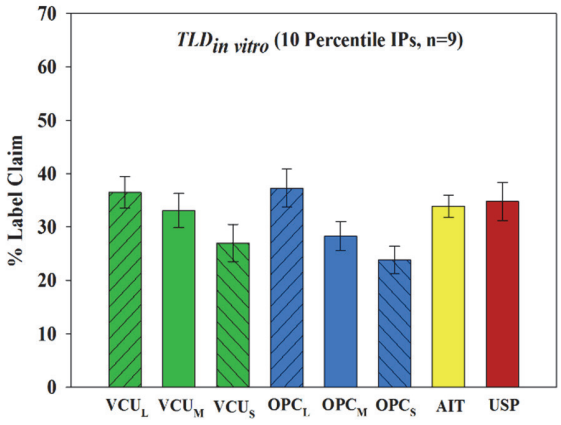

Statistical Comparisons for $TLD_{in\ vitro}$ (10 Percentile IPs)

	VCU_L	VCU_M	VCU_S	OPC_L	OPC_M	OPC_S	AIT	USP
VCU_L			✓		✓	✓		
VCU_M			✓		✓	✓		
VCU_S	✓	✓		✓			✓	✓
OPC_L			✓		✓	✓		
OPC_M	✓	✓		✓		✓	✓	✓
OPC_S	✓	✓		✓	✓		✓	✓
AIT			✓		✓	✓		
USP			✓		✓	✓		

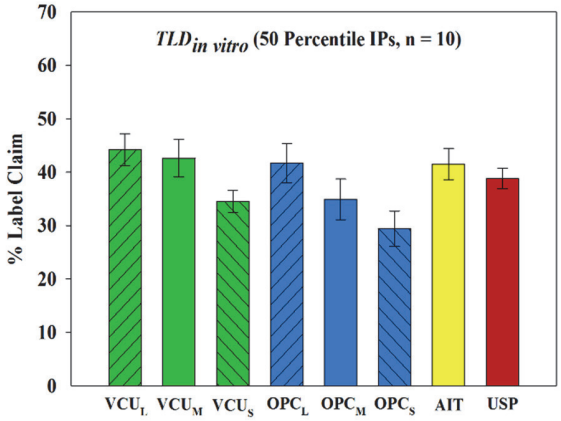

Statistical Comparisons for $TLD_{in\ vitro}$ (50 Percentile IPs)

	VCU_L	VCU_M	VCU_S	OPC_L	OPC_M	OPC_S	AIT	USP
VCU_L			✓		✓	✓		✓
VCU_M			✓		✓	✓		
VCU_S	✓	✓		✓		✓	✓	✓
OPC_L			✓		✓	✓		
OPC_M	✓	✓		✓		✓	✓	
OPC_S	✓	✓	✓	✓	✓		✓	✓
AIT			✓		✓	✓		
USP	✓		✓			✓		

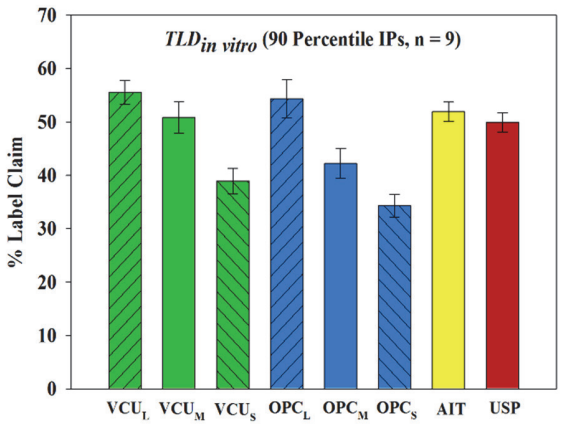

Statistical Comparisons for $TLD_{in\ vitro}$ (90 Percentile IPs)

	VCU_L	VCU_M	VCU_S	OPC_L	OPC_M	OPC_S	AIT	USP
VCU_L		✓	✓		✓	✓		✓
VCU_M	✓		✓		✓	✓		
VCU_S	✓	✓		✓		✓	✓	✓
OPC_L			✓		✓	✓		✓
OPC_M	✓	✓		✓		✓	✓	✓
OPC_S	✓	✓	✓	✓	✓		✓	✓
AIT			✓		✓	✓		
USP	✓		✓	✓	✓	✓		

Figure 3.6. Percent of manufacturer's label claim (120 mcg albuterol sulfate) escaping the MT model (mean $TLD_{in\ Vitro}$) from Salbulin Novolizer after randomized testing using 10, 50 and 90 percentile IPs. Results are presented as mean±SD (n≥9). The subscripts L, M and S represent large, medium and small MT models, respectively. Statistically significant differences (✓) in mean values are shown after one-way ANOVA ($p<0.05$) and Tukey's HSD. Further statistical analyses following two- and three-way ANOVA to evaluate the effects of the MT models, IPs and model sizes on values for mean $TLD_{in\ Vitro}$ are described in the text.

The direct one-way ANOVA comparisons (above and Figure 3.6) were mirrored by two-way ANOVA to evaluate the effects of MTs (VCU vs. OPC vs. AIT vs. USP) and IPs (10 percentile vs. 50 percentile vs. 90 percentile) on $TLD_{in\ vitro}$. The following hypotheses were tested:

H_1: MTs have no effect on $TLD_{in\ vitro}$

H_2: IPs have no effect on $TLD_{in\ vitro}$

H_3: There is no interaction between MTs and IPs

The results showed that both MTs and IPs had significant effects on $TLD_{in\ vitro}$ ($p<0.0001$ in both cases; H_1 and H_2 were rejected), while no significant interaction was observed between the two factors ($p=0.6523>0.05$; H_3 was not rejected). Tukey's HSD indicated that effects of MT on $TLD_{in\ vitro}$ appeared to be: VCU = AIT = USP > OPC, while effects of IP on $TLD_{in\ vitro}$ showed that: 90 percentile IP > 50 percentile IP > 10 percentile IP.

Three-way ANOVA was used to compare the VCU and OPC MTs. The effects of MTs (VCU vs. OPC), model sizes (small vs. medium vs. large) and IPs (10 percentile vs. 50 percentile vs. 90 percentile) on $TLD_{in\ vitro}$ were evaluated by testing the following hypotheses:

H_4: MTs have no effect on $TLD_{in\ vitro}$

H_5: Model sizes have no effect on $TLD_{in\ vitro}$

H_6: IPs have no effect on $TLD_{in\ vitro}$

H_7: There is no interaction between MTs and model sizes

H_8: There is no interaction between MTs and IPs

H_9: There is no interaction between model sizes and IPs

H_{10}: There is no interaction between MTs, model sizes and IPs

The results showed that there was no significant interaction between the three factors (MT*size*IP, p=0.8812>0.05; H_{10} was not rejected), while significant interactions were observed for MTs and model sizes (MT*size, p<0.0001; H_7 was rejected), MTs and IPs (MT*IP, p=0.0419<0.05; H_8 was rejected), and model sizes and IPs (size*IP, p<0.0001; H_9 was rejected). Tukey's HSD indicated that effects of MT*size on $TLD_{in\ vitro}$ appeared to be: VCU Large MT = OPC Large MT, VCU Medium MT > OPC Medium MT, VCU Small MT > OPC Small MT. Tukey's HSD furthermore showed the effects of MT*IP on $TLD_{in\ vitro}$ appeared to be: VCU > OPC for both the 50 and 90 percentile IPs while VCU = OPC for the 10 percentile IP. Effects of size*IP on $TLD_{in\ vitro}$ appeared to be: Large MT > Medium MT > Small MT, and Large IP > Medium IP > Small IP.

3.4 DISCUSSION

The $TLD_{in\ vitro}$ results of Delvadia et al. (2012) for Budelin Novolizer (200 mcg budesonide per delivered dose) appeared to correlate well with reported literature values for $TLD_{in\ vivo}$ when experiments were conducted in VCU MT models and the simulated IPs were based on those used in the clinic (Newman et al., 2000). Most notable from that work (Delvadia et al., 2012), was the apparent agreement between the overall range of results for $TLD_{in\ vitro}$ when the results were derived from tests across IPs using the small, medium and large VCU MT models, compared with the literature values for $TLD_{in\ vivo}$ (for example, $TLD_{in\ vivo}$ ranged from 9.4–41.0% of the metered dose for *fast* inhalation, while that of *in vitro* spanned 9.7–40.4%). In the work discussed in this chapter, the

experimental range of $TLD_{in\ vitro}$ in VCU models was 22–59% label claim, while in OPC models it was 21–63% label claim. In these terms, VCU and OPC models were similar. Because *in vivo* results are not available for Salbulin however, there was no way that a preference can be stated for either model on this basis. Nevertheless, the medium VCU and OPC geometries produced statistically significant differences in values for $TLD_{in\ vitro}$ from Salbulin Novolizer at all tested inhalation profiles. While the meaning of this difference in "medium result" needs to be further explored, the predicted range of possible deposition results across an adult population was more consistent between the differently sized VCU and OPC models, indicating that a much smaller number of *in vitro* experiments than those described in this paper may be sufficient to provide reliable estimates of $TLD_{in\ vitro}$ at the extremes (e.g. small IP–small MT to large IP–large MT, from either model series). Figure 3.7 and Table 3.2 show the range of results for $TLD_{in\ vitro}$ from all the tests conducted with Salbulin Novolizer.

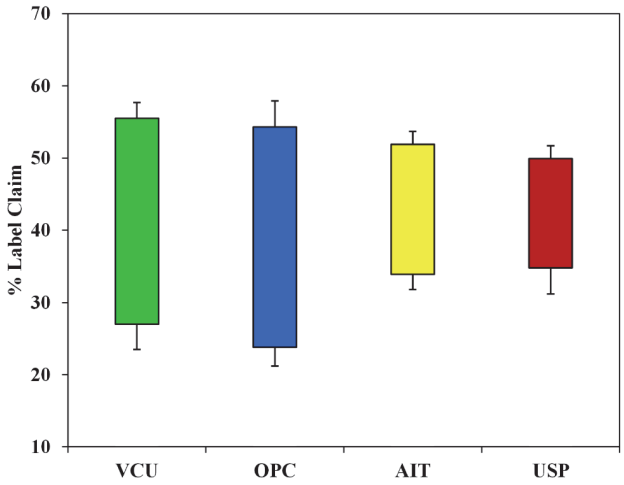

Figure 3.7. The range of mean results for Salbulin Novolizer's $TLD_{in\ vitro}$ (% label claim) tested across all MT Models using 10, 50 and 90 percentile IPs. Results for the single geometry AIT and USP models show the range of results due solely to the change in IP. Results are percent of manufacturer's label claim (120 mcg albuterol sulfate as delivered dose). Upper and lower error bars are SD values from the large IP–large model and small IP–small model, respectively, as shown numerically in Table 3.3.

Table 3.2. Numerical results from Figure 3.7; a statistically significant difference between VCU and OPC model results ($p<0.05$; $n=18$) occurred when testing to determine the value for the mean minimum $TLD_{in\ vitro}$.

	Mean (SD)[a]	
	Small	Large
VCU	27.0 (3.5)	55.5 (2.2)
OPC	23.8 (2.6)	54.3 (3.6)
AIT	33.9 (2.1)	51.9 (1.8)
USP	34.8 (3.6)	49.9 (1.8)

[a] Mean and standard deviations (SD) of $TLD_{in\ vitro}$ following testing with small model and 10 percentile IP ("Small") vs. large model and 90 percentile IP ("Large"). For AIT and USP, where only a single model is available, "Small" and "Large" refer to the results from testing with 10 and 90 percentile IPs, respectively.

The colored portion in each of the bar graphs of Figure 3.7 shows the range between the mean results when the 10 percentile IP was tested with the small MT model (mean minimum $TLD_{in\ vitro}$) and the 90 percentile IP was tested with the large MT model (mean maximum $TLD_{in\ vitro}$); the error bars in Figure 3.7 show a single standard deviation about those means in each case. While the means for minimum $TLD_{in\ vitro}$ showed statistically significant differences (Student's t test, $p<0.05$; Table 3.3), there was a distinct overlap in the experimental results (Figure 3.7) and no statistically significant difference between each model series for mean maximum $TLD_{in\ vitro}$. Clearly, this range of values could be collected using only the small and large versions of each set of MT models, at least as far as this inhaler was concerned. Moreover, because the experimental range of results for $TLD_{in\ vitro}$ seen by Delvadia et al. (2012) was much more representative of the results seen *in vivo*, there is good evidence to suggest that DPI testing needs to be

conducted across a range of MT geometries (and not a single model as seen with either AIT or USP; Figure 3.7).

The choice between the three VCU and three OPC MT models became one in which the advantages and disadvantages of these models needed to be compared in order to practically justify the use of one over the other. While further studies are possibly needed to thoroughly compare values of *in vitro* lung doses for the different models, the practical advantages and disadvantages of these MT models were listed in Table 3.3 to facilitate selection of the MT models for realistic *in vitro* testing. As shown in this table, OPC models are not provided with a standardized mouth opening. Moreover, their complex internal structure (Figure 1.6) required solvent based drug extraction for periods up to 10 minutes, in order to ensure complete drug recovery (for albuterol sulfate in this study, VCU models could be extracted in less than 1 minute). In this thesis therefore, the VCU models were selected for all further studies because their advantages outweighed their disadvantages, the models were readily available, and they had already been shown to produce an apparent IVIVCs with Budelin Novolizer and four other marketed DPIs (Delvadia et al., 2013a; Delvadia et al., 2012). In addition, the results from the VCU models were similar to those from the OPC models when tested with Salbulin Novolizer.

Table 3.3. Practical advantages and disadvantages of the test MT models.

	Advantages	Disadvantages
VCU	▪ Small, medium and large MTs are available ▪ Polyurethane versions are now available for use with an attached NGI adapter ▪ Constructed in one piece for ease of use ▪ Clear and easy to observe particle deposition ▪ Geometrically validated via the literature (Delvadia et al., 2012) ▪ IVIVC validated to five marketed DPIs	▪ Accura 60 is not resistant to use of all solvents
OPC	▪ Small, medium and large MTs are available ▪ Constructed in one piece for ease of use ▪ Universal outer geometry allows a single mouth-piece adapter to be used ▪ NGI/ACI adapter attached	▪ Chunky and less easy to handle ▪ Internal volumes inconsistent with those reported in the literature* (Burnell et al., 2007); not geometrically validated ▪ Mouth entrance arbitrarily occluded due to selection of individual subject geometries (Oropharyngeal Consortium, 2013)
AIT	▪ Robust construction in polished aluminum ▪ Particle deposition site can be observed after splitting into two-halves ▪ NGI/ACI adapter attached	▪ Only the medium model is available ▪ Constructed in two-halves with a gasket that can leak ▪ Not easy to handle
USP	▪ Constructed in one piece for ease of use ▪ NGI/ACI adapter attached	▪ Geometry is not realistic ▪ Only one model is available

*The internal volumes of the small, medium and large OPC models (constructed from sintered polyamide) were determined experimentally to be 27.6, 91.7 and 84.4 cm^3, respectively, compared to reported internal volumes of 25.8 (small), 78.1 (medium) and 71.0 cm^3 (large) (Burnell et al., 2007).

CHAPTER 4

SIMULATING VARIATIONS IN HUMAN BREATH PROFILES FOR REALISTIC DPI TESTING

This Chapter is in press. It is to be published in the Journal of Aerosol Medicine and Pulmonary. Drug Delivery. In the Journal it carries the title and authors: **In Vitro Tests for Aerosol Deposition. IV: Simulating Variations in Human Breath Profiles for Realistic DPI Testing.** Renishkumar R. Delvadia, Xiangyin Wei, P. Worth Longest, Jurgen Venitz and Peter R. Byron. Renishkumar Delvadia performed the clinical trial with assistance from Xiangyin Wei. The raw breath profile data and statistical analyses of the descriptive inhalation parameters (PIFR, V, etc.) were performed by Renishkumar Delvadia with the assistance of Jurgen Venitz and included in his thesis in 2012 (Delvadia, 2012). In this thesis, Peter Byron and Worth Longest advised Xiangyin Wei during her reanalysis, simulation and curve fitting of the data describing the 10, 50 and 90 percentile inhalation profiles under the various conditions described in full below. The chapter is reproduced entirely as it is to be published below.

4.1 INTRODUCTION

In this series of publications on realistic inhaler testing we sought to offer improved, clinically-relevant test methods for aerosol drugs and possible *in vitro-in vivo* correlations (IVIVC) for lung deposition (Delvadia et al., 2013a; Delvadia et al., 2012; Delvadia et al., 2013b). The experimental setup and brief description of the test method is shown in Figure 4.1.

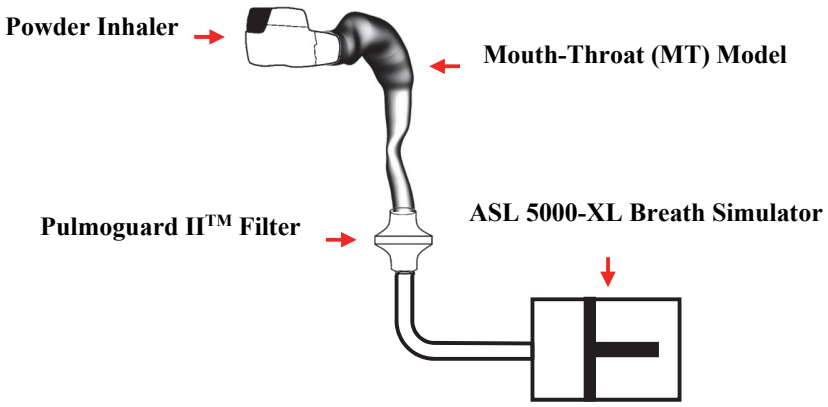

Figure 4.1. Experimental setup for realistic *in vitro* testing. A passive powder inhaler with known airflow resistance, R, is primed and inserted into small, medium or large mouth-throat (MT) model(s) that span 95% of the volumetric range seen in human adults. Internal surfaces of MT are coated to retain powder particles. A breath simulator with sufficient capacity is programmed to withdraw a volume V through a low resistance filter using a range of simulated IPs, as described in this paper. The mass of drug that reaches the filter, $TLD_{in\ vitro}$, depends on the product, and the MT-IP combination (Byron et al., 2010; Byron et al., 2013; Delvadia et al., 2013a; Delvadia et al., 2012; Delvadia et al., 2013b; Longest, 2012; Olsson et al., 2013; Wei et al., 2014).

By assessing the aerosol drug dose exiting small, medium and large realistic mouth-throat (MT) models (Longest, 2012) while using inhalation profiles (IPs) believed to simulate the breathing maneuvers used during clinical testing, we found that (a) the mean value for $TLD_{in\ vitro}$, from several different dry powder inhalers (DPIs) was consistent with literature values for lung deposition following clinical testing (Delvadia et al., 2013a) and (b) the range of values from a single DPI agreed with the published range of values

for $TLD_{in\ vivo}$ following gamma-scintigraphic testing in a mixed-gender adult population (Delvadia et al., 2012). It is well known that performance of passive DPIs is air flow rate dependent; indeed the seminal work of Clark and Hollingworth (1993), led to compendial test methods requiring that dose emissions and size distributions be determined at flow rates that maintain an appropriate pressure drop across each inhaler (U.S. Pharmacopeial Convention, 2013). It is also well known that DPI performance depends on the way that patients use these inhalers. While this can be influenced by instruction leaflets, training and of course, the subject's lung capacity, present DPI development is largely empirical and often retrospective because of *in vitro* performance testing that fails to concern itself with the way that patients actually inhale through a chosen device. Reports that a large proportion of patients fail to use DPIs correctly are common; failure to exhale before inhalation, failure to inhale rapidly and deeply, as well as incorrect mouthpiece positioning may all influence regional drug deposition and clinical outcome (Broeders et al., 2009; van Beerendonk et al., 1998).

In this article we report the results of a clinical study that enabled us to document the variability in the IPs of inhaler-naïve normal adults inhaling through a series of air flow resistances typical of those used in commercial DPIs. The study enabled us to recommend a range of IPs for testing DPIs with different airflow resistances. The IPs may be simulated using sinusoidal equations that adequately describe the flow rate vs. time profiles spanning the 10 through 90 percentile values for a mixed-gender, lung-normal, adult population. Because inhaler-naïve volunteers were recruited for the study, it was also possible to compare the effectiveness of "training by package insert" to formalized training from a pharmacist in the use of passive DPIs; this by comparing the different IPs

elicited by the two procedures in the same subjects. Use of the protocol described here should enable IPs to be selected for inhaler testing to span those likely to be used by normal human volunteers in clinical trials. While recognizing that inhalation profiles may differ in patient groups with different demographics and lung disease (Baba et al., 2011; Broeders et al., 2004; Malmberg et al., 2010; Sarinas et al., 1998), the approach to data analysis and IP simulation that is described here can likely be generalized to cover different populations so that product development scientists can select IPs for inhaler testing *in vitro* that are realistic and representative of the way new inhalers should eventually be used.

4.2 MATERIALS AND METHODS

A protocol was designed to document the IPs commonly used by healthy volunteers inhaling through powder inhalers. Volunteers were trained first by reading the directions for use provided in a typical package insert, and second, by receiving a demonstration and direct oral instructions from a pharmacist. The objectives were (a) to collect a range of typical flow rate vs. time profiles from normal adult subjects inhaling through air flow resistances that mimicked those seen in commercial DPIs, (b) curve-fit and analyze those IPs before and after receipt of training and thus, (c) establish a data base and equations for simulation of typical IPs used by normal subjects inhaling through different air flow resistances. We envisaged the use of these equations by inhaler designers seeking to optimize product performance *in vitro*, in advance of clinical trials. As it is well known that aerosol drug delivery performance of passive DPIs is dependent on air flow rate and air flow resistance (Clark & Hollingworth, 1993; U.S. Pharmacopeial

Convention, 2013), a drug-free “inhalation flow cell (IFC)” with a disposable mouthpiece and variable airflow resistances was constructed and instrumented with a digital volumetric flow meter, as shown in Figure 4.2, to record the air flow rate vs. time profiles used by each of the volunteers.

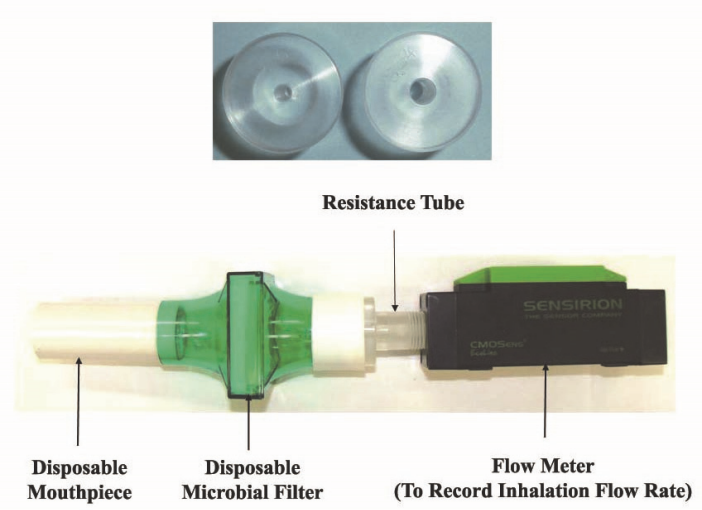

Figure 4.2. The inhalation flow cell (IFC) with top views of two “Resistance Tubes” with identical external, but different internal, dimensions. Six IFC resistances were chosen for IP recordings in the clinic: 0.0179, 0.0200, 0.0241, 0.0344, 0.0432 and 0.0462 $kPa^{0.5}$ L^{-1} min. These values were determined experimentally from the slope of plots measured pressure $drop^{0.5}$ (flowmeter inlet to mouthpiece) vs. the volumetric airflow rate exiting the mouthpiece (ASL 5000-XL, Ingmar Medical, Pittsburgh, PA). In the clinic, flow rates entering IFC were recorded every 50msec using a calibrated digital flow meter (EM1, Sensirion Inc., CA). All flow rates in this paper are expressed as the volumetric flow rate exiting the mouthpiece and are identical to those used to program the breath simulator (Figure 4.1).

Each recorded flow rate value was converted to the volumetric flow rate exiting the mouthpiece using an algorithm to account for the change in the volumetric gas flow into and out of the IFC with variations in pressure and resistance (Delvadia, 2012). All of the IPs and flow rates described in this paper are flow rates exiting the mouthpiece. Therefore, all IP data can be used directly to program breath simulators in the “realistic” *in vitro* tests we described elsewhere (Byron et al., 2010; Byron et al., 2013; Delvadia et

al., 2013a; Delvadia et al., 2012; Delvadia et al., 2013b; Olsson et al., 2013; Wei et al., 2014). Air flow resistance values [$kPa^{0.5}.L^{-1}$ min] for the IFC were determined from the slope of experimental plots of (pressure drop across IFC)$^{0.5}$ vs. volumetric flow rate out of the mouthpiece, by linear regression.

Clinical Study: Collection of inhalation profiles (IPs)

Adult human volunteers were recruited from the general population of Richmond, Virginia, via advertisements. Healthy, non-pregnant, non-smoking subjects were recruited who were 18 to 65 years old, above 147 cm in height, 50 to 120 kg in weight, without history of recent congestion, lung disease and/or inhaler use. Volunteers had never used, or been trained to use, a DPI before admission to the study. The study was approved by VCU's Institutional Review Board and entered on www.clinicaltrials.gov. Eligible subjects were enrolled; twenty (10M, 10F) completed the study. None had evidence of acute medical or psychiatric illness and all were found to have FEV1 > the predicted lower limit of normal (LLN) after spirometric screening performed during an initial visit.(Marion et al., 2001; M. R. Miller et al., 2005) On the second visit, each volunteer was asked to inhale approximately 18 times through the IFC (Figure 4.2). Individual IPs were recorded digitally every 50 msec as the volumetric flow rate vs. time profile of air exiting the mouthpiece of the calibrated inhalation cell after Instruction A and B were provided, sequentially, to each volunteer.

Instruction A. Each volunteer was asked to read the instructions shown in Figure 4.3. Those written instructions were based on leaflets, supplied as package inserts with marketed powder inhalers, showing patients how to inhale from a primed DPI. After

reading the instructions, volunteers were asked to inhale through the drug-free IFC, as if they were conforming to the written instructions. Inhalation profiles were recorded for each of six different resistance tubes placed in the IFC in random order. Subjects were allowed to rest between inhalations to avoid fatigue.

Instruction B. Verbal instruction and a practical demonstration of how to use a powder inhaler correctly was then delivered individually to each volunteer by a pharmacist trained and experienced in the use of powder inhalers. The same pharmacist provided the same demonstration and instructions to each volunteer that emphasized: (Step 1) breathe out *completely*, (Step 2) ensure *good lip closure around the IFC mouthpiece*, (Step 3) inhale as *fast and deep as possible through the mouth*; and to *continue until replete*, (Step 4) *hold breath and remove IFC from mouth*.

Following this formal training, volunteers were again asked to inhale through the IFC in the way they had been instructed and, during each inhalation, they were encouraged to continue inhaling as they began to show signs of reduced effort. IPs were recorded for each of the six different resistance tubes placed in the IFC in random order. Each flow profile was repeated to give a second IP, or flow rate exiting the mouthpiece vs. time, for each subject and resistance. The results from these duplicate experiments were designated “Instruction B1” and “Instruction B2”.

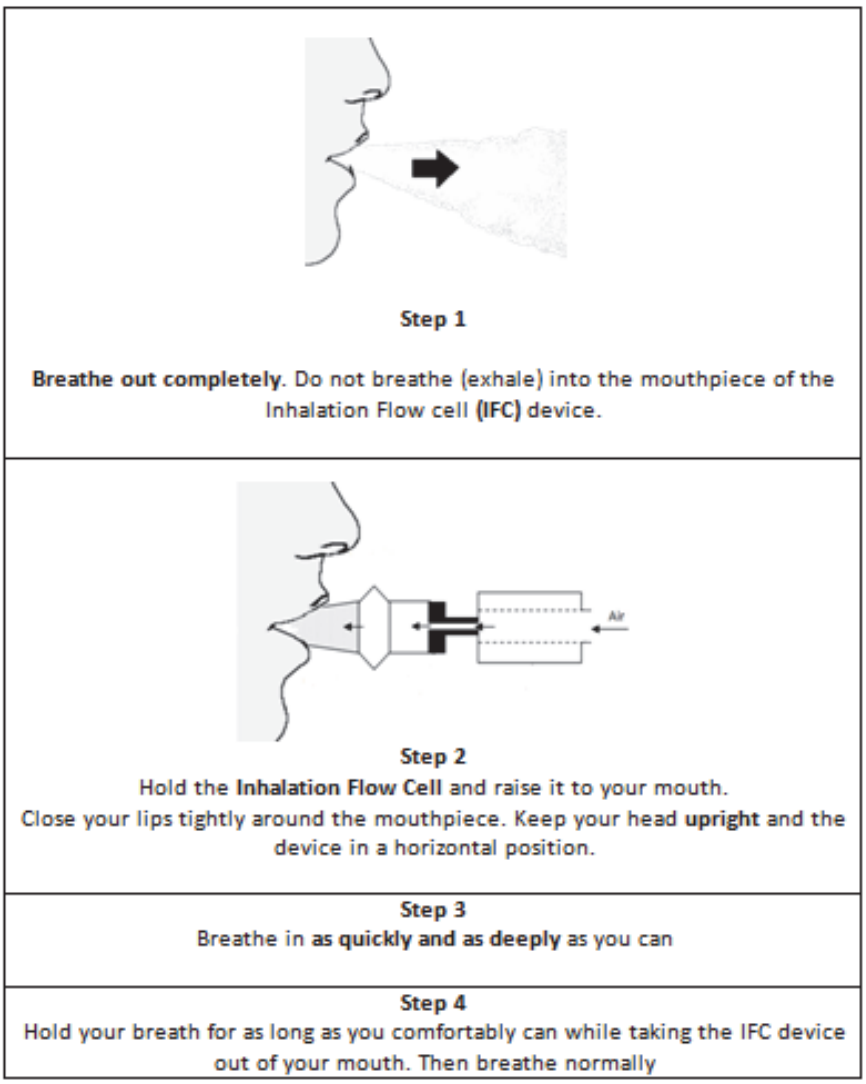

Figure 4.3. Written instructions for inhalation. **Instruction A** (Artwork adapted from patient information leaflets).

Data Analysis and Statistics

Overall, the trial produced a series of 20 IPs per air flow resistance (total = 120) for each of three instruction conditions: A, B1 and B2. These IPs were analyzed to determine their overall dependence on airflow resistance, R, and training status. In order

to do this, the parameters defined in Figure 4.4 were extracted from each IP and tabulated. The descriptive statistics: mean, median, standard deviation, minimum and maximum values, coefficient of variation [CV (%) = 100*standard deviation/mean] were estimated for each of the inhalation variables (PIFR, $T_{PIFR`}$, V and T; Figure 4.4) *by gender* and *across gender*. Further inferential statistics were estimated as follows: for each individual dataset (Instruction A, B1 or B2) for a given volunteer, the quantitative relationship between each inhalation variable and air flow resistance (R) was assessed by linear regression analysis. Four functions of R, [f(R)], were explored in this way: R, 1/R, LogR and $R^{0.5}$. Best f(R) was selected based on the best fit (e.g. the coefficient of determination, r^2, that was largest). To assess the effects of training on IP statistically (e.g. comparing instruction A, B1 or B2) it was necessary to pool the results for each training condition. Accordingly, secondary variables were derived that were resistance-independent: in cases where significant relationships existed between the inhalation variable and R (e.g. PIFR), the values of that variable were normalized by resistance and averaged across all resistances in order to obtain a secondary, resistance-independent, normalized, inhalation variable. In case of insignificant relationships between a variable and R, the inhalation variables were averaged across resistances, without normalization, again to obtain a secondary, resistance-independent, inhalation variable. The effect of formal training (Instruction B1 and B2) on these secondary inhalation variables was assessed using repeated-measures ANOVA. The level of significance was preset at 0.05. Normality of the residuals was judged by normal quantile plots and visual inspection of the distribution of residuals. JMP 8.0 (SAS Corp, RTP, NC) was used for all statistical analyses.

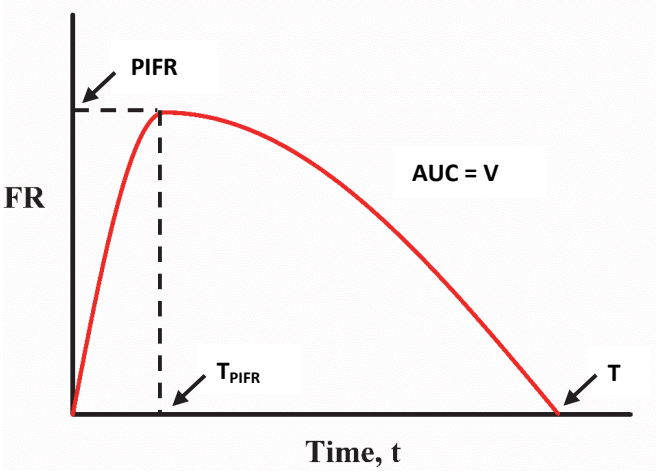

Figure 4.4. Idealized IP and the primary variables: PIFR = peak inspiratory flow rate; T_{PIFR}, the time at which PIFR occurs; AUC = Area Under the Curve = Inhaled Volume, V. Total inhalation time, T, is a secondary variable, dependent on PIFR and V.

4.3 RESULTS

Air flow resistances of the Inhalation Flow Cell (Figure 4.2) were 0.0462, 0.0432, 0.0344, 0.0241, 0.0200 and 0.0179 $kPa^{0.5}$ L^{-1} min. These were comparable with the values 0.0467, 0.0435, 0.0352, 0.0241, 0.0198 and 0.0176 $kPa^{0.5}$ L^{-1} min, determined from linear regression of pressure $drop^{0.5}$ vs. flow rate data for Spiriva® HandiHaler®, Salbutamol Easyhaler®, Pulmicort® Turbuhaler®, Budelin® Novolizer®, Relenza® Diskhaler® and Foradil® Aerolizer®, respectively. Twenty (10F, 10M) of an initial 22 volunteers, with the demographics and pulmonary function results shown in Table 4.1, completed the study. Each subject followed the instructions and inhaled through the six, randomly-presented, airflow resistances that are typical of those in marketed DPIs, using the apparatus shown in Figure 4.2. The resulting IPs are used in the discussion to provide data on the type and range of inspiratory maneuvers that need to be catered for by powder inhaler designers seeking to deliver aerosol drug clouds to the lungs of inhaler-naïve human adults with essentially normal pulmonary function, and where the subjects

selected for product development trials have either been given written instructions on how to inhale or received formal training in DPI use by a professional.

Table 4.1. Summary of subject demographics and pulmonary function tests (mean±SD).

	Males	Females	Overall
Total	10	10	20
Caucasian	6	3	9
African	1	3	4
Asian	1	2	3
Hispanic	0	1	1
Others	2	1	3
Age [yrs]	31.1 ± 10.31	34.0 ± 8.81	32.6±9.23
Height [cm]	176.6 ± 5.64	161.8 ± 6.49	169.2±9.40
Weight [kg]	81.7 ± 16.75	60.7 ± 7.29	71.2±16.16
PFT[a]			
FVC [L]	5.02 ± 0.60	3.31 ± 0.35	4.15±0.98
FEV1 [L]	4.23 ± 0.41	2.81 ± 0.32	3.51±0.80
FEV1/FVC	0.84 ± 0.04	0.85 ± 0.06	0.85±0.05
FEF 25-75% [L/s]	4.72 ± 0.70	3.29 ± 0.87	3.99±1.03
PEF [L/s]	10.08 ± 1.28	7.12 ± 0.77	9.15±1.92
FET [s]	6.46 ± 1.01	6.91 ± 3.77	6.69±2.63

[a]Pulmonary function tests

Dependence of inhalation variables on air flow resistance and training

A complete and detailed description of the analyses performed on the inhalation variables collected clinically is available in Delvadia (2012); the thesis included analyses of residual distributions, normal quantile plots, statistical evaluation of gender effects,

assessment of interactions between training status, gender and data from pulmonary function tests and a complete compilation of all numerical data on which the analyses in this paper are based. While those results enable us to present IP data, conclusions and equations for IP simulation at each resistance and training condition, the material is too lengthy to present in its entirety. Therefore, essential material in Delvadia (2012) is presented to justify our recommendations to test dry powder inhalers *in vitro*, using the apparatus shown in Figure 4.1, with a range of differently simulated IPs that describe the pooled data including confidence limits at each resistance and training condition.

The experimental values for PIFR, T_{PIFR} and V (Figure 4.4) were assessed for functional dependence on airflow resistance, R. The results showed that 1/R gave the best fit for PIFR from the four functions tested, while T_{PIFR} and V showed no detectable dependence on resistance. Accordingly, the statistics describing the mean, median, standard deviation, minimum and maximum values and coefficient of variation [CV (%) = 100*standard deviation/mean] for each “resistance-normalized” variable (Figure 4.4; R*PIFR, T_{PIFR} and V) are presented in Table 4.2 *by gender*, *across gender* and *by training status* to show the effects of gender and training.

Table 4.2. Descriptive result summary of the IP data for "resistance-normalized", R*PIFR ($kPa^{0.5}$), mean volume, V (L), and mean T_{PIFR} (sec), by training status and gender.

	Female			Male			Overall		
	Instr. A Mean (R*PIFR)	Instr. B1 Mean (R*PIFR)	Instr. B2 Mean (R*PIFR)	Instr. A Mean (R*PIFR)	Instr. B1 Mean (R*PIFR)	Instr. B2 Mean (R*PIFR)	Instr. A Mean (R*PIFR)	Instr. B1 Mean (R*PIFR)	Instr. B2 Mean (R*PIFR)
Mean	1.895	2.402	2.381	2.619	3.029	2.920	2.257	2.715	2.650
SD	0.432	0.287	0.316	0.589	0.259	0.235	0.625	0.417	0.387
Min	0.893	2.012	1.900	1.291	2.529	2.510	0.893	2.012	1.900
Max	2.507	3.009	3.033	3.391	3.376	3.287	3.391	3.376	3.287
CV	22.8	11.9	13.3	22.5	8.5	8.1	27.7	15.4	14.6
Median	1.879	2.375	2.372	2.654	3.053	2.920	2.244	2.661	2.583
	Mean V (L)	Mean V (L)	Mean V (L)	Mean V (L)	Mean V (L)	Mean V (L)	Mean V (L)	Mean V (L)	Mean V (L)
Mean	1.562	2.025	2.100	3.009	3.781	3.793	2.285	2.903	2.947
SD	0.532	0.410	0.370	0.925	0.758	0.814	1.044	1.078	1.064
Min	1.065	1.393	1.486	2.366	2.982	2.713	1.065	1.393	1.486
Max	2.484	2.687	2.679	5.349	5.595	5.488	5.349	5.595	5.488
CV	34.0	20.2	17.6	30.7	20.0	21.5	45.7	37.2	36.1
Median	1.384	2.031	2.167	2.620	3.688	3.799	2.384	2.834	2.696
	Mean T_{PIFR} (sec)	Mean T_{PIFR} (sec)	Mean T_{PIFR} (sec)	Mean T_{PIFR} (sec)	Mean T_{PIFR} (sec)	Mean T_{PIFR} (sec)	Mean T_{PIFR} (sec)	Mean T_{PIFR} (sec)	Mean T_{PIFR} (sec)
Mean	0.803	0.497	0.529	0.914	0.614	0.582	0.858	0.555	0.555
SD	0.447	0.153	0.210	0.456	0.192	0.275	0.443	0.179	0.240
Min	0.453	0.222	0.255	0.540	0.225	0.250	0.453	0.222	0.250
Max	1.893	0.734	0.978	1.944	0.872	1.179	1.944	0.872	1.179
CV	55.7	30.8	39.6	49.9	31.3	47.3	51.7	32.3	43.2
Median	0.667	0.473	0.491	0.744	0.619	0.520	0.683	0.550	0.495

While the move from Instruction A to Instruction B1 or B2 showed the importance of formal training, the data from the duplicate IPs designated “Instruction B1” or “Instruction B2” showed no statistical difference between the pooled first or second measurement sets. Accordingly, data from B1 and B2 were pooled for further analysis and designated “Instruction B”.

Gray profiles in Figures 4.5 and 4.6 show the IP results from all subjects (M and F) following Instructions A and B, respectively. The profiles shown in red at each resistance and training condition, are taken from the gray profiles after processing to show the 10, 50 and 90 percentile flow rate for the population at each 50 msec sampling time.

The functional dependence of the 10, 50 (median) and 90 percentile PIFR values (Figures 4.5 and 4.6) on reciprocal resistance is plotted in Figure 4.7 for this population. Figure 4.7 is valid for values of R in the range 0.018 – 0.046 $kPa^{0.5}$ L^{-1} min although beyond this range, curvature of PIFR vs. 1/R is expected (in order to meet a zero intercept as R tends to infinity). There was no need to explore curvature at impractically large resistance values however, as the selected linear functions were clearly appropriate for resistances that are encountered practically.

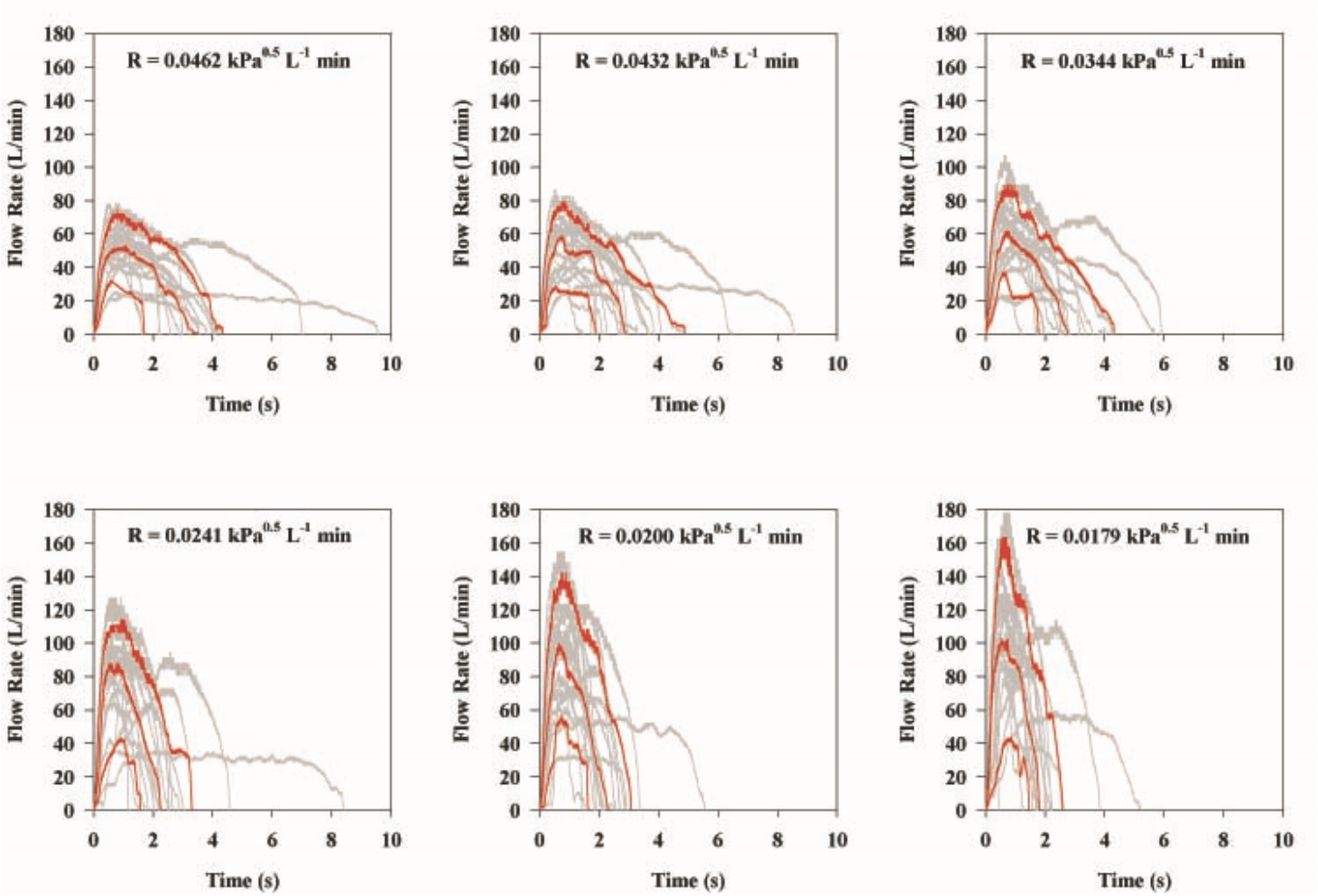

Figure 4.5. Individual flow profiles (gray) or volumetric flow rates exiting the mouthpiece of IFC vs. time from 20 volunteers (10M, 10F; 20 gray profiles per panel) after reading written instruction A (Figure 4.3). IFC airflow resistance, R, is shown in each panel. Red profiles show the 10, 50 and 90 percentile IP in each case.

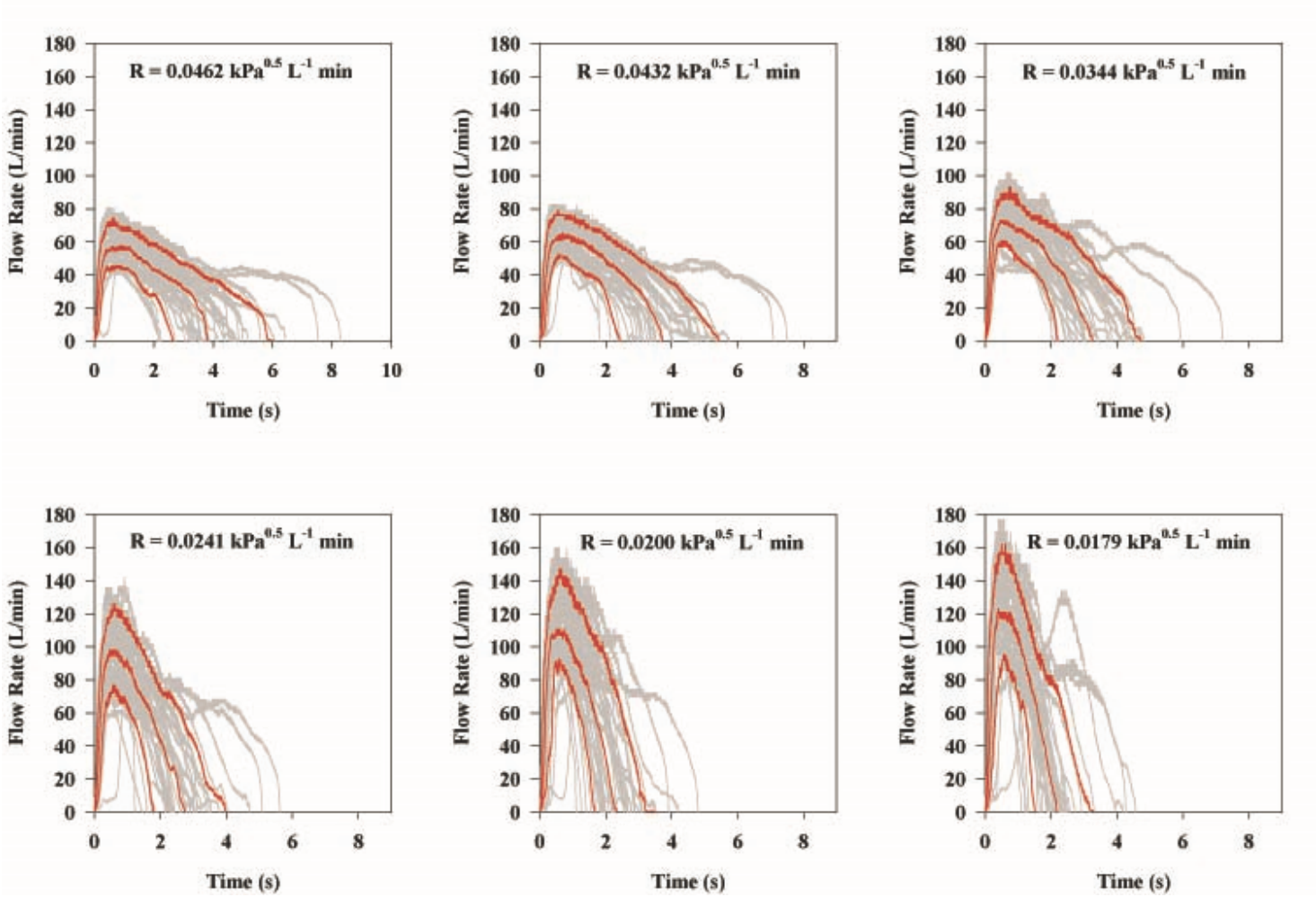

Figure 4.6. Individual flow profiles (gray) or volumetric flow rates exiting the mouthpiece of IFC vs. time from 20 volunteers (10M, 10F) after Instruction B (40 gray profiles, from B1 and B2, per panel). IFC airflow resistance, R is shown in each panel. Red profiles show the 10, 50 and 90 percentile IP in each case.

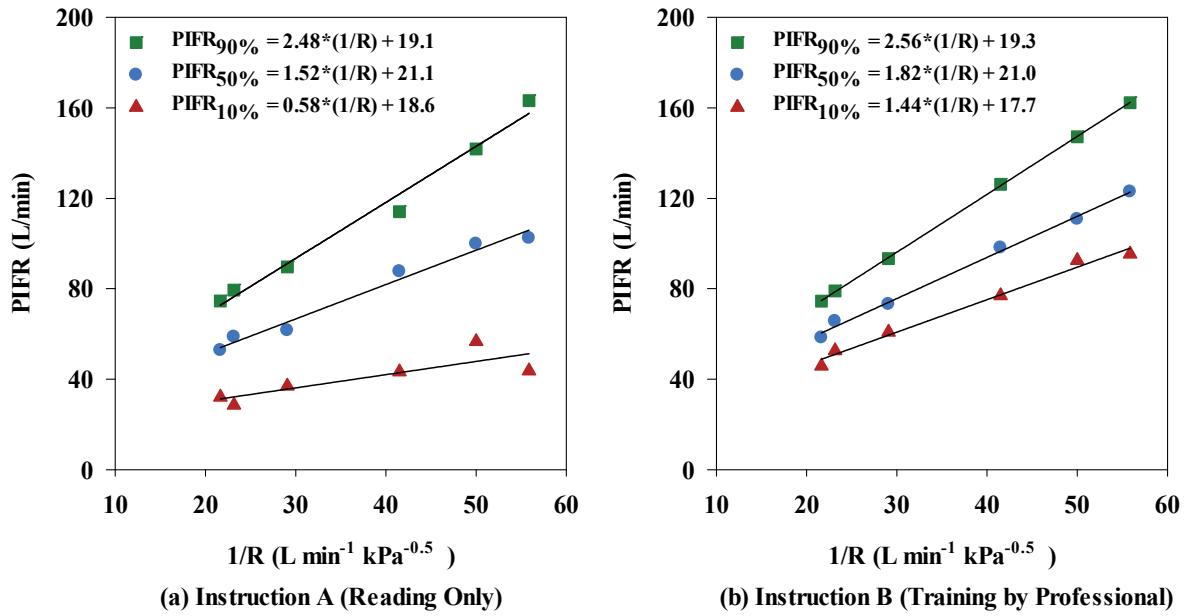

Figure 4.7. PIFR vs. I/R from pooled data collected after (a) Instruction A (reading only) and (b) Instruction B (training by professional; r^2>0.995). 10, 50 and 90 percentile values can be predicted based on a pre-selected value for R in the range of 0.018–0.046 $kPa^{0.5}.L^{-1}$ min.

Inhalation profiles were less erratic after subjects received professional training (Instruction B) and values for PIFR appeared to increase. Equations 4.1–4.3 and Figure 4.7a describe the 90, 50 and 10 percentile values for PIFR in this population due to Instruction A; Equations 4.4–4.6 and Figure 4.7b apply to Instruction B.

Instruction A:

$$PIFR_{90\%} = 2.48\ (1/R) + 19.1 \qquad \text{Equation 4.1}$$

$$PIFR_{50\%} = 1.52\ (1/R) + 21.1 \qquad \text{Equation 4.2}$$

$$PIFR_{10\%} = 0.58\ (1/R) + 18.6 \qquad \text{Equation 4.3}$$

Instruction B:

$$PIFR_{90\%} = 2.56\ (1/R) + 19.3 \qquad \text{Equation 4.4}$$

$$PIFR_{50\%} = 1.82\ (1/R) + 21.0 \qquad \text{Equation 4.5}$$

$$PIFR_{10\%} = 1.44\ (1/R) + 17.7 \qquad \text{Equation 4.6}$$

Where R < 0.046 > 0.018 $kPa^{0.5}.L^{-1}$ min and PIFR and R have units of L min^{-1} and $kPa^{0.5}.L^{-1}$ min, respectively. Overall (Table 4.2), males had higher mean PIFR compared to females and volunteers inhaled at larger flow rates with lower inter-subject variability when formally trained (Instruction B; there was no significant difference between normalized PIFR values for Instruction B1 and B2). Residuals from plots of PIFR vs. 1/R were randomly distributed and the observed positive linear relationship between PIFR and 1/R was consistent with the physiological literature where the slope of the regression line of PIFR vs. 1/R has been reported to give the square root of the "maximum" pressure drop across an inhaler for a given volunteer; this pressure drop reportedly stays approximately constant across the air flow resistances seen in marketed DPIs (Smutney et al., 2009).

Values for inhaled volume, V, and the time to the peak inspiratory flow rate, $T_{PIFR,}$ (Table 4.2) were resistance-independent. As expected however, V was clearly influenced by gender. Consistent with their larger total lung capacity (Hankinson et al., 1999) males had a mean value for V = 3.009 L after Instruction A. This was 1.45 L more than females (mean V = 1.562 L). After Instruction B, these values increased to 3.787 and 2.063 L, respectively. Formal training (Instruction B), caused a statistically significant improvement in V across gender (n = 20); mean V overall was 0.64 L greater than that seen after

Instruction A ($p < 0.0001$). There was no apparent effect of gender on T_{PIFR} but training once again was influential. A significant reduction of 0.3 seconds in mean T_{PIFR} was observed after formal training ($p < 0.0001$).

4.4 DISCUSSION

This study describes the data resulting from a clinical study of the breath profiles produced by differently trained, inhaler-naïve, normal human adults inhaling through variable resistances typical of those seen in marketed DPIs (Delvadia et al., 2013a; Delvadia et al., 2012). Because the leaflets supplied with different powder inhalers use different phrases to describe the actual inhalation maneuver, we adopted a standardized phrase for Step 3 of our written Instruction A: “breathe in as quickly and as deeply as you can” (Figure 4.3). Our choice of phrase may have influenced the profiles shown in Figure 4.5 given that the respective phrases in leaflets for Aerolizer®, Diskhaler®, Novolizer®, Turbuhaler®, Easyhaler® and HandiHaler® were: “breathe in quickly and deeply”, “breathe in through your mouth steadily and as deeply as you can” “inhale the powder with a deep breath”, “breathe in as deeply and as hard as you can”, “take a strong and deep breath” and “breathe in deeply until your lungs are full”. Nevertheless, volunteers inhaled faster and deeper when they were trained using written instructions in combination with formal training from a pharmacist skilled in the use of inhalers, compared to the use of written instructions alone. The study showed that formal training helped to reduce inter-subject variability in inhalation flow rate vs. time profiles; an observation that may translate into reduced variability in aerosol drug deposition in the lung. IP analysis showed that decreased air flow resistance produced increases in PIFR

while V was unchanged. The results also showed that males inhaled faster and more deeply than females although no significant relationships were observed between the spirometric results (Table 4.1) of volunteers and their observed inhalation variables (Figure 4.4). Because the scope of the present study was limited to 20 healthy volunteers, most of whom were in their prime, the reported IPs probably do not reflect those for subjects with significant reductions in lung capacity. While the time of PIFR, T_{PIFR}, and the total inhaled volume V were unrelated to R in this study, the findings may not hold in all subjects. Sarinas et al. (1998), for example, showed that in CF, COPD and asthma, V fell as resistance was increased. Gender and age, that influence mouth inspiratory pressure, MIP, have also been shown to influence inspiratory flow (Baba et al., 2011; Broeders et al., 2004; Malmberg et al., 2010). In spite of this limitation, the analysis below shows a general way of selecting standard IPs for use in realistic *in vitro* tests of inhalers during development. Indeed, because many drug and device development efforts, including aerosol deposition studies used for bridging purposes, begin with normal volunteers or largely asymptomatic patients, the present study was designed to ensure that the equations and general procedures for IP simulation that were developed could span the likely range of “normal” IPs needed to program a breath simulator for use with a realistic *in vitro* test method (Figure 4.1). In addition we sought to offer IP ranges for volunteers who were representative of patients who had to teach themselves how to inhale after reading an instruction leaflet.

Simulating Inhalation Profiles for DPIs with Different Airflow Resistances

Even though it is possible to program breath simulators with IPs that are almost identical to the individual breath profiles of volunteers, or the 10, 50 and 90 percentile IPs shown in red in Figures 4.5 and 4.6, and this is practiced by some scientists (Olsson et al., 2013), profiles that are statistically representative of groups of subjects, that can be selected *a priori*, seem preferable for testing and development purposes.

To program a breath simulator to mimic IPs that were representative of those shown in Figures 4.5 and 4.6, we sought suitable equations and functions able to adequately describe the red profiles representing the 10, 50 and 90 percentile flow rate vs. time curves shown in each panel. Ideally, parameters in the resulting equations should have physiologic meanings that relate to the variables shown in Figure 4.4. While we and others have described and used alternate methods previously,(Delvadia et al., 2013a; Delvadia et al., 2012; Delvadia et al., 2013b; Longest et al., 2012a; Longest et al., 2012b) we sought a simplified approach for use in future research with DPIs, in which it was only necessary to select the inhaler resistance, R, in order then to be able to define ranges of PIFR, T_{PIFR} and V; whence to generate a fan of appropriate IPs with which to test a new DPI. Because the approach and algorithm is simple, we hope that the method proposed here can be generalized to include realistic tests that extend to treatment of different patient groups with differently designed inhalers and use instructions.

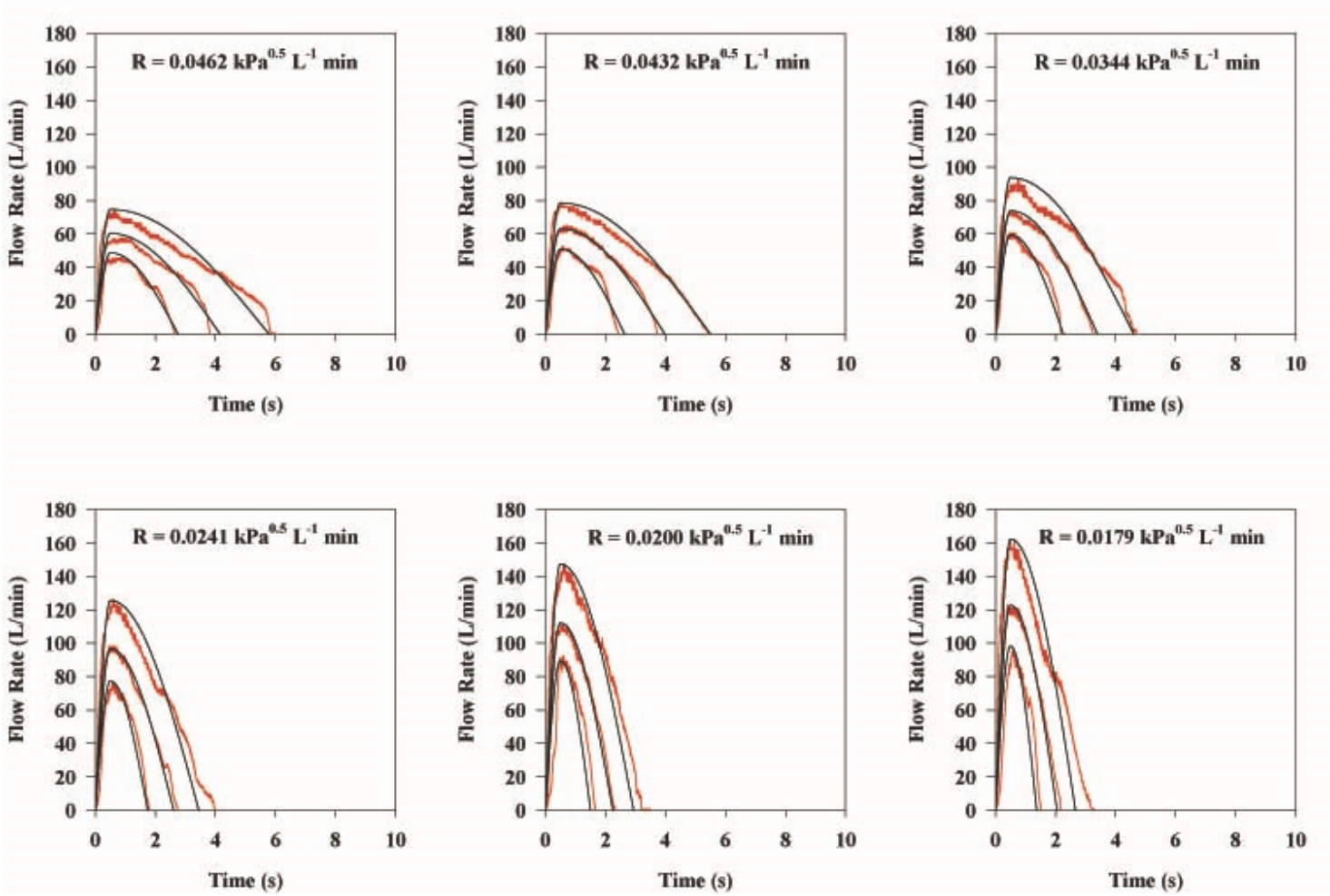

Figure 4.8. Simulated inhalation profiles (black curves) generated using Equations 4.7–4.10 for resistances shown in each panel and the algorithm described in the text. PIFR was calculated from Equations 4.4–4.6 (Instruction B); $T_{PIFR} = T_{PIFR50\%}$ = 0.49s for all black curves while values for $V_{10\%}$, $V_{50\%}$ and $V_{90\%}$ were 1.4, 2.7 and 4.6 L. Red curves shown for comparison are the 10, 50 and 90 percentile IPs from Figure 4.6.

The black curves in Figure 4.8 are the simulated flow rate vs. time profiles that resulted from the following routine. They are clearly good descriptions of the real profiles (reproduced from Figure 4.6) that represent the 10, 50 and 90 percentile IPs (Instruction B). The same approach can be used to generate curves that follow the red profiles in Figure 4.5 (Instruction A; not shown), while intermediate curves, for testing inhalers with different resistances can also be generated. Each panel of IPs (black curves; Figure 4.8) was generated as follows from Equations 4.7–4.10:

$$FR(t) = PIFR \times \sin\left(\frac{\pi}{2}\frac{t}{T_{PIFR}}\right) \qquad 0 \le t < T_{PIFR} \qquad \text{Equation 4.7}$$

$$FR(t) = PIFR \times \cos\left(\frac{\pi}{2}\frac{(t - T_{PIFR})}{(T - T_{PIFR})}\right) \qquad T_{PIFR} \le t \le T \qquad \text{Equation 4.8}$$

Because AUC = V (Figure 4.4) is given by integrating and adding Equations 4.7 and 4.8,

$$V[L] = \frac{PIFR[L \cdot \min^{-1}] \times T[s]}{30\pi} \qquad \text{Equation 4.9}$$

Therefore,

$$T[s] = \frac{30\pi \times V[L]}{PIFR[L \cdot \min^{-1}]} \qquad \text{Equation 4.10}$$

First, $PIFR_{90\%}$, $PIFR_{50\%}$, $PIFR_{10\%}$ was calculated based on the DPI resistance, R (quoted in panel of Figure 4.8) using Equations 4.4, 4.5, 4.6, respectively, assuming that we were concerned with well-trained normal subjects. Second, a median value for $T_{PIFR50\%}$ = 0.49 sec was selected and held constant; if required however, alternate values for $T_{PIFR50\%}$ may be employed to produce different values for airflow acceleration (see distribution and legend in Figure 4.9). Notably, T_{PIFR} was independent of R and log-

normally distributed across the 240 IPs from this population. In spite of that observation, because the rising slope d(FR)/dt falls with decreasing PIFR (Figure 4.6) and PIFR decreases with increasing R (Figure 4.7), de Boer et al.'s reported relationship between the "flow increase rate (FIR)" and device resistance (de Boer et al., 1997) still holds.

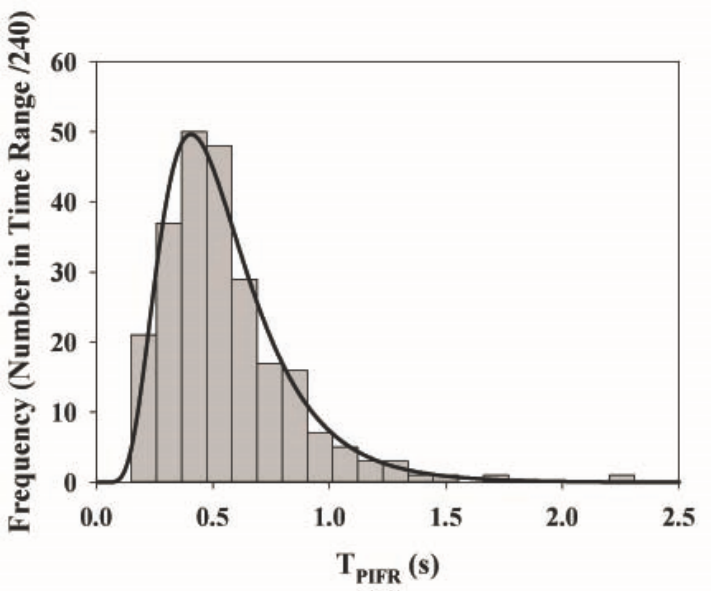

Figure 4.9. Distribution of values for T_{PIFR} (seconds) across genders after Instruction B. The 10, 50 and 90 percentile values were 0.28, 0.49 and 0.88 seconds, respectively. Instruction A yielded a similar distribution with 10, 50 and 90 percentile values of 0.43, 0.66 and 1.68 seconds, respectively. Selection of the values for T_{PIFR} and PIFR permits the study of device behavior at different flow accelerations according to Equation 4.7.

Third, $V_{90\%}$, $V_{50\%}$ and $V_{10\%}$ values were assigned (4.6, 2.7 and 1.4 L, respectively), based on "across gender" data for V (Table 4.2; because values for V in males and females differ significantly, IPs simulated for single gender studies should be adjusted). Fourth, values were calculated for the inhalation time $T_{90\%}$, $T_{50\%}$ and $T_{10\%}$ from Equation 4.10. Coupling the calculated and assigned values for PIFR, T_{PIFR}, V and T at their chosen percentiles, enables the calculation of flow rates leaving the mouthpiece at each value of time, t, from Equations 4.7 ($t<T_{PIFR}$) and 4.8 ($t\geq T_{PIFR}$). These simulated profiles were plotted as the large, medium and small profiles shown in black on Figure 4.8. In practice,

breath simulators, such as the ASL 5000-XL can be programmed directly using these sine wave equations, or data may be supplied directly in the form of a spreadsheet of simulated flow rates over time. An example of the use of these IPs to test a DPI with known resistance was described previously (Byron et al., 2014).

4.5 CONCLUSION

A general method of selecting and simulating a range of inhaled flow rate vs. time profiles for use in the realistic testing of powder inhalers has been described. Equations and an algorithm are presented that enable simulation of the range of inhalation flow rate vs. time curves used by normal human adult volunteers of both genders both before and after formal training in the use of powder inhalers. The approach enables the product designer to select breath profiles with which to study aerosol device performance across the likely inter-subject variability seen with DPIs of different resistances following either leaflet training alone, or formal training from a professional in addition to leaflet training.

CHAPTER 5

DETERMINING AERODYNAMIC PARTICLE SIZE DISTRIBUTIONS OF IN VITRO LUNG DOSES FOR BUDELIN® NOVOLIZER® UNDER REALISTIC INHALATION CONDITIONS

5.1 INTRODUCTION

Coupling realistic mouth-throat (MT) models with simulated, but representative human inhalation profiles (IP) that mimic inhaler use in the clinic (as described in Chapter 4) has been found to be promising when building *in vitro–in vivo* correlations (IVIVCs) for orally inhaled drug products. Studies of several inhalers have shown that the *in vitro* measured lung doses (designated as the drug doses exiting the MT models) appear to predict the mean and extreme values for the *in vivo* total lung deposition data obtained from gamma scintigraphic or pharmacokinetic (PK) methods (Delvadia et al., 2013a; Delvadia et al., 2012; Olsson et al., 2013; Weers et al., 2014; Zhang et al., 2007). While total lung dose (TLD) is important in evaluating inhaler *in vivo* performance, regional drug deposition in the lung may also be a determinant of the therapeutic effects of inhaled drugs, especially for compounds intended for topical activity like budesonide (Anderson & Newman, 2009; Usmani & Barnes, 2012; Usmani et al., 2005).

As particle size is one of the major factors affecting aerosol drug deposition, and it is known to be influenced significantly by the airflow through Novolizer (de Boer et al., 2004), evaluating size distribution of drug aerosols able to enter the lung, following deaggregation and dispersion under realistic inhalation conditions, is an essential part of realistic *in vitro* testing. We may expect that the drug deposition patterns in gamma scintigraphy studies, usually reported as P/C ratios [designated as radioactive counts in the peripheral (P) to central (C) lung ratio] are some function of the aerodynamic particle size distribution (APSD) of the TLD. A summary of the mean values and variations for P/C ratio obtained from gamma scintigraphy studies in the literature for different DPIs is provided in Appendix I. While variations in regional deposition may be caused by combined effects of variations in APSDs, inhalation flow rates, and airway geometries, if we are to fully evaluate the variations in regional drug distribution in the lung using modeling approaches like computational fluid dynamic (CFD) simulations (Longest & Holbrook, 2012), it is necessary to evaluate the possible ranges of APSDs of drugs exiting the MT models during realistic testing.

The challenge of coupling realistic IP conditions for aerosol generation with the constant flow demand of cascade impactor testing can be overcome by using devices like the Electronic Lung™ (Burnell et al., 1998b) or the Nephele Mixing Inlet (N. C. Miller, 1997; N. C. Miller et al., 2000). The Electronic Lung™ was developed by GlaxoSmithKline scientists who created powder aerosols using different IPs in a large chamber; aerosols were subsequently drawn into a calibrated cascade impactor at a fixed flow rate (Brindley et al., 1994; Burnell et al., 1998a; Burnell et al., 1998b). The method, that generates an apparent APSDs of the sampled drug cloud, suffers from a significant problem because

of settling and drug losses in the sample chamber (Burnell et al., 1998b). The use of the Nephele Mixing Inlet to provide variable aerosol dilution over time in a “flow balancing” set up (described in Figure 5.3 later in this chapter) can overcome this difficulty under certain circumstances. Several examples of using this approach to measure particle size distributions exiting MT models have been reported (Below et al., 2013; Casaro et al., 2014; Chrystyn et al., 2015; Olsson et al., 2013). Because the method is obliged to use additional makeup air to create the constant air flow required by the cascade impactor, the highest flow rate possible for a test IP, i.e. peak inhalation flow rate (PIFR), is presently limited by the upper flow limit of the calibration range of the chosen cascade impactor. The most accepted cascade impactor for pharmaceutical studies of inhalers with a high flow rate calibration is the Next Generation Pharmaceutical Impactor [NGI; Apparatus 5, USP (U.S. Pharmacopeial Convention, 2013)]. The NGI is calibrated for use at air flow rates between 15 and 100 L/min, so that presently, the maximum usable PIFR in the set up used in the literature is 100 L/min (Below et al., 2013; Casaro et al., 2014; Chrystyn et al., 2015; Olsson et al., 2013). This is a big limitation of the method given that Chapter 4 and other studies have reported that both healthy subjects and patients may generate PIFRs much greater than 100 L/min through DPIs, especially when the inhalers in use are low resistance devices (Azouz et al., 2015a; Azouz et al., 2015b; Virchow et al., 2014).

The present study sought to develop and evaluate methods for measuring APSDs of drug aerosols from Budelin® Novolizer® 200 mcg (Meda Pharmaceuticals, Hertfordshire, U.K.) exiting the Virginia Commonwealth University (VCU) MT models under a range of realistic IPs. While Budelin was chosen for this study in part because its regional distribution in the lung has been reported in the literature (Newman et al., 2000),

the method sought to extend the range of testable IPs to allow the assessment of APSDs of $TLD_{in\ vitro}$ from Budelin at flow rates over 100 L/min. The chapter describes methods of extending the test limit of NGI to allow the APSDs of the *in vitro* lung doses to be determined across a range of realistic IPs. A recalibration of NGI using polydisperse budesonide aerosols is also described. The details of Budelin Novolizer 200 mcg regional distribution are summarized from the literature (Newman et al., 2000) in Appendix I.

5.2 MATERIALS AND METHODS

Mouth-Throat Models

Small, medium and large Virginia Commonwealth University (VCU) MT models [(Longest, 2012); noted as VCU-MT_S, VCU-MT_M, VCU-MT_L in the following text], previously designed and validated to describe the geometric variations seen in adult humans (Delvadia et al., 2012), were externally modified to improve connectivity to the NGI and Nephele Mixing Inlet (NMI) (N. C. Miller, 1997; N. C. Miller et al., 2000) (Figure 5.1). Internal dimensions of these models were not changed. The three-dimensional (3D) geometry of the MT models were altered in Autodesk® Inventor® 2014 (Autodesk, Inc., San Rafael, CA), and a quick-fit adapter to NGI was added to the trachea of each model to ensure an airtight connection between MT, NGI and NMI. The tapered “quick-fit” female dimensions atop the NGI inlet and NMI inlet are identical. The NMI outlet also has a tapered male connection designed to mate with the NGI inlet. Dimensions of the modified MT geometry can be found in Appendix II. Physical models were constructed in ultraviolet-laser-cured resin (Accura® 60, 3D System, Valencia, CA) using a rapid

prototyping process of stereolithography (Viper si2™ SLA® system, 3D Systems, Valencia, CA), with vertical layer thickness of 0.1 mm.

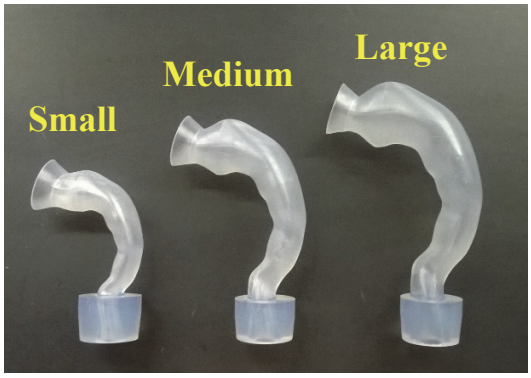

Figure 5.1. Small, medium and large Virginia Commonwealth University (VCU) mouth-throat (MT) models [(Longest, 2012); noted as VCU-MT_S, VCU-MT_M, VCU-MT_L in the following text] with quick-fit adapters to fit the Next Generation Impactor (NGI) and Nephele Mixing Inlet (NMI). Dimensions of the modified MT geometries are described in Appendix II.

Inhalation Profiles

IPs were simulated using the sinusoidal waveforms described in Chapter 4 (Equations 4.7–4.10) to represent the *fast*, *moderate* and *slow* inhalation used by subjects in a lung scintigraphy study of Budelin Novolizer 200 mcg (Newman et al., 2000). Variations in subjects' inhalation maneuvers were estimated by adding and subtracting two standard deviations (SD) from the mean values for peak inhalation flow rate (PIFR) and inhaled volume (V) (Newman et al., 2000) to represent the 95% conference intervals around each of the reported means. These values were paired (Table 5.1) to generate the small, medium and large volume IPs for each inhalation condition (Figure 5.2).

Table 5.1. Mean and likely confidence intervals for peak inhalation flow rate (PIFR) and inhaled volume (V) at each of the reported inhalation conditions (Newman et al., 2000).

Inhalation Condition		Inhalation Profile	
		PIFR[a] (L/min)	V[a] (L)
Fast	Small	73 (Mean–2SD)	1.11 (Mean–2SD)
	Medium	99 (Mean)	3.13 (Mean)
	Large	125 (Mean+2SD)	5.15 (Mean+2SD)
Moderate	Small	59 (Mean–2SD)	1.30 (Mean–2SD)
	Medium	65 (Mean)	2.96 (Mean)
	Large	71 (Mean+2SD)	4.62 (Mean+2SD)
Slow	Small	40 (Mean–2SD)	0.83 (Mean–2SD)
	Medium	54 (Mean)	2.77 (Mean)
	Large	68 (Mean+2SD)	4.71 (Mean+2SD)

[a]Mean values for PIFR and V for each inhalation condition were as reported (Newman et al., 2000), whereas the ranges (large and small values) were estimated by adding and subtracting two standard deviations [SD; also reported by Newman et al. (2000)] from the mean.

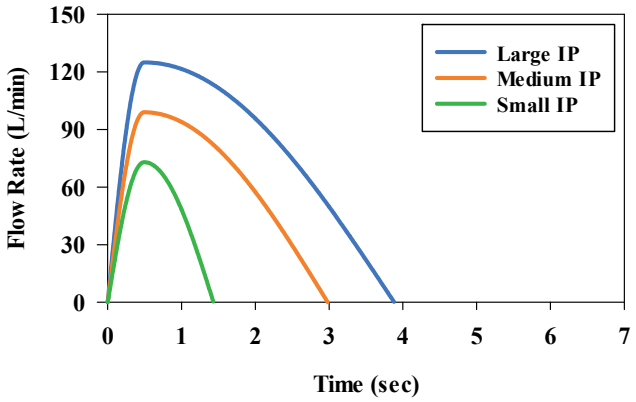

(a) *Fast* Inhalation

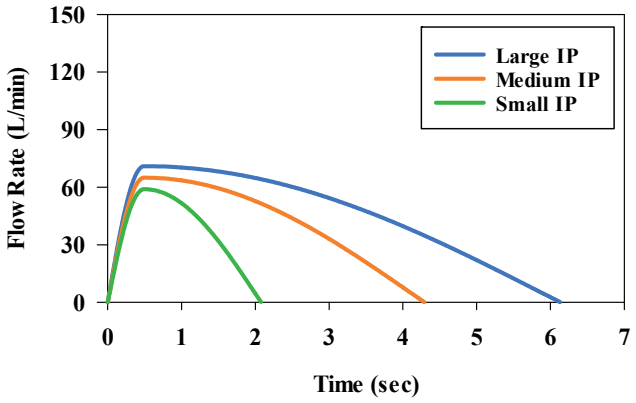

(b) *Moderate* Inhalation

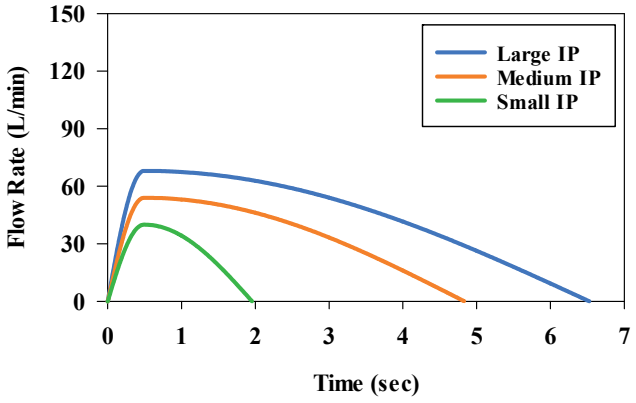

(c) *Slow* Inhalation

Figure 5.2. The small, medium and large simulated test IPs used to represent the median and extremes (95% confidence intervals; see IP definition page xix) for the (a) *fast*, (b) *moderate* and (c) *slow* inhalations described in the clinical study (Newman et al., 2000).

Mixing Inlet–Cascade Impactor System

Apparatus

The NMI (Model III for NGI; RDD Online, Richmond, VA) is a precisely engineered and patented tool for mixing high density, non-homogeneous aerosol clouds, like those from inhalers, with variable volumes of dilution air. It contains a central tube for receiving the aerosol clouds and an outer inlet for receiving and introducing dilution air; the design enables a sheath air flow to be created around the aerosol flow to minimize wall losses due to impaction. Losses within the NMI have been reported to be <2% (N. C. Miller, 1997; N. C. Miller et al., 2000). The NGI (MSP Corporation, Shoreview, MN) was modified by replacing the jets and orifice plates with those from the Westech W7 Cascade Impactor (Westech Scientific Inc., Marietta, GA), a precisely-engineered copy of the original NGI and purchased with detailed mensuration data and certification. The use of the W7 jet plate enables the removal of individual jets and the Micro-Orifice Collector (MOC) when these are found to create sonic (or critical) flow conditions in the instrument (i.e. situations where the air flow rate through the impactor cannot be increased given further increase of vacuum power). Notably, the unmodified NGI does not enable jet removal and high flow rate testing. To extend the flow limits of NGI and allow its operation outside the specific flow range for which it is calibrated [15–100 L/min; (Marple et al., 2003a; Marple et al., 2004; U.S. Pharmacopeial Convention, 2013)], MOC was replaced with a high flow internal filter holder containing an 81 mm diameter disposable type A/E glass fiber filter (Pall Corporation, Port Washington, NY) capable of complete aerosol capture. The programmable breath simulator ASL 5000-XL (a larger-volume version of the commercial model ASL 5000, redesigned for VCU by IngMar Medical, Pittsburgh, PA), was used in

this study to simulate the complete range of realistic IPs for Budelin Novolizer (Figure 5.2). Two vacuum pumps were used to generate constant air flow through NGI: a lower capacity ERWEKA vacuum pump VP 1000 (ERWEKA International, Annandale, NJ) for air flow rates ≤100 L/min, and a higher capacity 3-phase DOERR vacuum pump LR22132 (Emerson Electric, St Louis, MO) for air flow rates >100 L/min.

Experimental Setup and General Procedure

The setup for characterizing the APSDs of drug exiting MT models, following deaggregation and dispersion under realistic inhalation conditions, is illustrated in Figure 5.3. The NMI was placed atop the NGI-W7 impactor (noted as “NGI” in the following text), with its upper inlet connected to the MT model for receiving aerosol clouds from Budelin Novolizer, and side inlet connected to a compressed air source (with a pressure regulator and a flow control valve) for receiving dilution air. The vacuum pump was connected to the outlet of NGI, and depending on the PIFR of the test IP, either the lower capacity or higher capacity pump was selected to draw air through NGI at the designated flow rate (Table 5.2). The breath simulator was interposed between the NMI and compressed air source using a T-junction. While not strictly necessary, Parafilm® M (Bemis, Oshkosh, WI) over-wraps were used throughout to ensure airtight connections between apparatus components.

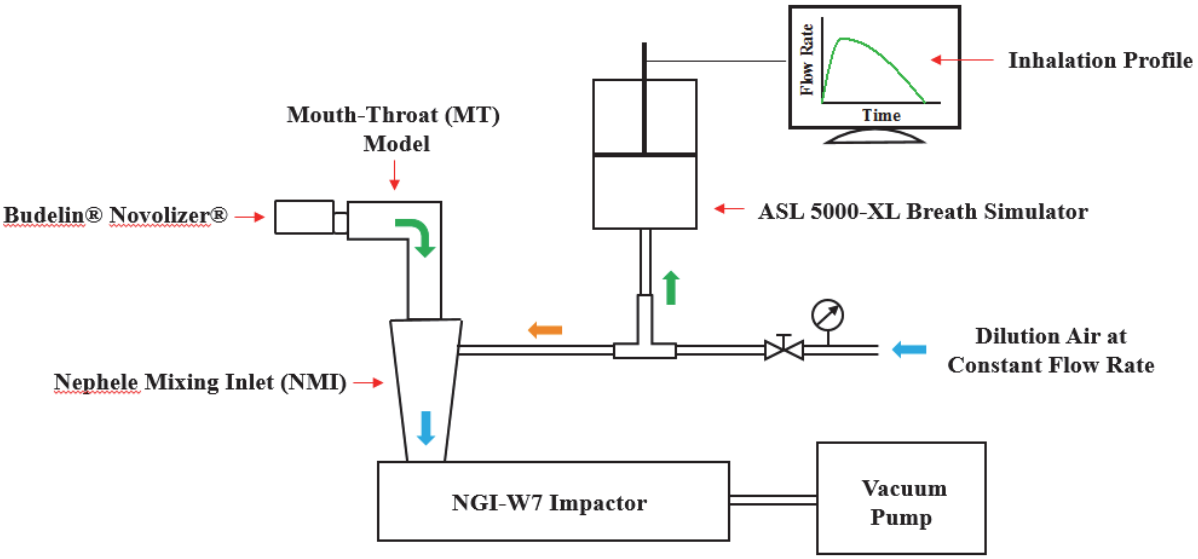

Figure 5.3. Experimental setup and apparatus used to measure aerodynamic particle size distributions of drugs exiting the MT model under realistic inhalation conditions for Budelin® Novolizer®. Equipment details are described in the text.

Prior to each experiment, internal surfaces of the MT models and NGI plates were coated twice with Molykote® 316 silicone release spray (Dow Corning, Midland, MI) using procedures described by Hindle et al. to avoid particle re-entrainment after impaction (Hindle et al., 1996). After each spraying, excess coating solution was retained inside the MT model, and the model shaken regularly to ensure uniform internal surface coverage. The complete coating procedure took 30 minutes per coating, after which all solvents had evaporated. The apparatus was assembled as shown in Figure 5.3 except that prior to each test, a low-resistant digital flow meter SFM 3000 (Sensirion Inc., Westlake Village, CA) was connected at the mouth opening of MT, in place of the inhaler, to monitor the air flow rate entering MT with time. The vacuum pump was switched on to draw air through the MT into the NGI and air flow was adjusted until it reached the designated flow rate for the NGI in the chosen experiment (either 100 or 140 L/min in this study). The vacuum

flow was then held constant, and compressed air introduced as dilution air to the side port of NMI. This dilution air flow was adjusted until it balanced the vacuum flow through NGI to produce a flow meter reading at the entry to MT = 0±2 L/min. The breath simulator, programmed to create a chosen IP (Figure 5.2), was activated to draw air through MT into NMI while constant air flow was maintained through NGI. The designated IP was recorded at the mouth opening of MT to ensure that PIFR and V were within 2% of their designated protocol values (Table 5.1). Once this condition was met, the setup was accepted and the flow meter removed from the entrance to MT. Budelin Novolizer was then primed, inserted into the MT model and sealed with Parafilm® M, and a single IP used to disperse and draw a budesonide dose through the system. After commencing the designated IP, the inhaler was removed from MT, and the compressed air source and vacuum pump switched off in sequence. The apparatus was disassembled after each dose, and budesonide was recovered by rinsing the inhaler (with drug cartridge removed), MT, NMI, NGI stages 1–7 and filter using known volumes of 70%/30%:methanol/water (v/v) and analyzed using high-performance liquid chromatography (HPLC). Budesonide assay was performed using Symmetry® C18 column (3.5µm, 4.6×100mm, Waters, Milford, MA), 69% methanol / 31% 0.1% (v/v) acetic acid buffer (v/v) as mobile phase (flow rate: 1.0 mL/min), and UV detection at 280 nm (2996 Photodiode Array Detector, 1515 Isocractic HPLC Pump, 717 plus Autosampler, Waters). Injection volume was 100 µL and calibration curves were linear in the range of 0.2–10.0 mcg/mL ($r^2 > 0.999$). The limit of quantification (LOQ) = 0.025 mcg/mL.

Aerodynamic Particle Size Distributions of Budelin's $TLD_{in\ vitro}$

The mixing inlet–cascade impactor system (Figure 5.3) and different VCU MT models (Figure 5.1) were employed to enable drug clouds to be withdrawn from Budelin Novolizer 200 mcg according to each of the designated IPs (Figure 5.2) so that the APSDs of drugs exiting MT ($TLD_{in\ vitro}$) could be characterized under constant flow conditions. To evaluate the likely ranges of APSDs of Budelin's $TLD_{in\ vitro}$, the VCU-MT_S, VCU-MT_M, and VCU-MT_L were paired with the small, medium and large IPs, respectively, for each inhalation condition (*fast*, *moderate*, *slow*). The NGI was operated either at 100 L/min if PIFR for the test IP was smaller than 100 L/min or 140 L/min if PIFR > 100 L/min. Combinations of MT models, IPs and NGI flow rates used for measurement of APSDs of Budelin's $TLD_{in\ vitro}$ are summarized in Table 5.2. Because NGI is only calibrated in the flow range of 15–100 L/min (Marple et al., 2003a; Marple et al., 2004; U.S. Pharmacopeial Convention, 2013), additional experiments were performed to evaluate the data collected at 140 L/min. In practice, it was necessary to recalibrate the instrument at 140 L/min. To to do this, four MT-IP combinations where PIFR of the test IP < 100 L/min were selected from Table 5.2 (*fast* inhalation, small MT-IP and medium MT-IP; *slow* inhalation, medium MT-IP and large MT-IP). The same MT-IP combinations were employed to determine the apparent APSDs of $TLD_{in\ vitro}$ at the 140 L/min NGI flow condition given that the same budesonide aerosol should be generated under the same conditions, regardless of the change in NGI flow. In this way, the data collected at 100 L/min could be used as polydisperse aerosol calibration standards to compare with the data generated at 140 L/min. All experiments were randomized. Single actuations were applied and five replicates were performed for each protocol.

Table 5.2. MT models, IPs and NGI flow rates used for measurement of APSDs of $TLD_{in\ vitro}$ for Budelin Novolizer. IPs (small, medium, large) for each of the inhalation conditions (*fast*, *moderate*, *slow*) in the literature (Newman et al., 2000) and as defined in Table 5.1 and Figure 5.2.

Inhalation Condition	MT Model	Inhalation Profile	NGI Flow Rate (L/min)
Fast	VCU-MT_S	Small	100 and 140*
	VCU-MT_M	Medium	100 and 140*
	VCU-MT_L	Large	140
Moderate	VCU-MT_S	Small	100
	VCU-MT_M	Medium	100
	VCU-MT_L	Large	100
Slow	VCU-MT_S	Small	100
	VCU-MT_M	Medium	100 and 140*
	VCU-MT_L	Large	100 and 140*

*The MT-IP combination was tested at both 100 and 140 L/min NGI flow conditions to evaluate the validity of APSD measurements of Budelin's $TLD_{in\ vitro}$ at 140 L/min.

Data Treatment

The amount of budesonide depositing on inhaler, MT, NMI, NGI stages 1–7 and filter were calculated from the products of drug concentrations and sample volumes. Values for $TLD_{in\ vitro}$ were calculated as total amount of budesonide depositing on NMI and NGI, and compared with $TLD_{in\ vivo}$ reported in the gamma scintigraphy study (Newman et al., 2000) for each inhalation condition. The APSDs of $TLD_{in\ vitro}$ for budesonide exiting the MT model were analyzed in accord with USP (U.S. Pharmacopeial

Convention, 2013), where the cutoff aerodynamic diameters for NGI's stages at a specific flow rate (Q), $D_{50,Q}$, were calculated using Equation 5.1:

$$D_{50,Q} = D_{50,Qn}\left(\frac{Qn}{Q}\right)^{x} \qquad \text{Equation 5.1}$$

Where Qn is the nominal flow rate (60 L/min) and $D_{50,Qn}$ is the stage cutoff diameter at Qn. USP's values for $D_{50,Qn}$ and the exponent x (Table 5.3) are based on an archival NGI calibration that accords with NGI's stage mensuration data and impaction theory in the flow range of 30–100 L/min (Marple et al., 2003a). To facilitate initial data analysis, Equation 5.1 was extrapolated so that values for $D_{50,Q}$ could be calculated for both the 100 and 140 L/min NGI flow conditions, assuming that the values for the exponent x were unchanged (Table 5.3). Apparent APSDs of Budelin's *TLD*$_{in\ vivo}$ measured at different conditions were then compared by plotting the cumulative percent mass less than the stated cutoff diameter vs. the cutoff diameter of the corresponding stage (D_{50}) (Equation 5.2). Statistical analyses were performed for total recovered dose and total drug mass in NGI using one-way ANOVA and Student's t-test at a significant level of 0.05 in JMP Pro 11 (SAS Institute Inc., Cary, NC).

$$Cumulative\ \%\ Mass\ < D_{50}\ of\ Stage\ i = \frac{\sum Drug\ Mass\ Below\ Stage\ i}{Total\ Drug\ Mass\ in\ NGI} \times 100\% \qquad \text{Equation 5.2}$$

Table 5.3. The cutoff aerodynamic diameters for NGI's stages at the nominal flow rate (Qn), $D_{50,Qn}$, and the exponent x in Equation 5.1 (U.S. Pharmacopeial Convention, 2013).

Stage	$D_{50,Qn}$	x
1	8.06	0.54
2	4.46	0.52
3	2.82	0.50
4	1.66	0.47
5	0.94	0.53
6	0.55	0.60
7	0.34	0.67

Re-calibration of NGI's Stage Cutoff Diameters

While the theoretical value of the exponent x in Equation 5.1 is 0.5 given "ideal" impaction theory (Reist, 1993), all impactors require experimental calibration corrections so it is not surprising that x ranges 0.47 through 0.67 for NGI stages 1–7 in the flow rate range of 30–100 L/min (Table 5.3) (U.S. Pharmacopeial Convention, 2013). In order to employ NGI at a flow rate above this calibration limit (e.g. 140 L/min), it was necessary to:

(a) Remove the last stage (MOC) from NGI to prevent flow limitation due to the flow through the MOC becoming critical or sonic;

(b) Assess the validity of Equation 5.1 at 140 L/min with USP's values for the exponent x by comparing the APSDs of budesonide aerosols produced from Budelin under the same MT-IP conditions when drawn into NGI at both air flow rates;

(c) Amend the values of D_{50} for certain stages (perhaps by modifying the exponential term x for those stages) at 140 L/min.

The recalibration of a cascade impactor using polydisperse pharmaceutical aerosols was reported by Kotian et al. (2009) and a similar approach was employed here. Four sets of n = 5 cumulative percent mass undersize data obtained from the NGI at 100 L/min from the experimental protocols described in Table 5.2 (*fast* inhalation: small MT-IP, medium MT-IP; *slow* inhalation: medium MT-IP, large MT-IP) were used as calibration standards. Data were fitted using least square nonlinear regression analysis to determine best estimates for the mass median aerodynamic diameter (MMAD) and the geometric standard deviation (GSD) of each cloud by fitting the data to the cumulative lognormal distribution function (CDF) (Andrews, 1992; Kotian et al., 2009) shown in Equation 5.3:

$$y = 100 * \left(0.5 + 0.5 ERF \left\{ \left[\frac{1}{2^{0.5} * \sigma} \right] * \left[\log_e (x) - MEAN \right] \right\} \right) \qquad \text{Equation 5.3}$$

Where ERF is the error function = $\frac{2}{\pi^{0.5}} \int e^{-\left\{ \left[\frac{1}{2^{0.5} * \sigma} \right] * \left[\log_e (x) - MEAN \right] \right\}^2} dx$, and e^{MEAN} and e^{σ} are the MMAD and GSD of the lognormally distributed data. No weighting factors were assigned and the analysis was performed using MATLAB® R2012b (MathWorks, Natick, MA). The cumulative percentage of drug, y, depositing below the cutoff diameter, D_{50}, of each stage at 100 L/min, x, was fitted by allowing $MEAN$ and σ to float in order to minimize the sum of squared deviations of the data from the line of best fit for each MT-IP combinations (Table 5.2). Best estimates of MMAD and GSD were tabulated for each product, alongside their 95% confidence intervals (CI) in accord with Kotian et al. (2009).

To recalibrate NGI at 140 L/min, the individual values for cumulative percent mass penetrating below each stage were tabulated for that flow condition. The curves of best fit for the NGI data at 100 L/min were assumed to also describe the NGI data at 140 L/min. Values for MMAD and GSD for each aerosol at 100 L/min were fixed at their best estimates following curve fitting, and solutions for the stage D_{50} values at 140 L/min were then solved analytically using the cumulative lognormal distribution curves for each aerosol and MT-IP combination. This was performed in Microsoft Excel 2013 (Microsoft Corporation, Redmond, WA) by setting the value for the cumulative percent undersize (y in Equation 5.3) to its experimentally determined value for the chosen MT-IP combination when tested with NGI flow = 140 L/min; the function was then solved for x using the LOGNORM.INV function and the solution assigned to D_{50} for the selected stage and data set. Mean values of each D_{50} were calculated for each stage from the four separate calculations and assigned as the re-calibrated cutoff diameters for the NGI when operated at 140 L/min.

5.3 RESULTS

Mass Balance

The mean total (SD) budesonide recovered from the deposition sites (mass from inhaler mouthpiece, MT, NMI + NGI) ranged from 222.1±7.6 to 240.5±21.9 mcg showed no statistical differences (one-way ANOVA, $p>0.05$) across all testing conditions (Table 5.4). This statement was true even through the combination of small MT and small IP resulted in greater inhaler retention and reduced delivered dose in all cases. The same

trend of reducing delivered doses was seen for Salbulin Novolizer (same inhaler, different drug and formulation) as shown in Figure 3.4.

Table 5.4. Mean budesonide dose (±SD) collected from Budelin Novolizer 200 mcg inhaler, mouth-throat model (MT), Nephele Mixing Inlet (NMI), Next Generation Impactor (NGI) alongside the total recovered dose for different testing conditions. Total lung dose, $TLD_{in\ vitro}$, was designated as the drug dose exiting the MT model, or the sum of the drug mass collected in NMI and NGI. Total recovered drug was calculated as the sum of drug dose collected from inhaler, MT, NMI and NGI. Data were presented as mean±SD (n=5). Drug deposition on NMI was <LOQ in most cases (noted as "0.0").

Experimental Protocol			Budesonide Dose (mcg)					
			Inhaler	MT	NMI	NGI	TLD	Total
Fast Inhalation[a]	Small MT-IP	100 L/min	78.0 (17.6)	117.6 (22.2)	0.0 (0.0)	36.1 (5.2)	36.1 (5.2)	231.7 (17.7)
	Small MT-IP	140 L/min	74.0 (28.0)	129.6 (38.2)	0.0 (0.0)	31.4 (8.9)	31.4 (8.9)	235.0 (7.7)
	Medium MT-IP	100 L/min	21.9 (4.1)	137.9 (11.7)	0.2 (0.5)	75.2 (6.1)	75.5 (5.9)	235.3 (7.8)
	Medium MT-IP	140 L/min	23.7 (4.1)	123.6 (7.4)	0.2 (0.5)	74.6 (4.9)	74.8 (4.7)	222.1 (7.6)
	Large MT-IP	140 L/min	21.6 (9.8)	114.9 (8.0)	0.5 (0.7)	89.3 (9.9)	89.8 (10.5)	226.3 (13.6)
Moderate Inhalation[a]	Small MT-IP	100 L/min	70.5 (16.3)	131.0 (14.9)	0.0 (0.0)	32.8 (7.9)	32.8 (7.9)	234.3 (7.3)
	Medium MT-IP	100 L/min	25.0 (9.9)	152.5 (13.6)	0.0 (0.0)	54.2 (7.0)	54.2 (7.0)	231.7 (22.4)
	Large MT-IP	100 L/min	22.2 (3.4)	150.6 (18.7)	0.0 (0.0)	67.6 (8.1)	67.6 (8.1)	240.5 (21.9)
Slow Inhalation[a]	Small MT-IP	100 L/min	62.4 (28.1)	162.2 (35.3)	0.0 (0.0)	12.2 (2.9)	12.2 (2.9)	236.7 (10.5)
	Medium MT-IP	100 L/min	18.9 (3.2)	174.1 (11.8)	0.0 (0.0)	42.3 (6.1)	42.3 (6.1)	235.2 (18.5)
	Medium MT-IP	140 L/min	25.1 (8.6)	172.8 (7.2)	0.2 (0.5)	37.0 (2.5)	37.2 (2.9)	235.1 (4.9)
	Large MT-IP	100 L/min	20.0 (4.6)	147.5 (6.5)	0.0 (0.0)	66.8 (1.7)	66.8 (1.7)	234.4 (9.4)
	Large MT-IP	140 L/min	20.3 (7.1)	154.7 (7.2)	0.5 (0.7)	56.9 (4.4)	57.4 (4.9)	232.3 (6.2)

[a]Newman et al. (2000) training conditions.

Notably, the amount of drug collected in the NMI was <2% of $TLD_{in\ vitro}$ in all cases, consistent with the claims for the NMI (N. C. Miller, 1997; N. C. Miller et al., 2000) and

indicating that the addition of NMI to the NGI (Figure 5.3) had negligible effects on the data for particle size distributions of $TLD_{in\ vitro}$. This observation was consistent with Olsson et al.'s findings (Olsson et al., 2010) and this again shows the advantage of NMI over the Electronic™ Lung approach (Burnell et al., 1998b) when seeking to couple realistic IPs with the constant flow conditions required for cascade impaction. The degree of IP control that proved possible with the apparatus and general method described in Figure 5.3 and associated text is illustrated in Figure 5.4.

For experiments using the same MT-IP combinations tested at two NGI flow conditions (*fast* inhalation: small MT-IP, medium MT-IP; *slow* inhalation: medium MT-IP, large MT-IP), the flow rate vs. time profiles, or IPs, measured at the mouth opening of MT were indistinguishable and completely comparable for a selected inhalation condition, regardless of the change in NGI flow rates (Figure 5.4). Because aerosol generation and dispersion from Budelin is flow-dependent (de Boer et al., 2004), when the inhaler is tested using the same MT-IP combination, the budesonide clouds and drug doses collected from inhaler, MT, NMI and NGI should be comparable between the 100 and 140 L/min NGI flow conditions within the dosing variations imposed by the product. This comparability was confirmed by the results from the small and medium MT-IP combinations tested under *fast* inhalation conditions (Table 5.4, Row 2–5), and the medium MT-IP combinations under *slow* inhalation conditions (Table 5.4, Row 11–12) that showed no statistically significant differences in mass distribution across the columns (e.g. for comparable MT-IP combinations). While small but statistically significant differences (Student's t-test, assuming equal-variance, $p<0.05$) were observed for the collected mass in NGI between 100 and 140 L/min NGI conditions for the large MT-IP

combination (*slow* inhalation; Table 5.4, Row 13–14), this was only seen once and the variation was consistent with those reported for Novolizer (Munzel et al., 2005). It appeared reasonable to believe that budesonide aerosols, generated from Novolizer using the same MT-IP combinations, had comparable particle size distributions when tested in the apparatus shown in Figure 5.3, irrespective of whether the flow rate through the NGI was 100 or 140 L/min.

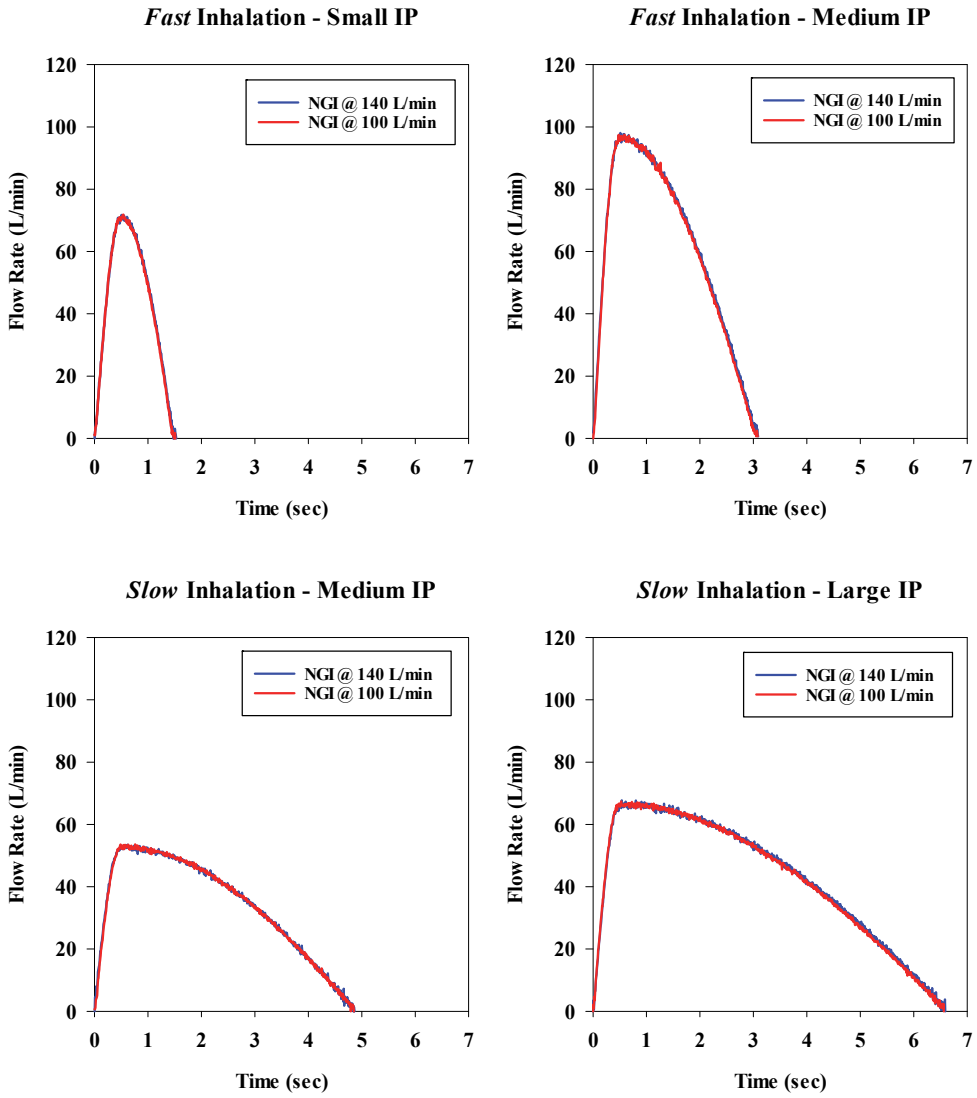

Figure 5.4. Comparison of inhalation profiles recorded at the entrance to MT under the same MT-IP combinations with NGI flow rates = 100 and 140 L/min, respectively.

In Vivo – In Vitro Correlations

The method produced values for $TLD_{in\ vitro}$ (drugs recovered from NMI and NGI) that were comparable to those described previously following aerosol capture in upper airway models and filters (Delvadia et al., 2012) in spite of the fact that the method used to simulate the IPs (Chapter 4 and Figure 5.2) differed slightly from the technique reported for the Budelin Novolizer inhaler by Delvadia et al. (2012) and the large, fast IP utilized a value for V = 5.15 L (Table 5.1) in the present study. The results produced the IVIVCs shown in Figure 5.4 for the percent of the total recovered dose exiting MT, illustrating once more the importance of variations in mouth-throat geometry and breath profiles for aerosol drug delivery from Budelin Novolizer. For a selected inhalation condition, the extremes of lung deposition seen clinically appeared to correlate to the values for $TLD_{in\ vitro}$ seen between the large MT–large IP and small MT–small IP test configurations (Figure 5.5). The *in vitro* lung doses determined using these test methods ranged from 11.5% to 45.8% for *fast* inhalation, from 10.1% to 31.0% for *moderate* inhalation, and from 3.5% to 31.2% for *slow* inhalation. These values are comparable to those reported by Delvadia et al. (2012) for the same inhaler where $TLD_{in\ vitro}$ ranged from 9.7% to 40.4% for *fast* inhalation, from 8.0% to 28.7% for *moderate* inhalation, and from 4.8% to 28.0% for *slow* inhalation.

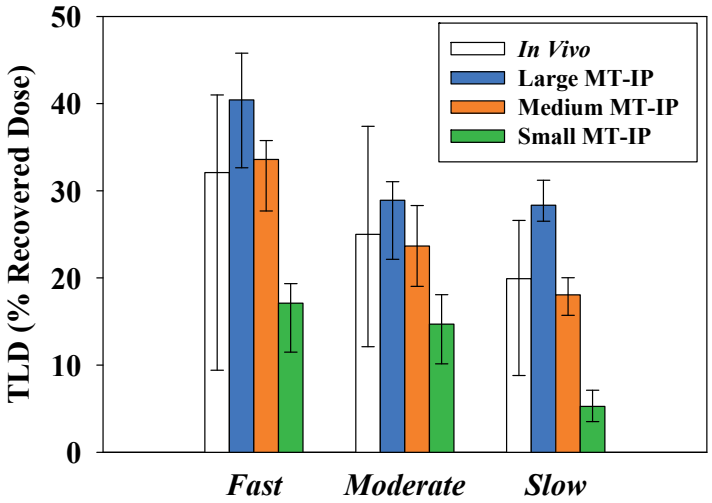

Figure 5.5. Comparison of *in vivo* and *in vitro* total lung dose (TLD) as % total recovered drug dose (inhaler + MT + NMI + NGI) for Budelin Novolizer at *fast*, *moderate* and *slow* inhalation conditions. Both the *in vivo* (Newman et al., 2000) and *in vitro* data were presented as median (range) (n = 5). TLD values were calculated from the experiments where NGI was operated at 100 L/min except for the large MT-IP combination tested at *fast* inhalation which employed an NGI flow rate of 140 L/min.

Aerodynamic Particle Size Distributions

Deposition of $TLD_{in\ vitro}$ for budesonide within the NMI and NGI was determined for each of the MT-IP and NGI flow rate conditions described above (Tables 5.2) in replicate (n = 5). The mean results are shown in Table 5.5. Cutoff diameters for NGI stages were first calculated for both 100 and 140 L/min flow conditions using Equation 5.1 with values for x taken from Table 5.3, and the results are shown in Table 5.6.

Table 5.5. Mean deposition of budesonide $TLD_{in\ vitro}$ in micrograms (±SD) in NMI (Nephele Mixing Inlet), S1–S7 and F (NGI stages 1–7 and filter of NGI) when tested using the "General Procedure" described in Methods. Drug deposition on NMI, S6 and S7 was <LOQ in most cases (noted as "0.0").

Experimental Protocol			Budesonide Dose (mcg)								
			NMI	S1	S2	S3	S4	S5	S6	S7	F
	Small	100	0.0	1.1	7.0	7.5	13.0	6.0	1.3	0.0	0.0
	MT-IP	L/min	(0.0)	(0.1)	(0.7)	(1.0)	(2.0)	(1.3)	(0.3)	(0.0)	(0.0)
	Small	140	0.0	2.5	9.8	6.6	8.9	3.0	0.5	0.0	0.0
	MT-IP	L/min	(0.0)	(0.3)	(1.9)	(1.6)	(3.1)	(1.5)	(0.5)	(0.0)	(0.0)
Fast	Medium	100	0.2	2.0	12.3	14.1	26.6	15.4	4.8	0.0	0.0
Inhalation[a]	MT-IP	L/min	(0.5)	(0.2)	(0.5)	(0.7)	(1.6)	(2.3)	(1.3)	(0.0)	(0.0)
	Medium	140	0.2	4.8	19.5	14.2	22.7	10.4	2.9	0.0	0.0
	MT-IP	L/min	(0.5)	(0.3)	(1.0)	(0.8)	(1.6)	(1.1)	(0.5)	(0.0)	(0.0)
	Large	140	0.5	5.3	22.4	16.7	27.6	13.2	4.1	0.0	0.0
	MT-IP	L/min	(0.7)	(0.5)	(2.7)	(1.7)	(2.8)	(1.7)	(0.9)	(0.0)	(0.0)
	Small	100	0.0	1.2	7.8	7.4	11.3	4.5	0.6	0.0	0.0
	MT-IP	L/min	(0.0)	(0.2)	(1.1)	(1.5)	(3.1)	(1.7)	(0.6)	(0.0)	(0.0)
Moderate	Medium	100	0.0	2.3	12.7	12.0	17.7	7.9	1.7	0.0	0.0
Inhalation[a]	MT-IP	L/min	(0.0)	(0.1)	(1.1)	(1.5)	(2.8)	(1.2)	(0.3)	(0.0)	(0.0)
	Large	100	0.0	3.0	15.6	14.3	22.3	10.1	2.3	0.0	0.0
	MT-IP	L/min	(0.0)	(0.5)	(0.9)	(1.3)	(2.7)	(2.2)	(0.8)	(0.0)	(0.0)
	Small	100	0.0	1.1	4.5	2.8	3.1	0.6	0.0	0.0	0.0
	MT-IP	L/min	(0.0)	(0.2)	(0.7)	(0.6)	(0.9)	(0.6)	(0.0)	(0.0)	(0.0)
	Medium	100	0.0	2.6	11.7	9.5	12.8	4.9	0.8	0.0	0.0
	MT-IP	L/min	(0.0)	(0.4)	(1.4)	(1.2)	(1.9)	(0.9)	(0.4)	(0.0)	(0.0)
Slow	Medium	140	0.2	4.9	13.9	7.1	8.3	2.5	0.3	0.0	0.0
Inhalation[a]	MT-IP	L/min	(0.5)	(0.5)	(0.7)	(0.7)	(1.0)	(0.5)	(0.4)	(0.0)	(0.0)
	Large	100	0.0	3.4	15.7	13.8	21.6	9.9	2.3	0.0	0.0
	MT-IP	L/min	(0.0)	(0.3)	(0.3)	(0.3)	(0.7)	(0.4)	(0.2)	(0.0)	(0.0)
	Large	140	0.5	6.7	19.2	11.0	14.1	4.8	1.2	0.0	0.0
	MT-IP	L/min	(0.7)	(0.6)	(1.1)	(0.9)	(1.4)	(0.7)	(0.2)	(0.0)	(0.0)

[a]Newman et al. (2000) training conditions.

Table 5.6. Calculated cutoff diameters for NGI stages at 100 and 140 L/min flow rates calculated from Equation 5.1 and Table 5.3.

Stage	$D_{50,\ 100L/min}$	$D_{50,\ 140L/min}$
1	6.12	5.10
2	3.42	2.87
3	2.18	1.85
4	1.31	1.11
5	0.72	0.60
6	0.40	0.33
7	0.24	0.19

Re-calibration of NGI's Stage Cutoff Diameters

For the four selected MT-IP combinations tested at both the 100 and 140 L/min NGI flow conditions (*Fast* Inhalation: small MT-IP, medium MT-IP; *Slow* Inhalation: medium MT-IP, large MT-IP), data were plotted as the cumulative percent of drug mass less than the stated cutoff diameter against the calculated stage cutoff diameters (D_{50}) from Table 5.6. While the same size distribution was expected and hoped for in the case of each selected MT-IP combination at the different NGI flow rates, the profiles shown in Figure 5.6 showed some discrepancies between the 100 and 140 L/min conditions for all cases, mostly related to deposition on stages 1 through 3 of NGI. The jets above those stages are associated with high Reynolds numbers (Re) and increasing airflow turbulence (Marple et al., 2003b). This suggested that the USP calibration (Equation 5.1) (U.S. Pharmacopeial Convention, 2013) failed to be applicable when calculating the stage

cutoff diameters at 140 L/min, necessitating experimental recalibration of the cutoff diameters.

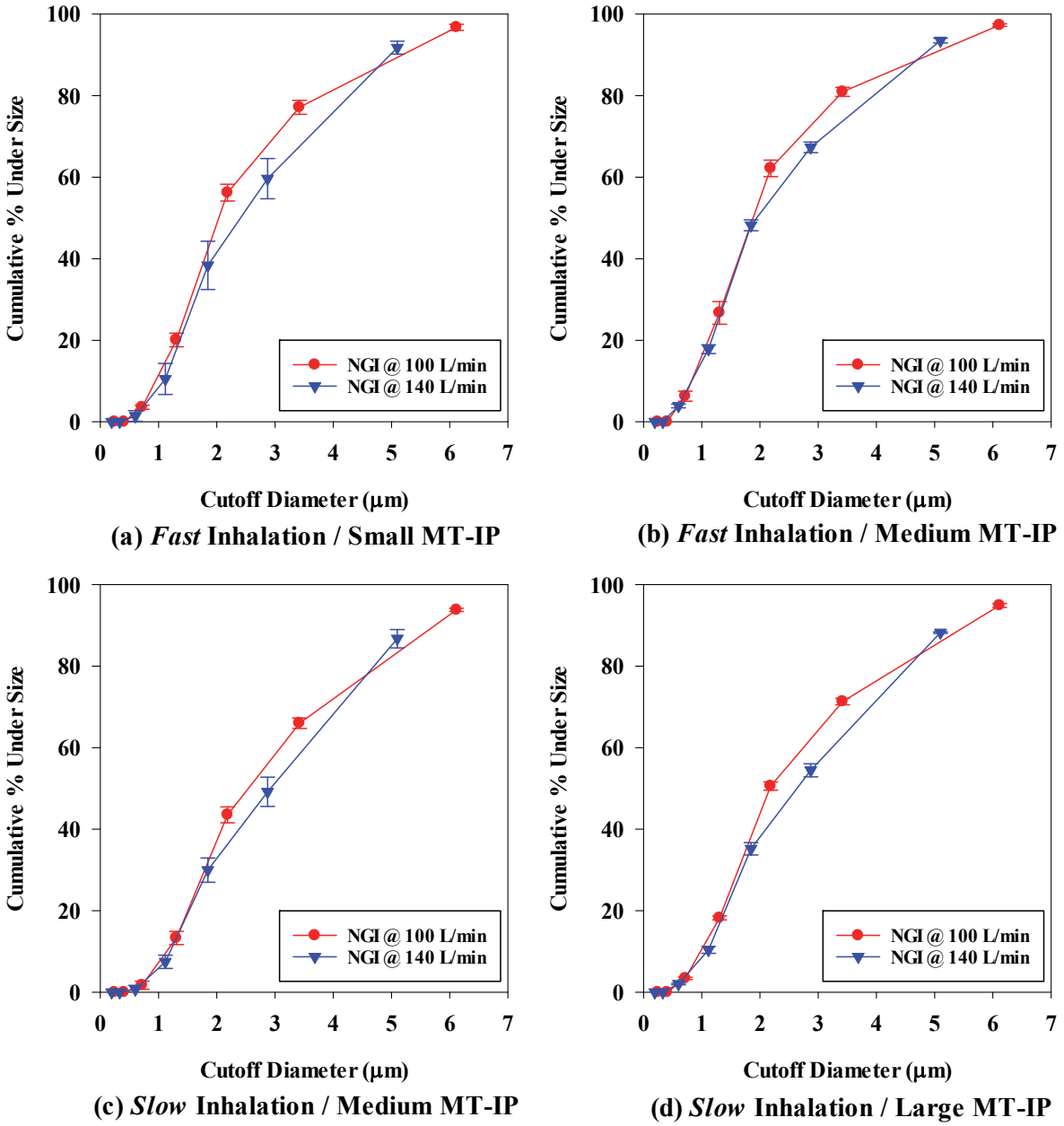

Figure 5.6. Apparent cumulative percent of drug mass under size vs. calculated stage cutoff diameters (Table 5.6) for budesonide collected in NGI following realistic aerosol testing in different MT models. Data are presented as mean±SD (n=5) for the four selected MT-IP combinations tested at the 100 and 140 L/min NGI flowrates.

The cumulative percent under size vs. stage cutoff diameter data for the four selected MT-IP combinations tested at 100 L/min were fitted to the cumulative lognormal distribution function (Equations 5.3–5.4) and results were shown in Figure 5.7. Values for coefficients of determinations (r^2) are greater than 0.997 for all cases, suggesting aerodynamic particle size of aerosols exiting MTs can be well described using the lognormal distribution model. Best estimation for MMAD (e^{MEAN}) and GSD (e^{σ}), and their 95% CIs, were summarized for each MT-IP combination in Table 5.7.

Table 5.7. Mean values and 95% confidence intervals for $MEAN$, σ , MMAD (e^{MEAN}) and GSD (e^{σ}) estimated from the curves of best fit (Equation 5.3) for the four selected MT-IP combinations when tested with NGI flow rate = 100 L/min.

Experimental Protocol		$MEAN$ (95% CI)	σ (95% CI)	MMAD (e^{MEAN}) (95% CI)	GSD (e^{σ}) (95% CI)
Fast Inhalation[a]	Small MT-IP	0.73 (0.71-0.75)	0.60 (0.57-0.63)	2.08 (2.04-2.12)	1.82 (1.76-1.87)
	Medium MT-IP	0.63 (0.61-0.65)	0.62 (0.59-0.65)	1.88 (1.84-1.91)	1.86 (1.81-1.92)
Slow Inhalation[a]	Medium MT-IP	0.93 (0.91-0.95)	0.62 (0.59-0.65)	2.52 (2.47-2.57)	1.87 (1.81-1.92)
	Large MT-IP	0.82 (0.80-0.84)	0.64 (0.62-0.67)	2.27 (2.23-2.30)	1.90 (1.86-1.95)

[a]Newman et al. (2000) training conditions.

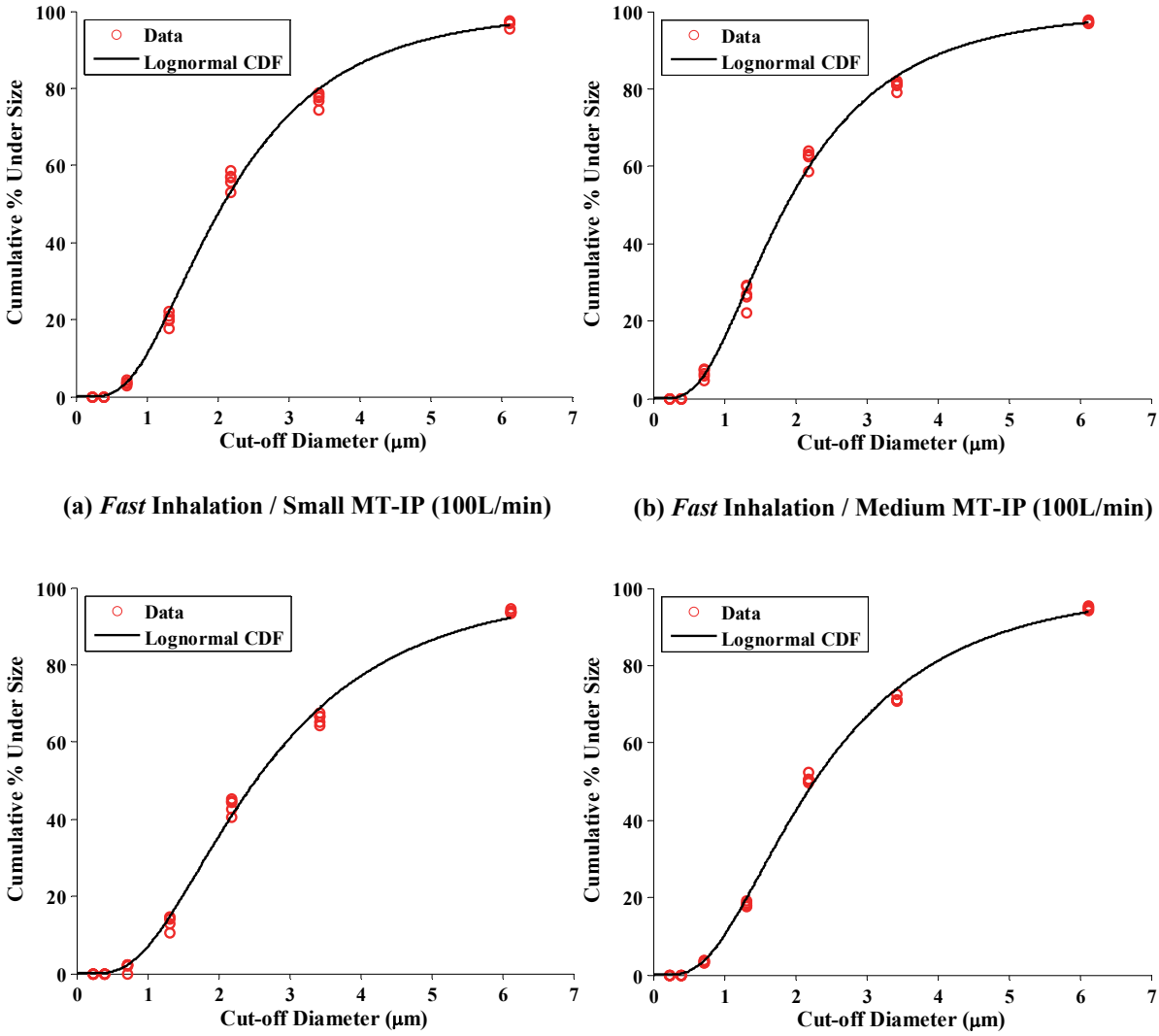

(a) *Fast* Inhalation / Small MT-IP (100L/min)

(b) *Fast* Inhalation / Medium MT-IP (100L/min)

(c) *Slow* Inhalation / Medium MT-IP (100L/min)

(d) *Slow* Inhalation / Large MT-IP (100L/min)

Figure 5.7. Cumulative percent of drug mass undersize vs. stage cutoff diameters for drugs collected in NGI following realistic testing. Data are presented as mean±SD (n=5) for the four selected MT-IP combinations tested at 100 L/min. Red circles are individual data points, while the black profiles are results of curve fitting to the cumulative lognormal distribution function (Equation 5.3). Coefficients of determination (r^2) were > 0.997 in all cases.

The curves in Figure 5.7 were generated according to Equation 5.3, to describe each budesonide APSD when characterized in NGI at 100 L/min. Calculated cutoff diameters (D_{50}) for stages 1–5 when NGI was recalibrated at 140 L/min are shown as the mean and standard deviations for the four selected MT-IP combinations in Table 5.8. Cutoff diameters for stages 6-7 are not listed as drug deposition on those stages could not be detected (washings resulted in budesonide mass < LOQ). The mean values for each stage were assigned as the re-calibrated D_{50} values at 140 L/min, and the results were compared with the USP calibrated cutoff diameter (U.S. Pharmacopeial Convention, 2013) in Table 5.9.

Table 5.8. Re-calibrated NGI stage cutoff diameters (D_{50}) at 140 L/min for selected MT-IP combinations. Data are presented as mean±SD (n=5). Drug deposition on stages 6 and 7 was <LOQ in all cases.

Stage #	Small MT-IP (*Fast*)[a]	Medium MT-IP (*Fast*)[a]	Medium MT-IP (*Slow*)[a]	Large MT-IP (*Slow*)[a]
1	4.81 (0.30)	4.82 (0.13)	5.08 (0.34)	4.86 (0.03)
2	2.42 (0.18)	2.48 (0.05)	2.49 (0.14)	2.44 (0.06)
3	1.75 (0.16)	1.83 (0.04)	1.82 (0.10)	1.77 (0.05)
4	0.98 (0.13)	1.06 (0.03)	1.02 (0.07)	1.01 (0.03)
5	0.63 (0.02)	0.63 (0.02)	0.68 (0.01)	0.60 (0.02)
6	NA	NA	NA	NA
7	NA	NA	NA	NA

[a]Newman et al. (2000) training conditions.

Table 5.9. Comparison of NGI's extrapolated USP calibration (U.S. Pharmacopeial Convention, 2013) or cutoff diameters (D_{50}) at 140 L/min (assuming that Equation 5.1 and Table 5.8 are valid) with the overall means for D_{50} after recalibration (from Table 5.8).

Stage #	USP D_{50} (μm) (Theoretical; 140 L/min)	Mean D_{50} (μm) (Experimental; 140 L/min)	Experimental D_{50} /Theoretical D_{50}
1	5.10	4.89	0.96
2	2.87	2.46	0.86
3	1.85	1.79	0.97
4	1.11	1.02	0.92
5	0.60	0.63	1.05
6	0.33	NA	NA
7	0.19	NA	NA

Aerodynamic Particle Size Distributions of Budelin's $TLD_{in\ vitro}$

Aerodynamic particle size distributions of $TLD_{in\ vitro}$, designated as drugs exiting the MT model following aerosol generation under realistic inhalation condition, were analyzed for all the MT-IP combinations shown in Table 5.2. The mean cumulative percent of budesonide depositing below D_{50} for each stage was calculated and plotted against the cutoff diameters using the archival USP calibration (U.S. Pharmacopeial Convention, 2013) when NGI flow = 100 L/min. In one case however, the high-flow IP protocol (large IP, *fast* inhalation) where NGI flow = 140 L/min, recalibrated cutoff diameters determined in the present study were applied (Table 5.9). No curve fitting was used to generate the results shown in Figure 5.8 for all three inhalation conditions. Values

for MMAD were calculated using linear interpolation for each MT-IP combination and data were summarized in Table 5.10. Perhaps the most important observation for Budelin's budesonide aerosols was the variation seen in particle size distribution resulting from the different MT-IP combinations, where the apparent MMADs ranged from 1.79 to 3.26 μm across all test conditions (Table 5.10). The results suggested that in addition to total lung dose, the size distribution for drugs likely to enter the trachea also depends on the combined effects of each subjects' MT geometry and inhalation profile. For Budelin, these effects were most pronounced for the *slow* inhalation condition (Figure 5.8) described clinically by Newman et al. (2000), where the mean values for MMAD varied from 2.17 to 3.26 μm. For all three inhalation conditions, the large MT-IP combination invariably produced the smallest MMAD and the largest $TLD_{in\ vitro}$, indicating that the best powder emptying and the best dispersion from Budelin occurred under large IP conditions. The amount of drug depositing on stage 1 was less than 10% of the total NGI dose in all cases, illustrating the high collection efficiency of the MT; MT appears to reduce the possible variations in APSDs significantly. There was also a lack of visually observable lactose deposition in the NGI, suggesting that at least the large lactose particles in the formulation were also captured by the coated MT models.

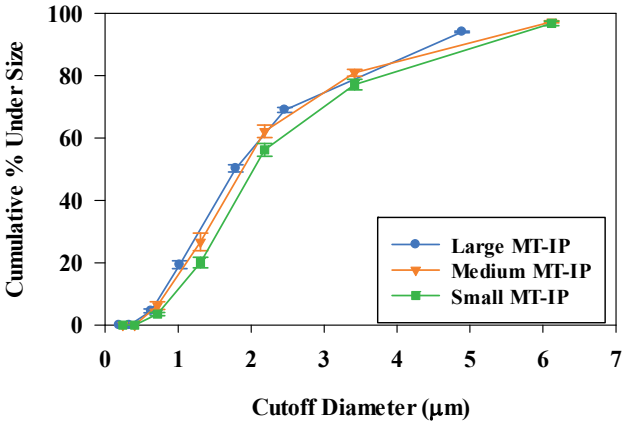

(a) *Fast* Inhalation

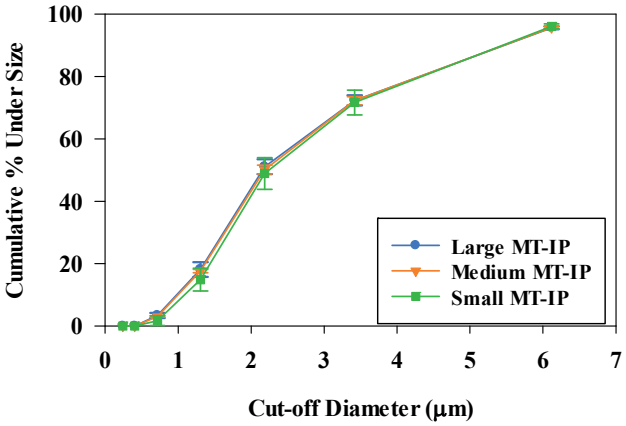

(b) *Moderate* Inhalation

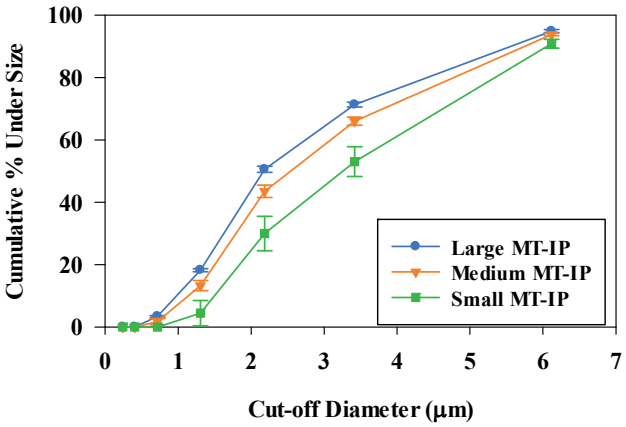

(c) *Slow* Inhalation

Figure 5.8. Cumulative percent of drug mass undersize vs. stage cutoff diameters for budesonide collected in NGI following realistic testing of Budelin Novolizer in the Apparatus shown in Figure 5.3. Data are presented as mean±SD (n=5) for (a) *fast*, (b) *moderate* and (c) *slow* inhalation conditions. NGI stage cutoff diameters were assigned according to USP (U.S. Pharmacopeial Convention, 2013) except for the high-flow IP protocol (large MT-IP, *fast* inhalation), where the NGI flow rate = 140 L/min and the re-calibrated cutoff diameters shown in Table 5.9 were used to process the data.

Table 5.10. Mass median aerodynamic diameter (MMAD) for different MT-IP combinations. Data were presented as mean±SD (n = 5).

	MMAD (μm)		
	Small MT-IP	Medium MT-IP	Large MT-IP
Fast Inhalation	2.03±0.05	1.88±0.06	1.79±0.03*
Moderate Inhalation	2.28±0.23	2.19±0.04	2.17±0.09
Slow Inhalation	3.26±0.27	2.54±0.09	2.17±0.03

*Calculated using cutoff diameters from Table 5.9.

5.4 DISCUSSION

The mixing inlet–cascade impactor system (Figure 5.3) allowed the aerodynamic particle size distributions of budesonide powder aerosols exiting MT models to be measured following testing of the DPI, Budelin Novolizer, according to realistic but different MT-IP conditions of use. A pre-requisite of the system was that the cascade impactor flow rate exceed the peak inhalation flow rate (PIFR) of the targeted breath profile; this to allow successful breath simulation through the inhaler and the MT model. Our previous clinical study (Chapter 4) showed that PIFR through an inhaler was dependent on the inhaler's airflow resistance, and that PIFR may well exceed 100 L/min, the present upper limit of NGI's calibration. Although the results described in Chapter 4 were for healthy adults only, studies performed on asthma or COPD patients also show that PIFR values often exceed 100 L/min when inhaling through a powder inhaler (Azouz et al., 2015a; Azouz et al., 2015b; Virchow et al., 2014). Therefore, to allow a complete range of DPIs to be tested realistically, using the mixing inlet–cascade impactor system shown in Figure 5.3, impactors like NGI must be modified and, if necessary recalibrated

to allow their use under high flow rate conditions. While complete recalibration using monodisperse, nonvolatile aerosols may be desirable (Marple et al., 2003a; Marple et al., 2004), for practical purposes, polydisperse pharmaceutical aerosols may also be used to estimate stage cutoff diameters outside the existing compendial specification range. This approach was shown to be successful previously (Kotian et al., 2009) and it also worked well in the present study. The largest difference between recalibrated cutoff diameters and USP calibrations (U.S. Pharmacopeial Convention, 2013) were seen for stage 2 (2.46 µm vs. 2.87 µm; Table 5.7) where the magnitude of the error was the main source of the discrepancies seen in APSD profiles between the 100 and 140 L/min NGI flow condition for all selected MT-IP combinations (Figure 5.6). This may have been caused by the non-ideal behavior of aerosols in NGI at high flow rates, where Re for stage 2 exceeds the generally desirable range of 500–3000 for impactor design (Marple et al., 2003b) (Calculated Re for stage 2 at 140 L/min= 6696).

What should also be noted is that the DPI, Budelin Novolizer, as used in the present study, is a medium-resistance inhaler [airflow resistance = 0.0241 $kPa^{0.5}.L^{-1}.min$; (Delvadia, 2012)]. Other DPIs with lower resistances (e.g. Aerolizer®), can enable subjects to achieve a much higher PIFR when inhaling forcefully through the device (Chapter 2). As even higher flow rates (>140 L/min) may be required to enable realistic testing of low-resistance inhalers, a complete redesign of cascade impactors or some of their stages may be needed to ensure correct measurement of particle size distribution at high flow conditions using the setup described in Figure 5.3.

The present study successfully coupled realistic *in vitro* testing (Chapter 3) with compendial cascade impactor methods (U.S. Pharmacopeial Convention, 2013). IPs

generated by breath simulation were re-producible at the mouth entrance of MT when air flow in the impactor is properly balanced with compressed air (Figure 5.4). Realistic MT models, when coated properly, proved to be highly efficient “preseparators” that captured large particles, thus eliminating the need to use an artificial preseparator before feeding an aerosol into the cascade impactor. The approach described here is different from that used elsewhere (Chrystyn et al., 2015; Goodey et al., 2014; Nadarassan et al., 2010; Yakubu et al., 2013), and standardization of the methods may be needed to facilitate application of realistic *in vitro* testing for inhaled drug products. Although other flow-balancing devices, for example the Electronic Lung™ (Brindley et al., 1994; Burnell et al., 1998b; Tarsin et al., 2006), may also be used to couple breath simulation with the constant flow needed for cascade impaction, yet the NMI was shown to minimize drug losses from the aerosol cloud once formed (N. C. Miller, 1997; N. C. Miller et al., 2000) by allowing sheath air flow to be generated and introduced around the central aerosol cyclone to “protect” drug aerosols from interior device collisions and minimize wall losses (<1% total recovered dose was lost in NMI across all experiments reported in this chapter).

An important observation in this study and the previously publications (Delvadia et al., 2012; Olsson et al., 2013) is that the large inter-subject variations in total lung dose seen in the gamma scintigraphy study for Budelin Novolizer (Newman et al., 2000) are most likely predictable (Figure 5.5) by using realistic *in vitro* testing that incorporates variations in human oropharyngeal geometry and the inhalation maneuver. The compendial cascade impactor method however, produced much smaller variations in fine particle fraction, FPF (designated as the percentage of particles likely to penetrate the lung, d<5 μm), with standard deviation <5% of label claim when Budelin was tested at the

flow rate equivalent to 4 kPa pressure drop (de Boer et al., 2004). Thus, the compendial test method fails to characterize the clinical variations in dose and aerosol delivery from powder inhalers like Budelin. Although FDA suggest that powder inhalers should be tested at “three flow rates [around the] reference labeled flow rate, and ±50% of the labeled flow rate” for the *in vitro* bioequivalent study (Saluja et al., 2014), in practice DPIs are usually tested at 30, 60 and 90 L/min during product development (Harris, 2015). This appears to be a gross oversimplification of the real situation as humans do not inhale at constant flow, and the three suggested flow rates cannot really represent the flow range that subjects were shown to produce in Chapter 4.

Variations in regional drug distribution in the lung, usually described as P/C ratio [drug deposition in peripheral lung (P) to central lung (C) ratio] in the gamma scintigraphy study, were also reported for Budelin (Newman et al., 2000). We showed in the present study that the combination of different MT models and realistic IPs produced variable size distributions for drugs exiting MT models, and the effects were most pronounced for the *slow* inhalation condition (Figure 5.8). The results were consistent with the “critical condition” reported for Budelin (de Boer et al., 2004), where the particle size distribution was seen to change significantly when the inhaled flow rate dropped below a certain threshold. This may partly explain the variations seen in the P/C ratios reported by (Newman et al., 2000). However, particle size distribution is not the only factor affecting aerosol deposition in the lung, many other factors like airway geometry and human inhalation maneuvers are also critical in determining the final destination of inhaled drug particles (De Backer et al., 2010; Farr et al., 1995; Newman et al., 1989). A better understanding of aerosol deposition in the airways, and the need to build IVIVCs for

regional drug distribution in the lung, require further studies using approaches like mathematical modeling [e.g. ICRP model (International Commission on Radiological Protection (ICRP), 1994)] or Computational Fluid Dynamic (CFD) simulations (Longest & Holbrook, 2012), as such measurement is beyond the present state-of-the-art for *in vitro* testing. A pilot study where realistic *in vitro* testing has been coupled with the modeling approach shown in this chapter will be described in Chapter 6.

Demonstrating bioequivalence for locally acting drugs is always a challenge due to the difficulty in proving equivalent [drug delivery] at the “site of action” ("Code of Federal Regulations," 2015). For powder inhalers, FDA suggests *in vitro* bioequivalence be demonstrated between inhalers for single actuation content and aerodynamic particle size distribution (Saluja et al., 2014). While such approaches may be adequate to control batch to batch quality, the difficulty in correlating the *in vitro* (e.g. fine particle dose) and *in vivo* (e.g. drug dose penetrating the lung) data (Newman & Chan, 2008) make it challenging to predict clinical performance for the test product. The present work and previous publication (Delvadia et al., 2012) clearly show that IVIVCs can be achieved for total lung dose, and more importantly, for clinical variations seen in dosing. We believe that if such IVIVCs (mean and variations) can be demonstrated and validated *in vitro*, that *in vitro* predicted lung dose may be considered to be a surrogate for some *in vivo* bioequivalence studies. The approach may at least prove useful for drug developers to evaluate how a change in device design or formulation may affect *in vivo* lung dose, especially for drugs with low therapeutic windows. Although we have yet to demonstrate IVIVCs for regional drug distribution in the lung, the methods reported in this study, when used to determine the variations in particle size distribution for drugs entering the lung should provide a

foundation for future studies when assessing the relationships between particle size distributions, drug deposition in airways and the clinical effects produced by inhalers.

5.5 CONCLUSION

A new method was developed and evaluated to enable the prediction of variations in APSDs of $TLD_{in\ vitro}$ from Budelin Novolizer 200 mcg. This powder inhaler, that doses reproducibly when subjected to USP testing (de Boer et al., 2004; Delvadia et al., 2012), showed significant variations in lung dose *in vivo* due probably to variations in oropharyngeal (MT) geometry and the way that subjects inhaled. When realistic *in vitro* tests were conducted, *IVIVCs* revealed and confirmed the importance of MT geometry and IP variations. Coupling these realistic tests with cascade impactor methods to evaluate the APSDs exiting the MT models from Budelin Novolizer 200 mcg, showed that these methods were sufficiently precise to distinguish between the different aerosol doses and aerosol sizes likely to enter the trachea. There is no reason to believe that the same techniques used to study Budelin in this chapter cannot be extended to review the data for other powder inhalers that are also used clinically by patients with variable MT geometry and breathing patterns. The clinical importance of these observations requires further evaluation.

CHAPTER 6

EVALUATING COMPUTATIONAL FLUID DYNAMIC (CFD) SIMULATIONS OF REGIONAL DRUG DEPOSITION FROM BUDELIN® NOVOLIZER® IN COMBINATION WITH REALISTIC IN VITRO TESTING TECHNIQUES

6.1 INTRODUCTION

The *in vitro* test methods described in Chapters 3–5 clearly enable drug development scientists to estimate the likely ranges of total lung dose (TLD) and the aerodynamic particle size distributions (APSDs) of those doses entering the trachea from DPIs like Budelin® Novolizer®. Even though an extensive primary and secondary literature exists that purports to relate regional deposition of aerosols to their APSDs in humans (International Commission on Radiological Protection (ICRP), 1994; Rostami, 2009; Stahlhofen et al., 1989), and several groups have converted such deposition models into computer programs that in certain cases (W.H. Finlay, 2013), account for inhaler effects on mouth-throat (MT) deposition for a DPI, neither models nor programs can presently be used to predict regional drug deposition from powder inhalers. In part this is because the methods used to determine APSDs for powder inhalers fail to account for oropharyngeal geometry and variations in breath profiles; topics that have been examined and for Budelin Novolizer at least, addressed in the earlier chapters of this

thesis. Even given the data for Budelin's APSD from Chapter 5 however, existing deposition models fail to enable the prediction of regional lung deposition during a typical powder inhalation profile (IP). It follows therefore, that the detailed regional drug deposition in the lung from Budelin remains unknown in the sense that its dependence on aerosol characteristics and breathing maneuvers cannot readily be determined. Product development scientists can only make guesses about regional drug deposition using clinical studies such as those reported by Newman et al. (2000). Fortunately however, new CFD programs have recently been described by Longest et al. and Tian et al. who reported that by using lung models consisting of realistic geometries of the VCU mouth-throat (MT) model coupled to an airway model up to generation 15 (terminal bronchioles) it was possible to facilitate the prediction of regional drug deposition from DPIs (Longest et al., 2012a; Longest et al., 2012b; Tian et al., 2015a; Tian et al., 2011). Very recently, the CFD modeling technique from those authors was used with the APSD data determined and reported in this chapter to predict regional drug deposition for Budelin Novolizer in both the MT and lung regions (Tian et al., 2015a). Because of the importance of that work to this thesis (Tian et al., 2015a), the paper is reproduced in full in Appendix III. The authors showed that their CFD predictions were consistent with the regional deposition results reported by Newman et al. following a clinical gamma scintigraphy study in which the subjects were instructed to target a 99 L/min peak inhalation flow rate (PIFR) [referred to as *fast* inhalation in this chapter; (Newman et al., 2000)] based on a selection of CFD model regions that were reported to be consistent with the imaging study. In this chapter, the CFD model and programming methods described by Tian and co-workers (Tian et al., 2015a) was applied with modifications and

evaluated for its ability to predict Budelin's regional deposition and the possible variations in the results given different initial conditions for aerosol entry into the trachea in the form of values for $TLD_{in\ vitro}$ and APSDs of $TLD_{in\ vitro}$ coupled to their corresponding breathing maneuvers or IPs. This "hybrid method" eliminates the need to model deposition in the MT geometry, and thus simplifies some of the more complex aspects of the CFD predictions. The semi-empirical results for Budelin were compared with the theoretical values reported earlier (Tian et al., 2015a) and the clinical assessments (Newman et al., 2000).

The motivation behind this study was to combine the new more realistic *in vitro* methods of predicting MT loss and TLD determinations developed in this dissertation together with CFD predictions of regional lung deposition to provide a more complete picture of dose distribution through the lungs. In this approach, the relative strengths of the *in vitro* and CFD methods could possibly be maximized while minimizing the weaknesses. The previous study of Tian et al. (2015a) demonstrated whole-airway CFD predictions of the aerosolized dose from a DPI with good agreement to *in vivo* data. Previous studies have also demonstrated good agreement between CFD predictions of MT depositional loss and *in vitro* predictions in identical geometries across a range of inhalers (Delvadia et al., 2013b; Longest & Hindle, 2009; Longest et al., 2012a; Longest et al., 2012b; Tian et al., 2011). Perhaps the most complex region of the whole-lung CFD calculation of inhaler dose is the MT geometry due to the presence of highly turbulent flow and the need to include transient flow effects (Tian et al., 2011). Furthermore, there are a number of difficult-to-define variables for inhaler aerosol simulations in the MT geometry, such as the exact emptying time course of a DPI for a given inhalation profile. In contrast, the *in vitro* techniques developed in this dissertation can directly predict MT

depositional loss and the particle size distribution entering the lungs on a realistic basis. This study explores a method in which *in vitro* experiments are used to predict the MT deposition fraction and APSD entering the lungs, and CFD simulations are then implemented to investigate regional lung deposition of that TLD. By removing the MT, the CFD simulations are significantly simplified. This reduction in complexity may enable the method to be more widely applied by scientists who do not specialize in CFD simulations. However, it is known that complex airflow currents and turbulence arising from the presence of the inhaler and the MT geometry, including the larynx, can influence flow patterns and particle deposition in the conducting airways, potentially down to the 6th generation (Xi et al., 2008). The extent to which removal of the MT influences regional lung deposition predictions compared with previous CFD simulations (Tian et al., 2015a) and *in vivo* data (Newman et al., 2000) for a DPI aerosol is not known. This study explores this newly proposed hybrid *in vitro*-CFD method with the aim of showing it to be a reasonably accurate new technique for predicting regional lung deposition of pharmaceutical aerosols. As demonstrated in previous studies, these new regional predictions of lung dose may possibly reveal important findings not available from current *in vitro* and imaging methods, such as the aerosol deposition fraction in the terminal bronchioles that are often involved with airway functional changes observed with asthma and COPD.

6.2 MATERIALS AND METHODS

Initial Particle Size Measurements

The APSDs from Budelin® Novolizer® 200 mcg (Meda Pharmaceuticals, Bishops Stortford, U.K.) were characterized using cascade impaction in three different ways: (a) a constant flow rate of 80 L/min (equivalent to a 4 kPa pressure drop across the device) was applied for 3 seconds; this method was used here to provide results for use in Tian et al.'s initial conditions for Budelin (Tian et al., 2015a); (b) a realistic breath profile or IP without an MT model or induction port was employed by linking the inhaler to the NGI via the Nephele Mixing Inlet (NMI; Model III; RDDonline, Richmond, VA); (c) three realistic breath profiles or IPs were used in the presence of the VCU medium MT model as described in Chapter 5. Experimental setups for the three different testing conditions are shown in Figure 6.1.

Methods (a) and (b) were designed to directly measure the APSDs for drugs emitted from the Budelin inhaler. Method (a) provided the initial conditions for use by Tian et al. (2015a) who used the results for APSD to define the particle sizes of the polydisperse aerosols entering the MT geometry of their CFD model. Method (a) was a slight modification of the compendial approach (U.S. Pharmacopeial Convention, 2013), where Budelin was connected directly to the pre-separator in the absence of a USP induction port. An in-house manufactured adapter (Ten-to-One silicone rubber, Micro-Mark, Berkeley Heights, NJ) was placed between the inhaler and preseparator to ensure airtightness of the system. The whole setup was flipped 90 degrees [i.e. preseparator placed horizontally and next generation impactor (NGI) vertically] to ensure correct inhaler

orientation. APSD was tested at 80 L/min to produce the 4 kPa pressure drop across the inhaler, following procedures described in USP (U.S. Pharmacopeial Convention, 2013). Method (b) added the NMI and dilution air supply between the inhaler and the NGI preseparator to enable the inhaler to be tested using a realistic IP. The primary purpose of the experiment was to determine the influence of the IP on this drug's APSD from Budelin, given that compendial test conditions [Method (a)] do not employ a transient (variable) flow rate. The setup was kept similar to Method (a), but the NMI was placed between inhaler and preseparator, with its side port connected to the breath simulator (ASL 5000-XL, IngMar Medical, Pittsburgh, PA) and dilution air supplied at 100 L/min. Method (c) was designed to measure the size distribution for drug aerosols exiting the MT model ($TLD_{in\ vitro}$), as described in Chapter 5. Methods (b) and (c) characterized the APSDs using realistic inhalation profiles for inhaler testing as described in Chapter 5. A schematic and the procedure for Method (c) was the same as that shown in Figure 5.3 and associated text. The three medium IPs described in Table 5.1 and shown in Figure 5.2 (orange curves; Chapter 5) were used for Method (c). These IPs are also shown in Figure 6.2 and they were simulated to represent the average inhalation maneuvers used by the human subjects under three different instruction protocols in the gamma scintigraphy study for Budelin (Newman et al., 2000). Only the medium IP for *fast* inhalation was used for Method (b) while the flow rate through NGI was maintained at 100 L/min for both Methods (b) and (c).

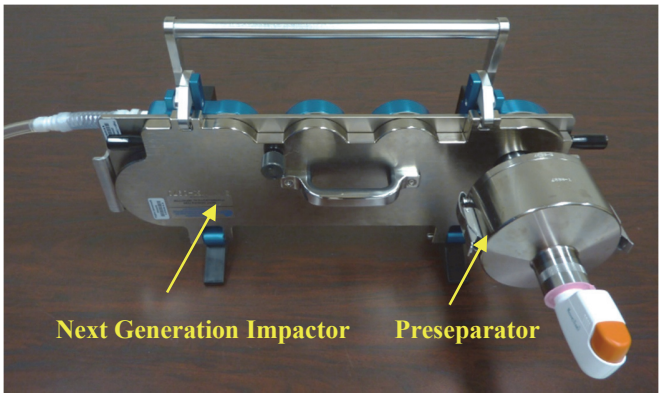

(a) Constant Flow Condition (80 L/min)

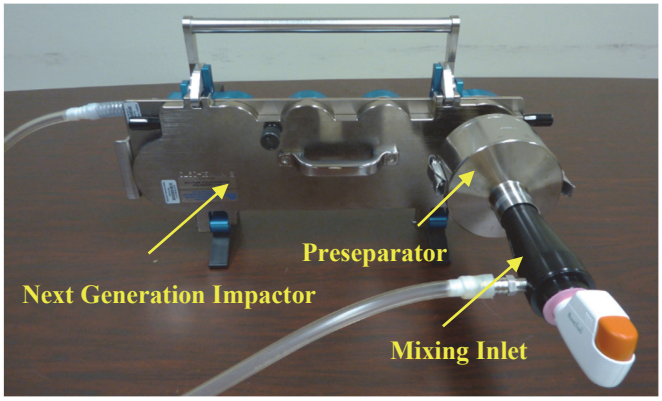

(b) Realistic IP without MT Model

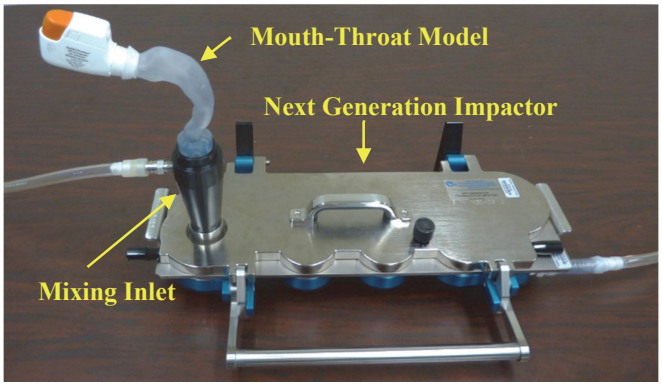

(c) Realistic IP with MT Model

Figure 6.1. Experimental setup for measurement of aerodynamic particle size distributions (APSD) of drug aerosols delivered from Budelin® Novolizer® 200 mcg. (a) Constant flow condition (80 L/min); (b) realistic IP without MT model; (c) realistic IP with MT model. The latter is identical to the apparatus and procedures described in Chapter 5.2.

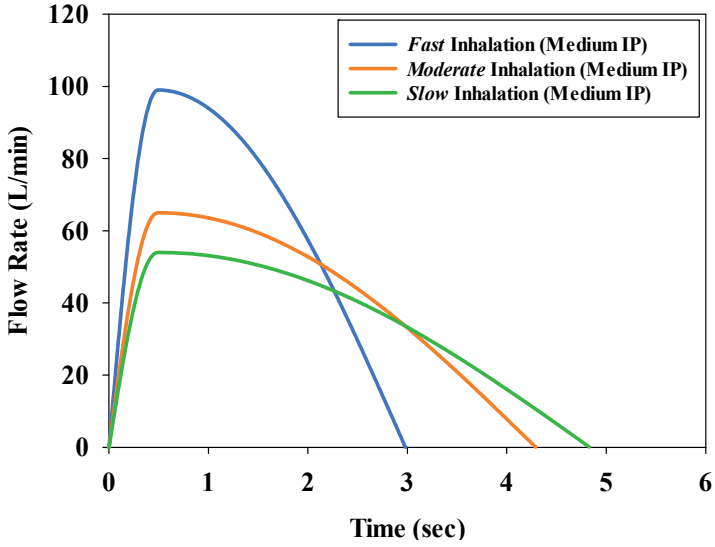

Figure 6.2. Inhalation profiles (IPs) simulated to mimic the average inhalation maneuvers used by subjects under three different instructions in the gamma scintigraphy study for Budelin (Newman et al., 2000). These medium IPs are identical to those described in Table 5.1 and shown in Figure 5.2 (Chapter 5). All three IPs were used for Method (c), while only the medium IP for *fast* inhalation (the blue curve) was used for Method (b). Experimental setups for methods (b) and (c) are shown in Figure 6.1.

Prior to all experiments, internal surfaces of the MT model, preseparator stage, and NGI plates were coated twice with Molykote® 316 silicone release spray (Dow Corning, Midland, MI) to avoid particle reentrainment after impaction. Single doses were collected in each experiment and five replicates performed for each protocol; budesonide deposition on inhaler, MT, NMI, preseparator, NGI plates and filter were collected using known volumes of 70%/30%:methanol/water (v/v), budesonide concentrations were determined using high-performance liquid chromatography (HPLC). The assay was performed using a Symmetry® C18 column (3.5µm, 4.6×100mm) and an HPLC system (Model 2996 Photodiode Array Detector, 1515 Isocratic HPLC Pump and 717 plus Autosampler; Waters Milford, MA) with 69% methanol / 31% 0.1% (v/v) acetic acid buffer (v/v) as mobile phase (flow rate: 1.0 mL/min), and UV detection at 280 nm. Injection

volume was 100 µL and calibration curves were linear in the range of 0.2–10.0 mcg/mL (r^2>0.999). Statistical analyses were performed using one-way ANOVA and Student's t-test at a significance level of 0.05 in JMP Pro 11 (SAS Institute Inc., Cary, NC).

CFD Simulation

The original airway model and CFD methods, designed for simulating particle motion in the human respiratory tract after aerosol release from a powder inhaler, were reported by Tian et al. (2015a). Briefly, the model consisted of a complete upper airway geometry from MT to the third airway bifurcation (B3) followed by a stochastic individual path (SIP) model from B4 to B15 of the left lower lobe (Figure 6.3a) with aerosol introduction into the model simulated via an 0.6 cm diameter jet, as produced by the Budelin Novolizer mouthpiece. To facilitate CFD simulation and prediction of budesonide deposition from Budelin, the model was divided into four parts: MT, B1 to B3, B4 to B7, and B8 to B15; particles penetrating beyond B15 (terminal bronchioles) were shown based on calculations with deposition correlations to fully deposit in the alveolar airways. Airflow appeared to be turbulent in the MT and B1 to B3 regions for the Novolizer, while it transitioned to laminar flow in B4 to B15. In regions where turbulent flow was expected, a low-Reynolds number (LRN) k–ω model was applied to characterize the airflow (Tian et al., 2015a) (e.g. in MT through B3), where realistic, transient IPs were employed. In the lower airways, steady-state flow simulations were used with average flow = V/T (ratio of inhaled volume, V, to total inhalation time, T) condition was applied from B4 to B15. Polydisperse aerosols consisting of nine types of spherical, monodisperse particles with aerodynamic diameters equivalent to the midpoint of NGI's stage cutoff diameters (D_{50})

at 80 L/min flow condition (preseparator, stages 1-7, and filter), were used to represent the budesonide particles delivered from Budelin Novolizer. The method then tracked particles in the airflows after their “injection” as polydisperse aerosols into the mouth inlet over a prescribed quick-and-deep (QD) inhalation profile lasting for 2.96 s. Particles were released during the first 0 - 0.5 s of this inhalation profile, to simulate transient emptying of the inhaler. During the simulation period, particle contact with the wall surface resulted in particle "deposition", and the wall contact location was recorded. Particle deposition data simulated in this way were then compared with the *in vivo* gamma scintigraphy data for Budelin (Newman et al., 2000) (Appendix I) by dividing the airway model into central (B1 to B7) and intermediate–peripheral (B8 to alveolar) regions (Tian et al., 2015a).

The same CFD method, described briefly here and in detail previously (Tian et al., 2015a) was also used in this chapter to track budesonide particles from Budelin Novolizer after their “injection” into the trachea as realistic APSDs known to exit MT, following testing according to Chapter 5. Three replicates were performed for each two-day simulation in this chapter. To couple the CFD simulation with the realistic *in vitro* test methods described in Chapter 5, where APSDs were measured at the exit of MT model, the original airway model and CFD methods (Tian et al., 2015a) were modified in the following ways:

Airway Model

MT and its geometry was removed from the original airway model (Tian et al., 2015a) to allow CFD simulation starting from the trachea (Figure 6.3b). Theoretical “particle injection” began in this study at the trachea after which, CFD modeling used the

programming methods of Tian et al. (2015a). Particles were released into the trachea using a blunt spatial distribution pattern with a wall offset distance of 0.01 mm.

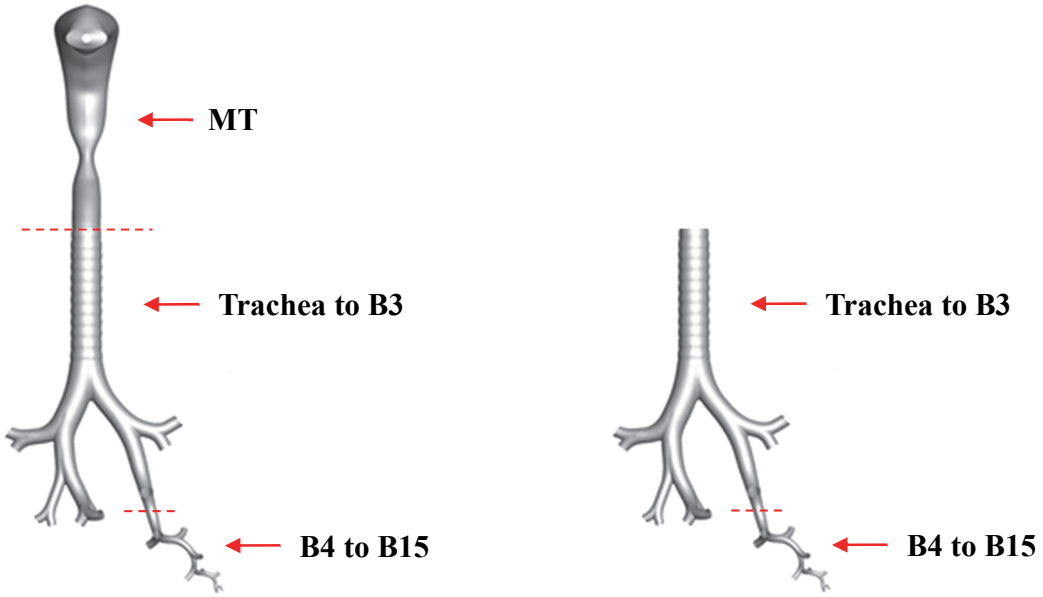

(a) Original Model (Tian et al., 2015a) (b) Modified Model (This Study)

Figure 6.3. Airway model (a) used for CFD simulations in Tian et al. (2015a), which began at the entry to MT via an 0.6 cm jet to represent the inhaler outlet. Simulations in this chapter used the modified model (b) and size distributions of $TLD_{in\ vitro}$. Both models include a complete geometry of the airways from trachea to B3, and a stochastic individual path (SIP) model from B4 to B15 of the left lower lobe; in those respects, the model geometries were identical.

Flow Conditions

The quick-and-deep inhalation profile employed by Tian et al. (2015a) and applied in the trachea to B3 region of that study was refined and replaced by the IPs used to mimic the average inhalation maneuvers of the subject groups trained by Newman et al. (2000) (Figure 6.2) as advocated in Chapter 4 of this thesis. Accordingly, the steady-state (constant) airflow rate applied from B4 to B15 region by Tian et al. (2015a) (60.8 L/min; defined as V/T) was replaced by 63.0 L/min, 41.4 L/min, and 34.4 L/min corresponding to

the average flow rates in the IPs for the *fast*, *moderate*, and *slow* inhalation conditions, respectively (V/T; Figure 6.2) consistent with the values for V reported by Newman et al. (2000).

Polydisperse Particles for Injection

The nine diameters of differently sized particles used in the simulations of Tian et al. (2015a) were replaced by eight monodisperse particle diameters with aerodynamic diameters equivalent to the midpoint of the upper and lower cutoff diameters of NGI's stages at the 100 L/min flow condition (Table 6.1). In the absence of the preseparator [Method (c)], an upper size limit for particles depositing on stage 1 of the NGI had to be assumed; a value of 10 μm was assigned based on the D_{50} value for the NGI preseparator at 100 L/min. These particles sizes (Table 6.1) were used to represent the polydisperse assembly of drug particles entering the trachea during an IP. 4,000 particles were used from each of eight size bins (32,000 particles in total) and "injected" into the trachea inlet over a period of 0–1.0 seconds at an initial velocity = V/(T*A), where V/T was equivalent to the average volumetric flow rate of the test IP and A is the cross sectional area of the tracheal opening. While Tian et al. (2015a) used 0–0.5 seconds for the particle injection period, this was extended in the present study because the "Air Classifier Technology" used by Novolizer was reported to prolong the inhaler's powder dispersion and delivery time (de Boer et al., 2006).

Table 6.1. NGI's stage cutoff diameters (D_{50}) for the 100 L/min flow condition and the corresponding aerodynamic diameters used to simulate the polydisperse aerosol particles for "injection" at the tracheal inlet for CFD simulation in this study.

	In Vitro Particle Size Characterization (NGI at 100 L/min)			Polydisperse Particles for CFD Simulation
	D_{50}[a] (μm)	Size Range (μm)	Midpoint (μm)	Aerodynamic diameter (μm)
Stage 1	6.12	6.12-10.00[b]	8.06	8.06
Stage 2	3.42	3.42-6.12	4.77	4.77
Stage 3	2.18	2.18-3.42	2.80	2.80
Stage 4	1.31	1.31-2.18	1.75	1.75
Stage 5	0.72	0.72-1.31	1.02	1.02
Stage 6	0.40	0.40-0.72	0.56	0.56
Stage 7	0.24	0.24-0.40	0.32	0.32
Filter	0.00	0.00-0.24	0.12	0.12

[a]Calculated using USP calibration method (U.S. Pharmacopeial Convention, 2013)
[b]The upper bound was given by the D_{50} value for the preseparator at 100 L/min

Analysis of Aerosol Deposition Data

Particle counts depositing (e.g intersecting with the airway walls) in each of the regions [MT (Tian et al., 2015a), trachea to B3, B4 to B7, B8 to B15, and beyond B15 (alveolar)] were generated using the CFD program and the techniques were described in detail by Tian et al. (2015a). Particle counts in each bifurcation were converted to mass fraction [defined as deposition fraction (DF) by Tian et al. (2015a)] of the injected "dose" by assuming that particle density and shape were size-independent and mass was

directly proportional to volume and diameter[3]. For example, the deposition fraction of particles in the trachea was given by:

$$DF_{trachea} = \frac{\sum m_j \times \left(N_j \times CF_j\right)}{\sum m_j \times \left(4000 \times CF_j\right)} \quad \text{Equation 6.1}$$

Where m_j is mass of a single particle of budesonide from size bin j and N_j is the number count of the corresponding particles trapped by the trachea. Because an equal number of particles (4,000) were injected from each of the eight size bins, a conversion factor (CF_j) was used to scale the number of particles in the actual APSD that should theoretically be injected; its value was given by:

$$CF_j = \frac{\frac{M_j / m_j}{\sum M_j / m_j} \times 32000}{4000} \quad \text{Equation 6.2}$$

Where M_j is mass fraction of budesonide with respect to the total mass of budesonide in the impactor that deposited at the corresponding NGI stage. Assuming particles were spherical, m_j was given by:

$$m_j = \rho \times \frac{1}{6} \pi d_j^{\,3} \quad \text{Equation 6.3}$$

Where ρ is particle density. Geometric diameter, d_j, was calculated from the aerodynamic diameter (d_{aej}) for the corresponding particle (Table 6.1) from:

$$d_j = \frac{d_{aej}}{\sqrt{\rho}} \quad \text{Equation 6.4}$$

All airway generations were treated similarly and values for regional drug deposition in each airway segment calculated in the same way as described by Tian et al. (2015a).

6.3 RESULTS AND DISCUSSION

Effects of Initial Conditions in the Original CFD Model (Tian et al., 2015a)

The CFD model developed by Tian et al. (2015a) allows particle motion and deposition in the human respiratory tract following aerosol release from a DPI to be simulated based on principles of fluid mechanics and known particle deposition mechanisms (inertial impaction, gravitational sedimentation, and Brownian diffusion). Simulations and particle tracking for Budelin Novolizer in Tian et al. (2015a) include the jet at the inhaler mouthpiece (and retention in the inhaler) in addition to the deposition analysis for polydisperse particles injected into the mouth inlet of the MT and the airway model (Figure 6.3a). Table 6.2 shows an expanded form of Tian's Table III (Tian et al., 2015a) that enables the CFD results from the two different approaches to be compared with the average *in vivo* results from Newman et al. (2000). Stated most simply, the results shown in the right hand column of Table 6.2 (based on realistic testing of Budelin according to the medium simulated IP and an APSD for $TLD_{in\ vitro}$ (as the initial condition for drug entry to the trachea), showed that Tian et al.'s slight underestimation (relative percent difference between *in vivo* and CFD: 2.7%) of Budelin's central lung deposition (Tian et al., 2015a) was further increased (new relative percent difference: 4.8%) by the approach described in this chapter in favor of intermediate and peripheral deposition.

Table 6.2. Deposition fractions (percent of aerosolized dose[a]) based on CFD predictions compared with the mean *in vivo* data for Budelin Novolizer (Newman et al., 2000) operated with a "QD waveform and PIFR of 99 L/min" as defined by Tian et al. (2015a) to mimic Newman's mean PIFR (99 L/min) and V (3.13 L) for normal human subjects trained in *fast* inhalation. The QD waveform of Tian et al. (2015a) was replaced in the present study with the breath-simulated curve shown in blue in Figure 6.2; size distributions for $TLD_{in\ vitro}$ were determined exiting the VCU medium MT model using the same IP. Regional drug deposition data for the *in vitro*–CFD method are presented as mean (SD), n = 3.

Deposition Regions	*In Vivo* (Newman et al.)[b]	CFD (Tian et al.)	*In Vitro*–CFD (This Chapter)
MP+MT	64.9	67.0	64.6
Central Lung[c] (Trachea Excluded)[d]	12.1	9.0	6.9 (0.2)
Intermediate and Peripheral Lung[e]	22.1	22.1	28.5 (0.2)
Trachea–B3 (Trachea Included)		2.7[f]	1.3 (0.1)[f]
B4–B7		8.2	5.6 (0.2)
B8–B15		1.8	2.3 (0.3)
Alveolar		20.3	26.2 (0.1)

[a]As reported in Tian et al. (2015a).
[b]The regional deposition reported by Newman et al. (2000) are percentages of the metered dose and therefore includes drug retained in the inhaler and not aerosolized. This fraction of the dose was not simulated during the CFD studies. In order to determine the *in vivo* deposition as a percentage of the aerosolized dose, the % radioactivity on the device was subtracted from the total recovered radioactivity to determine the total aerosolized dose and the regional deposition values were scaled as a percentage of this value.
[c]The central lung was defined as the B1–B7 region by Tian et al. (2015a). The same approach was applied in this chapter.
[d]Newman et al. (2000) excluded tracheal deposition from their calculations for the lung because swallowing and esophageal radioactivity interfered with the results for tracheal deposition.
[e]The intermediate and peripheral lung was defined as B8–alveolar region by Tian et al. (2015a). The same approach was applied in this chapter.
[f]Tracheal deposition accounted for 1.9% and 0.0% of the metered dose for Tian et al. (2015a) and this study, respectively.

While the exact deposition result breakdown is shown in Table 6.2 for the lung regions of interest for this *fast* mode of inhalation, it is important to realize that the original CFD approach used by Tian et al. (2015a) extended from the mouthpiece of the inhaler using an aerosol APSD that was measured using the modified compendial method (U.S. Pharmacopeial Convention, 2013) described as Method (a) above, where aerosol generation and release was characterized from Budelin at a constant flow of 80 L/min for 3 seconds. This was not the medium realistic inhalation condition for *fast* inhalation proposed for Budelin testing (Figure 6.2). For all passive DPIs, powder deaggregation is believed to be dependent on airflow, where the use of constant flow vs. a realistic IP may affect the APSD of the drug from the inhaler. In addition, the IP used for CFD simulation ["quick-and-deep", or "QD" profile for Budelin Novolizer (Tian et al., 2015a)] was different from that proposed in Chapter 5.2 and employed here in realistic *in vitro* testing (Figure 6.2, *fast* inhalation). Thus, before seeking to study the use of this combined *in vitro*–CFD approach further, it seemed prudent to answer two important questions: (a) to what extent did the APSD exiting the inhaler change from the distribution seen under constant flow, when Budelin was tested with the realistic IP for *fast* inhalation as shown in blue in Figure 6.2? and (b) how did the "QD" profile (Tian et al., 2015a) differ from the test IP employed *in vitro* in this chapter?

The first question was answered by comparing budesonide particle size distributions from Budelin, after testing at the exit of the inhaler under constant flow conditions [80 L/min; Method (a); same data as those used in Tian et al. (2015a)] and variable flow [realistic IP; Method (b)]. Data are summarized in Figure 6.4.

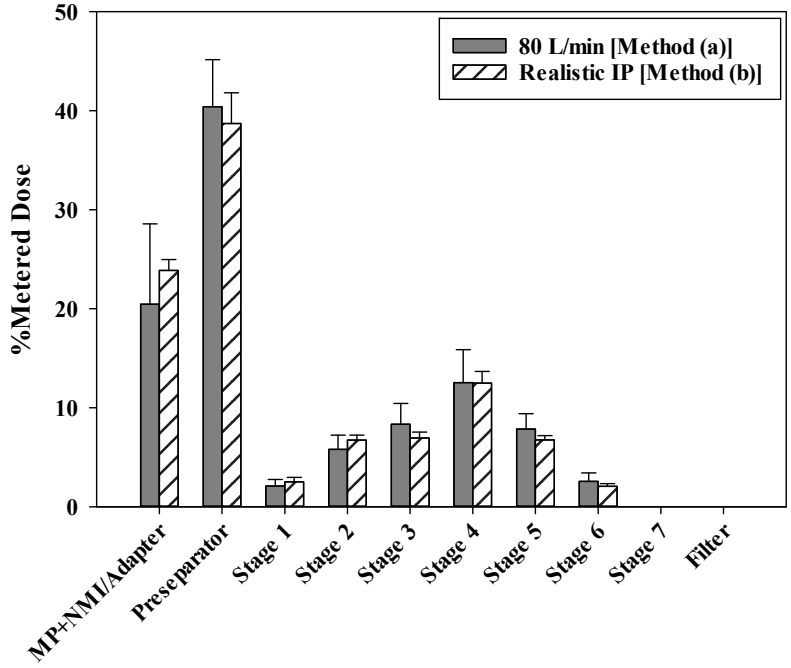

Figure 6.4 Distribution (percent of metered dose) of budesonide from Budelin Novolizer when tested in accord with Method (a) and (b), respectively [constant flow (80 L/min) or the medium simulated IP for *fast* inhalation (Figure 6.2)]. Data are presented as mean±SD (n = 5). The data generated from Method (a) in this study was used for CFD predictions in Tian et al. (2015a). The NGI flow rate employed in Method (b) was 100 L/min. MP = inhaler mouthpiece; NMI = Nephele Mixing Inlet. Total drug mass collected before (MP + NMI/adapter) or within (preseparator + stages 1–7 + filter) the cascade impactor were statistically comparable (Student's t-test, $p>0.05$) in both cases. Note that the cutoff diameters for each stage of NGI differ between the tests shown in this Figure because D_{50} values are a function of the air flow rate through NGI.

There was no significant difference in the total mass fraction collected before (MP + NMI/adapter) or within (preseparator + stages 1–7 + filter) the cascade impactor between the two methods (Student's t-test, $p>0.05$). The data from the cascade impactor was processed according to USP (U.S. Pharmacopeial Convention, 2013) and plotted as cumulative % drug mass undersize to enable the APSDs determined at the different NGI flow rates to be compared. Figure 6.5 showed, for Budelin Novolizer that the APSDs for budesonide following testing using a realistic IP (Figure 6.2) or, a constant flow rate of 80 L/min for 3 seconds produced results that were effectively identical (Figure 6.5).

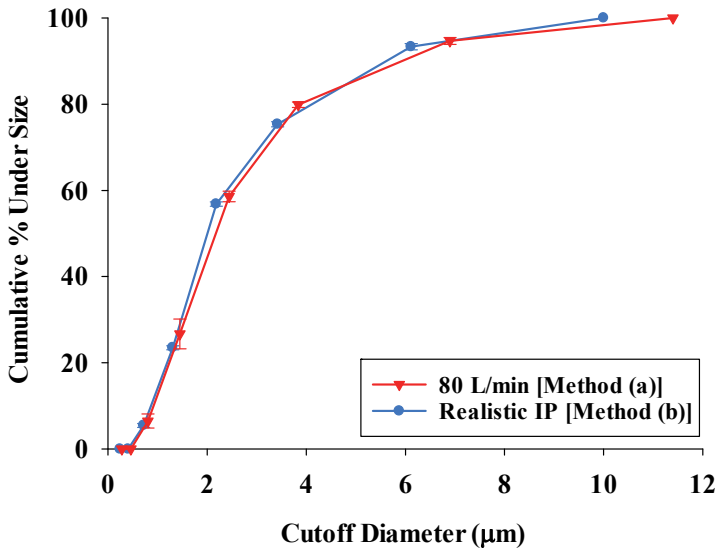

Figure 6.5. Mean cumulative % mass under size (±SD; n = 5) vs. NGI stage cutoff diameters (D_{50}) for drugs delivered from Budelin Novolizer at constant flow [80 L/min; method a; data used in Tian et al. (2015a)] and the test IP [Method (b)]. Size distributions are based on analysis of drug deposition within the NGI, and the cutoff diameters for NGI's stages and the preseparator were adjusted during size analysis in accord with USP's archival flow calibration (Marple et al., 2003a; U.S. Pharmacopeial Convention, 2013).

A further investigation compared the IP used by Tian et al. ["QD" profile; (Tian et al., 2015a)] to that used for realistic *in vitro* testing (Figure 6.2; *fast* inhalation) in this chapter. Figure 6.6 shows that the two IPs differed with respect to the air flow rate acceleration (linear vs. sinusoidal) but overall, the profiles were very similar. This agreement is because both studies attempted to match the fast inhalation conditions of Newman et al. (2000), but with slightly different value assumptions and profile equations (e.g., linear vs. sinusoidal inhalation). It is not clear from the data that Newman et al. provided which of these inhalation profiles is most correct.

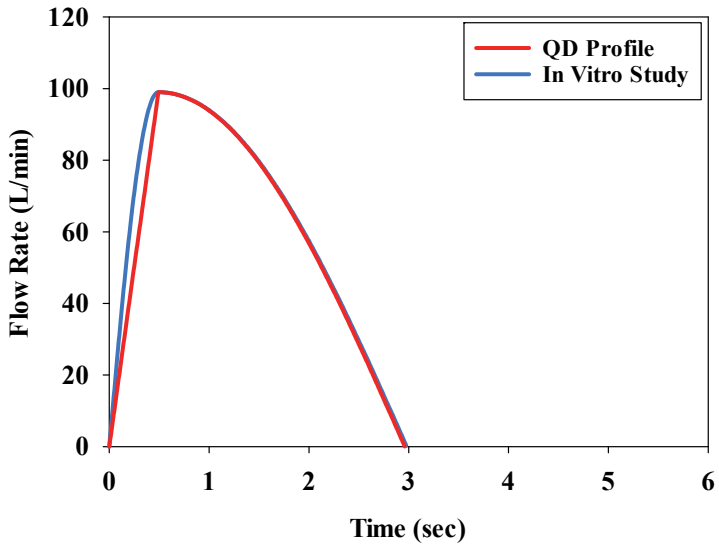

Figure 6.6. IPs simulated to represent those used by subjects trained by Newman et al. (2000). The red curve was reproduced from the "QD" profile reported by Tian et al. (2015a); the blue curve was used for realistic testing in the *in vitro* study (Figure 6.2, *fast* inhalation).

Based on these comparisons of Budelin's APSDs and IPs used in testing, it seemed reasonable to assume that comparable CFD results should be generated for regional deposition within the lung if we were to replace the APSD and IP reported by Tian et al. (2015a) with those advocated for realistic *in vitro* testing in this thesis (*fast* inhalation; Chapters 5 and 6). The results in Table 6.2 however, show small but finite differences in the CFD results for the individual segments. Trachea to B3 and B4 to B7 showed reduced deposition compared to the results of Tian et al. (2015a) while deposition in B8 to B15 and the "Alveolar" remainder were increased. The reduced deposition seen in the trachea itself [0.0% in the present study vs. 1.9% in Tian et al. (2015a); Table 6.2] likely points to the importance of particle trajectories at the tracheal entry point. In the present study, reduced particle impaction efficiencies were expected when particles were introduced vertically into the trachea compared to the flow curvature seen when the MT

was attached (Tian et al., 2015a). In addition, the exclusion of the larynx in Model (b) (Figure 6.3) may have eliminated the effects of the laryngeal jet on air turbulence and aerosol dynamics (Xi et al., 2008), resulting in an underestimation of aerosol deposition in the large airways. Another possible difference between the present study and that of Tian et al. (2015a) relates to the injection of particles in an accelerating transient flow over 0.5 seconds (Tian et al., 2015a) vs. an accelerating and plateauing flow over 1.0 second (this study; see Figure 6.6). A difference that may also be significant relates to the assignment of particle sizes introduced into the two models to "represent" and compute the deposition of the polydisperse budesonide aerosols released from Novolizer. Because of the difference in NGI flow rates that must be used to size the aerosols leaving the inhaler [e.g. 80L/min; Method (a) in Tian et al. versus 100 L/min; Method (c) in realistic testing], the midpoint of the size bins used to represent large particles in each of the CFD simulations differed. The difference in individual particle mass between the CFD-assigned diameter for particles landing on stage 1 of the NGI at 100 L/min (this study) could be about 5/7 ($8.06^3/9.15^3$) of the individual particle mass that was used in Tian et al. (2015a) and this may be expected to influence computed values for upper airway deposition.

APSDs of Budesonide Particles Entering Trachea

Budesonide particle size distributions at the exit of the MT were measured with Method (c) using the three IPs shown in Figure 6.2. Those IPs were simulated to mimic the average inhalation maneuvers of subjects trained under the three different breathing instructions in the gamma scintigraphy study for Budelin Novolizer (Newman et al., 2000). The medium IP for *fast* inhalation (the blue curve in Figure 6.2) was selected to match the

flow condition used in the CFD simulation by Tian et al. (2015a); that IP and the associated APSD of the drug exiting MT were used as initial conditions for the modified CFD model to evaluate whether the predicted regional drug deposition results were comparable with those produced by Tian et al. (2015a) as shown in Table 6.2. The medium IPs for *moderate* and *slow* inhalation (the orange and green curves in Figure 6.2, respectively) and their associated APSDs were used to further evaluate the method's ability to predict variations in regional drug deposition in the lung. Because only the medium airway model is currently available for CFD simulation, the small and large IPs and APSDs of Budelin's $TLD_{in\ vitro}$ produced from the small MT-IP and large MT-IP combinations (Chapter 5) were not studied or discussed in this chapter.

APSDs of budesonide aerosols exiting the MT for the mean *fast*, *moderate* and *slow* inhalation conditions are summarized in Figures 6.7 and 6.8. The three medium IPs in Figure 6.2 produced significantly different results for budesonide mass depositing in MT and on NGI stages 1, 3, 4, 5, and 6 (one-way ANOVA, $p<0.05$; Figure 6.7). The data from NGI was also processed according to USP (U.S. Pharmacopeial Convention, 2013), and the cumulative percent mass under size vs. NGI's stage cutoff diameters in Figure 6.8 clearly illustrate the variations in the APSDs of drugs likely to enter the trachea across these inhalation conditions. Values for the mass median aerodynamic diameters (MMAD) ranged from 1.88±0.06 μm for *fast* inhalation, to 2.19±0.04 μm for *moderate* inhalation, and 2.54±0.09 μm for *slow* inhalation.

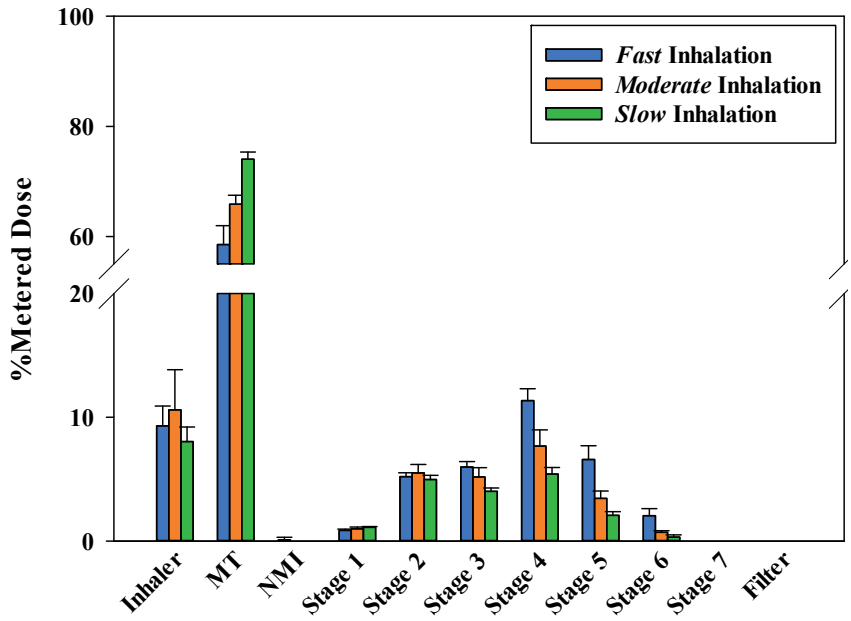

Figure 6.7. Distribution (percent of metered dose) of budesonide from Budelin Novolizer when tested in accord with Method (c) using IPs shown in Figure 6.2. Data are presented as mean±SD (n = 5). The NGI flow rate employed in this method was 100 L/min. MT = mouth-throat; NMI = Nephele Mixing Inlet. Significantly different values were observed for drugs depositing in MT and on NGI stages 1, 3, 4, 5, and 6 across the three inhalation conditions (one-way ANOVA, $p<0.05$).

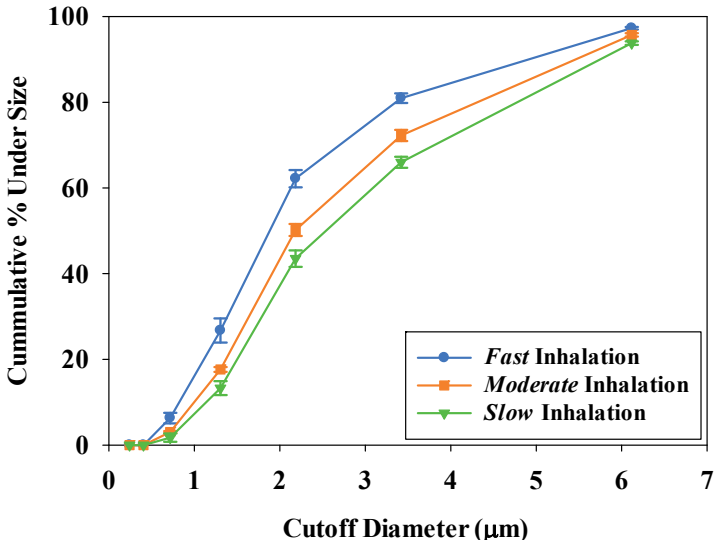

Figure 6.8. Mean cumulative percent mass under size (±SD; n = 5) vs. NGI stage cutoff diameters (D_{50}) for budesonide particles exiting MT when tested with Method (c) using IPs shown in Figure 6.2. Values for D_{50} (stage cutoff diameters) were plotted for the 100 L/min airflow test condition in accord with USP's archival flow calibration (Marple et al., 2003a; U.S. Pharmacopeial Convention, 2013).

Aerosol Deposition Results

Whole-Airway CFD Methods vs. Combined In Vitro–CFD Methods

One purpose of this chapter was to evaluate whether the CFD model and programming methods developed by Tian et al. (2015a), in which deposition was also modeled in MT, could be modified and coupled to the realistic *in vitro* test methods described in Chapter 5. The main differences between the two methods were the aerosol particle injection site at which particle tracking begins and their associated APSDs, and the effects of the existence or absence of the laryngeal jet on air turbulence and flow profiles entering the trachea. Given the absence of significant differences between the aerosol that enters a theoretical MT from Budelin in Tian et al. (2015a) and that entering the model MT (Figures 6.4 and 6.5), as well as the use of comparable IPs in both cases (Figure 6.6), Tian et al.'s CFD predictions for MT deposition (Tian et al., 2015a) should compare well with those seen experimentally with the caveats noted in the discussion above. Indeed, the percent of the drug dose depositing in MT and the inhaler from both techniques appeared to be comparable with the *in vivo* results for *fast* inhalation as shown in Table 6.2. There were discrepancies however. The APSD data used in the CFD simulations in both cases is presented in Figure 6.9a where the difference between the curves should represent MT deposition; this experimental data, and the CFD data on file from Tian et al. (2015a) enabled computation of the CFD-predicted APSD for MT deposition that in turn enabled computation of the theoretical APSD entering the trachea according to Tian et al. (2015a) (Figure 6.9b; red curve). While the curves were broadly similar at aerodynamic diameters ≤9 μm, the discontinuity in the red profile at approximately 11 μm indicated the injection of almost 5% of the dose into the trachea as

large particles in Tian et al. (2015a). This difference in APSD entering the trachea between the two methods appeared to justify the experimental determination of both $TLD_{in\ vitro}$ and the APSD of the aerosols exiting MT and entering the trachea. This being said however, it is quite possible that variations within and between inhalers (as well as the use of the mixing inlet as a conduit to NGI) may also contribute to the apparent reduction seen in large particles exiting MT when realistic testing was employed.

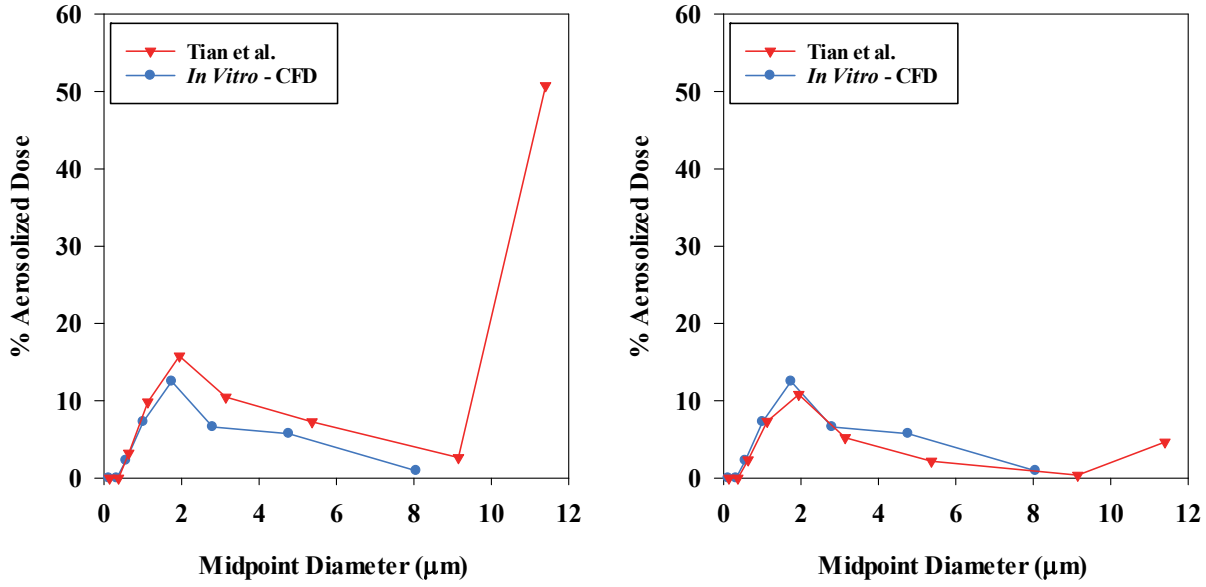

Figure 6.9. (a) APSD data used in CFD simulations for *fast* inhalation by Tian et al. (2015a) and in this chapter (particles introduced into trachea). These data were produced experimentally using Methods (a) and (c) described above. (b) APSD data for aerosols exiting the MT model. *In vitro*–CFD results (blue curve) are identical to those shown in the left panel. Results from Tian et al. (2015a) (red curve) were computed from the CFD results of Tian et al. (2015a) by subtracting the predicted MT deposition for *fast* inhalation (Tian, 2015). Data are presented as the mean percent of the metered dose vs. the midpoint of the upper and lower stage cutoff diameters at the designated flow rates in the fashion of Tian et al. (2015a).

Variations in Regional Drug Deposition in the Lung

To evaluate the ability of the *in vitro*–CFD method as a means of predicting variations in regional drug deposition in the airways, additional CFD studies were performed using different IPs and APSDs for Budelin's $TLD_{in\ vitro}$ and introducing these to the trachea of the modified airway model (Figure 6.3b). IPs were simulated to mimic the subject groups' *moderate* and *slow* inhalation conditions as described by Newman et al. (2000) (Figure 6.2); these IPs were paired with the mean APSDs produced using Method (c) [presented as the mean percent of the aerosolized dose depositing on a selected stage vs. the midpoint of the upper and lower stage cutoff diameters at the designated flow rates in the fashion of Tian et al. (2015a) as shown in Figure 6.10] and used as initial conditions for CFD simulations. Regional lung deposition results were compared across all three inhalation conditions (*fast*, *moderate*, *slow*) and also with the *in vivo* lung deposition data reported by Newman et al. (2000) in Figure 6.11 and Table 6.3.

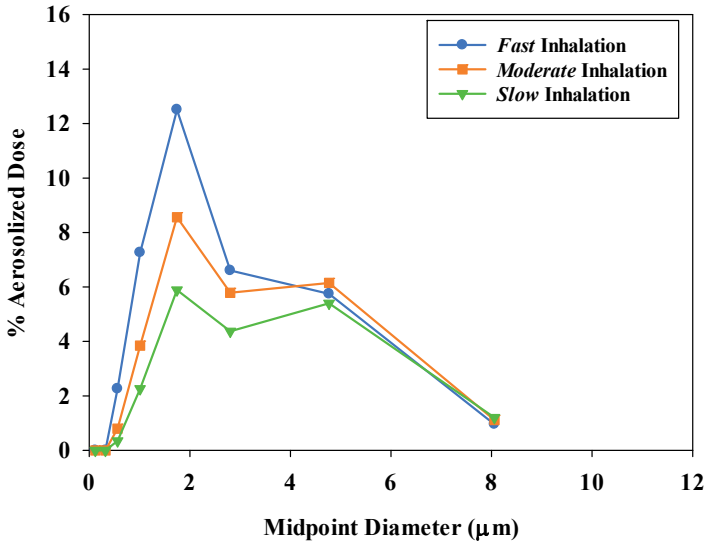

Figure 6.10. APSD data for the CFD simulations used for *fast*, *moderate* and *slow* inhalation conditions. Data are presented as the mean percent of the aerosolized dose depositing on a selected stage vs. the midpoint of the upper and lower stage cutoff diameters at the designated flow rates in the fashion of Tian et al. (2015a). These experimental results were calculated from the data shown in Figures 6.7 and 6.8 and produced using Method (c).

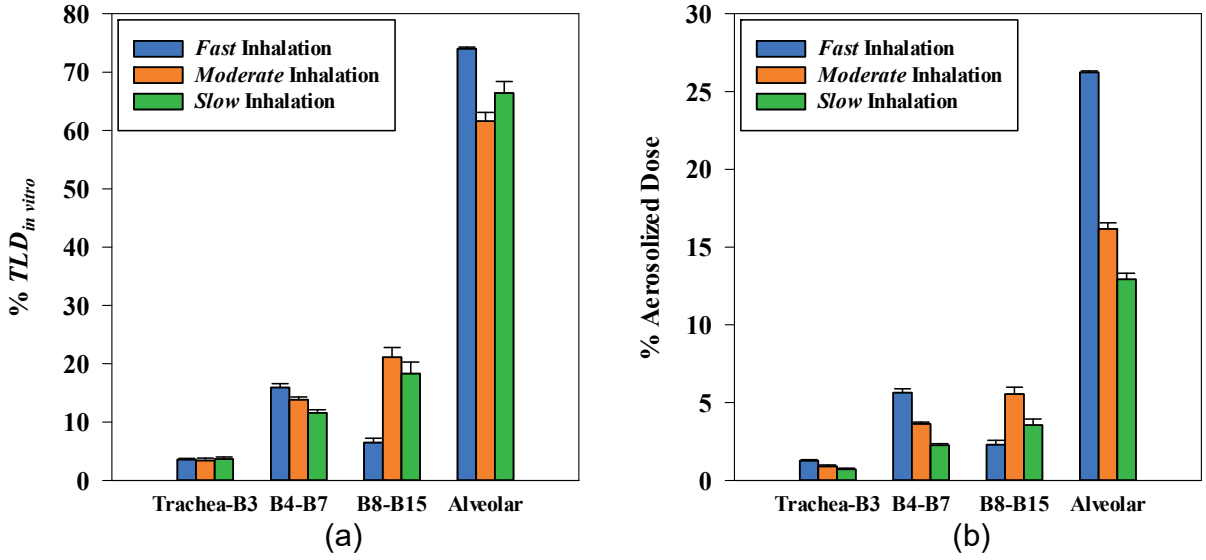

Figure 6.11. Regional drug deposition in the lung model as predicted using the *in vitro*–CFD approach for *fast*, *moderate* and *slow* inhalation conditions. Data are presented (a) as % total lung dose *in vitro* ($TLD_{in\ vitro}$; ±SD; n = 3) and (b) as % aerosolized dose (±SD; n = 3) for budesonide from Budelin Novolizer depositing theoretically at trachea to B3, B4 to B7, B8 to B15, and alveolar (>B15) regions of the modified lung model (Figure 6.3b). Significant differences were observed for the percent of $TLD_{in\ vitro}$ depositing in the B4 to B7, B8 to B15, and alveolar regions across the three inhalation conditions (one-way ANOVA, $p<0.05$).

Table 6.3. Deposition fractions (percent of aerosolized dose[a]) based on *in vitro*–CFD predictions compared with the mean *in vivo* data for Budelin Novolizer (Newman et al., 2000) operated with the three breath simulated curves shown in Figure 6.2; size distributions for $TLD_{in\ vitro}$ were determined exiting the VCU medium MT model using the same IPs. Regional drug deposition data for the *in vitro*–CFD method are presented as mean (SD), n = 3.

Deposition Regions	*Fast* Inhalation[b]		*Moderate* Inhalation		*Slow* Inhalation	
	In Vivo[c]	*In Vitro*–CFD	*In Vivo*[c]	*In Vitro*–CFD	*In Vivo*[c]	*In Vitro*–CFD
MP+MT	64.9	64.6	71.0	73.7	75.6	80.5
Central Lung[d] (Trachea Excluded)[e]	12.1	6.9 (0.2)	9.0	4.5 (0.1)	7.8	3.0 (0.0)
Intermediate and Peripheral Lung[f]	22.1	28.5 (0.2)	19.3	21.7 (0.1)	16.4	16.5 (0.0)
Trachea–B3 (Trachea Included)		1.3 (0.1)[g]		0.9 (0.1)[g]		0.7 (0.1)[g]
B4–B7		5.6 (0.2)		3.6 (0.1)		2.3 (0.1)
B8–B15		2.3 (0.3)		5.5 (0.4)		3.6 (0.4)
Alveolar		26.2 (0.1)		16.2 (0.4)		12.9 (0.4)

[a]As reported in Tian et al. (2015a)
[b]Data for *fast* inhalation are identical to those shown in Table 6.2.
[c]The regional deposition reported by Newman et al. (2000) are percentages of the metered dose and therefore includes drug retained in the inhaler and not aerosolized. This fraction of the dose was not simulated during the CFD studies. In order to determine the *in vivo* deposition as a percentage of the aerosolized dose, the % radioactivity on the device was subtracted from the total recovered radioactivity to determine the total aerosolized dose and the regional deposition values were scaled as a percentage of this value.
[d]The central lung was defined as B1–B7 region by Tian et al. (2015a) and the same approach was applied in this chapter.
[e]Newman et al. (2000) excluded the tracheal deposition from their calculations for the lung because swallowing and esophageal radioactivity interferes with the tracheal count.
[f]The intermediate and peripheral lung was defined as B8 to alveolar region by Tian et al. (2015a) and the same approach was applied in this chapter.
[g]CFD-predicted tracheal deposition accounted for 0.0% of the metered dose for all three inhalation conditions.

Budesonide aerosol deposition in trachea to B3, B4 to B7, B8 to B15, and alveolar (>B15) regions are summarized as %$TLD_{in\ vitro}$ in Figure 6.11a. For all three inhalation conditions, <5% of $TLD_{in\ vitro}$ deposited in trachea to B3, while the majority (>60% of $TLD_{in\ vitro}$) deposited in the alveolar region. When comparing the regional deposition of $TLD_{in\ vitro}$ across the three inhalation conditions, significant differences were observed for B4 to B7, B8 to B15, and alveolar (one-way ANOVA, $p<0.05$), suggesting that the combination of subjects' IPs and the associated APSDs in this study affected the regional drug deposition of the likely lung dose in each case. The effect was most pronounced for the *fast* inhalation condition, where much lower deposition was observed in B8 to B15 (and much higher deposition in alveolar) than those for the *moderate* and *slow* inhalation conditions, indicating the importance of the smaller aerosol produced during *fast* inhalation (Figure 6.8). Aerosol deposition data are also presented as % aerosolized dose in Figure 6.11b and Table 6.3 to evaluate the likely variations in regional drug dose in the lung. In general, *fast* inhalation produced the highest theoretical deposition in trachea to B3, B4 to B7 and the alveolar regions, but the lowest deposition in B8 to B15 among these three inhalation conditions. When comparing these data with the *in vivo* lung deposition results (Newman et al., 2000), we again found that the combined *in vitro*–CFD approach [when coupled with the airway mapping technique developed by Tian et al. (2015a)] appeared to underestimate drug deposition in the central lung and overestimate delivery to the periphery. However, because the fraction of peripheral overlap of the central airways assigned by gamma scintigraphy is unknown, a direct comparison between CFD prediction and two-dimensional (2D) scintigraphy has limitations. Future studies may be needed therefore, before making firm conclusions about the validity of either of approach.

Overall, theoretical regional drug deposition predicted using *in vitro* results coupled to the modified CFD model [Figure 6.1c coupled with Tian et al.'s CFD programming method (Tian et al., 2015a) in the modified lung model] were compared with those reported by Tian et al. (2015a) for *fast* inhalation and the *in vivo* data of Newman et al. (2000) for *fast*, *moderate* and *slow* inhalation. For ease of comparison with Tian et al. (2015a), Table 6.2 and 6.3 were constructed in the fashion of (Tian et al., 2015a). Both methods produced comparable results with the *in vivo* deposition data for *fast* inhalation (Newman et al., 2000) for drug retention on the inhaler and MT ("MP+MT"). To compare the regional lung deposition results based on CFD simulation with the *in vivo* data, Tian et al. (2015a) defined B1 to B7 as the central lung and B8 to alveolar as the intermediate and peripheral lung and used these regions to compare to those defined by Newman et al. (2000). This was based on using the lung division method of Newman et al. (2000) and applying it to the SIP CFD-based lung model. These same definitions were used in this chapter. The CFD methods used by Tian et al. (2015a) showed lower deposition in the central lung and higher deposition in the intermediate and peripheral lung than the published *in vivo* results (Newman et al., 2000) (Table 6.2), but a general trend of agreement between *in vivo* and *in vitro*–CFD results was seen to occur as the IP slowed from "*fast*" through "*slow*" inhalation (Table 6.3). Tian et al. (2015a) suggested that their underestimation of central lung deposition (which was within 10% relative error of the *in vivo* results) could be due to its overestimation by 2D gamma scintigraphy [because a significant fraction of the peripheral airways are captured in the central region by scintigraphy]. Their explanation is highly plausible. The "underestimation" of budesonide's central lung deposition seen by Tian et al. (2015a) was magnified by the combined *in*

vitro-CFD approach described here, in large part because of the absence of air turbulence introduced by the laryngeal jet (Xi et al., 2008) and values assigned for the APSD of each $TLD_{in\ vitro}$ (Figure 6.9b and 6.10) as aerosols entering the trachea.

In practice, the regional airway deposition of aerosols delivered from inhalers is known to be difficult to assess clinically. Extensive overlap between the central and peripheral airways can be expected when the three-dimensional (3D) lung geometry is projected onto the 2D plane in gamma scintigraphy studies. Schroeter et al. (2005) developed a 3D airway model using human morphological data and quantified the composition of different airways in the central, intermediate and peripheral lung (as those defined in gamma scintigraphy studies) by superimposing those regions on the planar view of their model. They found that over 18% of alveolar airways (>B17 in Schroeter et al.'s model) were captured in what appeared to be the central lung, and that these airways comprised about 80% of the total volume of airways in that region (Schroeter et al., 2005). Given that a large proportion of budesonide aerosols (>60% of TLD; Table 6.2) were predicted to deposit in the alveolar region (>B15) using both CFD methods discussed here, it appears to be necessary to account for a significant "peripheral fraction" appearing as central deposition when comparing results from CFD airway modeling with *in vivo* data from gamma scintigraphy.

6.4 CONCLUSION

A new technique was developed and evaluated to combine the realistic *in vitro* test methods described in Chapter 5 and a CFD model to maximize the strengths of both approaches in predicting total and regional drug deposition in the lung. Results for theoretical regional drug deposition in the airways were evaluated for the powder inhaler, Budelin Novolizer 200 mcg, under three inhalation conditions using this hybrid *in vitro*–CFD approach. Variations in results for drug deposition indicated that IPs and the APSDs of $TLD_{in\ vitro}$ appeared to affect drug deposition in the MT and airways of a model human adult respiratory tract. While future studies may be needed to incorporate variations in airway geometries across a population as well as effects of age and disease on those geometries, the combined approach appeared to show promise for predicting aerosol deposition in the lung. While changes in the inhalation profiles used by subjects using powder inhalers appeared likely to modify the dose of drug reaching the lung and its deposition across the airways, the model appeared to indicate that most of the dose from Budelin that escapes the MT region, was likely to reach beyond generation 15 into the lung periphery. This result indicated that the fraction of “peripheral deposition” that is usually reported in gamma scintigraphy studies is disproportionally low; a proportion of the counts usually attributed to deposition in the “central region” of the lung should be shifted to the periphery to allow for the presence of significant numbers of small (peripheral) airways that overlay the “central regions” in 2D lung scintigraphs.

CHAPTER 7

SUMMARY AND CONCLUSIONS

Realistic *in vitro* testing of inhaled drug products, coupling human mouth-throat (MT) models and inhalation profiles (IP) to allow drug aerosol generation from an inhaler and transport into the human respiratory tract to be mimicked under clinically-relevant conditions, has shown its potential in establishing *in vitro–in vivo* correlations (IVIVCs) for drug doses likely to enter the lung (TLD). The application of this approach however, remains challenging and scientists are left to decide which MT model(s) to choose and how to select representative IP(s). Furthermore, regional drug deposition in the lung remains unclear, although studies have shown that the deposition site of inhaled drugs may well be relevant to their therapeutic effects (Anderson & Newman, 2009; Usmani, 2015; Usmani & Barnes, 2012; Usmani et al., 2005). This dissertation describes the continuing research to develop realistic *in vitro* performance test methods for dry powder inhalers (DPI), with efforts to standardize and improve the existing DPI test methods to (a) enable the use of realistic *in vitro* tests by drug development scientists and regulators, and (b) explore the truth about the ranges of the aerodynamic particle size distributions (APSD) of drugs that are likely to enter the lung ($TLD_{in\ vitro}$) of healthy human adults from a marketed DPI. These goals were achieved through the four specific aims described in Chapter 2. In brief, these were: (i) select representative MT models for realistic *in vitro*

testing of DPIs; (ii) develop a general method for simulating the ranges of IPs for use with a DPI of known airflow resistance; (iii) develop methods for measuring APSDs of Budelin's $TLD_{in\ vitro}$ across different ranges of IPs; (iv) couple computational fluid dynamic (CFD) simulations with realistic *in vitro* testing techniques to predict regional lung deposition of budesonide aerosols from Budelin® Novolizer®. All these aims were achieved and the results presented in Chapters 3–6 were consistent with the accompanying hypotheses (Chapter 2).

The methods of selecting representative MT models for realistic *in vitro* testing were described in Chapter 3. Three main types of realistic MT models [the small, medium and large Virginia Commonwealth University (VCU) models, the small, medium and large Oropharyngeal Consortium (OPC) models, and the medium Alberta Idealized Throat (AIT)] were included in the study because those are commercially available and have been reported to produce IVIVCs with certain inhalers. The USP induction port was also included as a pharmacopeial control. A study was designed to evaluate the effect of MT model geometry on drug aerosol retention under realistic human inhalation conditions. This was accomplished by testing the eight, internally-coated MT models across a range of realistic IPs with Salbulin® Novolizer®. The models produced different values for $TLD_{in\ vitro}$ and most notably, the three medium MT models (VCU, OPC, AIT) did not show statistically comparable results. Interestingly however, the USP induction port produced comparable results with VCU and AIT models when tested with Salbulin in this study perhaps indicating some geometric similarities between those realistic MT models and the standardized USP induction port employed routinely for quality control of inhalers. Although we have yet to identify which medium MT is most "representative", as these

models were designed based on different philosophies and no clinical lung deposition data for Salbulin are available for evaluating its *in vitro* properties, the study suggested that caution should be applied when using different MT models to predict $TLD_{in\ vivo}$. A further implication of this study, and one that is perhaps more important, is that it may be necessary to incorporate both the variations in MT geometries and IPs when testing inhalers. The present study showed that the VCU and OPC models produced much larger ranges for $TLD_{in\ vitro}$ than the single medium AIT model and the USP induction port. Based on the previous studies (Delvadia et al., 2012; Olsson et al., 2013) that clinical variations seen in lung deposition could be accounted for by coupling the extremes of MT geometry with expected ranges of IPs, both the VCU and OPC models appeared to produce realistic variations in $TLD_{in\ vitro}$. While the practical advantages of the VCU models overweighed their disadvantages for the purposes of this thesis, future studies may be needed to test these realistic MT models across different inhalation systems (e.g. MDIs, Respimat®) and formulations (e.g. solution-based vs. suspension-based MDIs), before selecting the most representative MT models. In addition, CFD simulations may be applied to further our understanding of the flow and aerosol behaviors in these different MT geometries.

Chapter 4 describes the methods of selecting and simulating the range of representative IPs for use when testing a DPI with known airflow resistance. This study was designed to enable drug development scientists to select IPs for a new DPI *a priori* and predict inhaler performance in the clinic using realistic *in vitro* testing techniques. To achieve this goal, inhalation profile data from an existing VCU clinical trial (Delvadia, 2012) were reanalyzed, where a group of inhaler-naïve, mixed-gender, healthy human adults were trained (a) by leaflet reading and (b) by professional instruction to inhale through a

range of airflow resistances (R) typical of those used in commercial DPIs. Elaborate statistical analyses were performed by Delvadia (2012) and peak inhalation flow rate (PIFR) was found to have a linear correlation with 1/R, while time to reach PIFR (T_{PIFR}) and inhaled volume (V) did not show significant correlations with R. Based on those analyses, three equations were derived for PIFR as a function of R from the pooled data to enable the 10, 50 and 90 percentile values to be predicted for a DPI of known airflow resistance for each training status. Because T_{PIFR} and V were independent of R, their 10, 50 and 90 percentile values could be selected from the cross-gender data regardless of the DPI resistance. These statistically-derived inhalation variables allowed representative IPs and their realistic variations to be simulated using sinusoidal equations derived from curve fitting of the subjects' IPs (Chapter 4 and Appendix IV). The study provided a general method of selecting standard IPs for use in realistic *in vitro* tests of DPIs during the drug development process. Although the data analyses were based on profiles collected from healthy adults of both genders, and this was because clinical trial usually begins with healthy subjects or largely asymptomatic patients, the method is likely to be extended to select representative IPs and their likely variations for target patient groups (e.g. asthma patients, COPD patients) or age groups (e.g. pediatric patients, elderly patients). The data also showed clearly that professional training affected the subject group's inhalation maneuvers. This was consistent with reports in the literature (Azouz et al., 2015a; Azouz et al., 2015b). To fully evaluate DPI performance *in vitro*, it may be necessary to include IPs representative of patients who are "insufficiently trained" in the sense that they are left to figure out themselves how to use their inhalers. In addition, IPs

for other inhalation systems (e.g. MDIs, MDIs with spacers, Respimat®) may need to be collected and generalized to standardize realistic *in vitro* tests for those inhalers.

The selection of representative MT models and IPs enabled realistic *in vitro* test methods for DPIs to be developed further, to characterize the likely ranges of APSDs for $TLD_{in\ vitro}$ from Budelin® Novolizer® across different inhalation conditions (Chapter 5). The realistic *in vitro* test methods described in Chapters 3 and 4 were coupled to the compendial cascade impactor methods (U.S. Pharmacopeial Convention, 2013) by using the Nephele Mixing Inlet (NMI) supplied with dilution air to maintain constant airflow through a Next Generation Impactor (NGI). The modified test method enabled APSDs for the *in vitro* lung dose to be determined across a complete range of realistic IPs. To evaluate the method's ability to predict inter-subject variabilities in total and regional lung deposition, the small, medium and large VCU MT models were paired with the three sets of small, medium and large simulated IPs to mimic those used by subjects in the gamma scintigraphy study used with the inhaler that became Budelin® Novolizer® (Newman et al., 2000). Because the NGI was operated outside its specific flow range, over which the archival calibration is known to function (15–100 L/min), additional studies were designed to assess the validity of the theoretical stage cutoff diameters when these were calculated according to USP at high flow rate. Four sets of MT-IP combinations were tested at 100 and 140 L/min NGI flow conditions; the former was used as the calibration standard to recalibrate NGI's stage cutoff diameters at 140 L/min by curve fitting. An important observation from this study is that Budelin Novolizer, the DPI known to deliver consistent doses when subjected to USP testing (U.S. Pharmacopeial Convention, 2013), showed significant variations in lung dose *in vivo* (Newman et al., 2000); when realistic *in vitro*

tests were conducted and variations in MT geometries and IPs were accounted for, the inter-subject variabilities in the *in vivo* lung doses were likely to be predicted. IVIVCs were observed for all three inhalation conditions and this again revealed and confirmed the importance of incorporating MT geometry and IP variations in realistic *in vitro* tests of DPIs. Further analyses of the APSDs of Budelin's $TLD_{in\ vitro}$ showed that the size distributions of drug aerosols likely to enter the lung were also a function of both MT geometry and the subject's inhalation maneuver; the largest variations in APSDs were seen for the *slow* inhalation condition, suggesting that the methods developed in the present study were sufficiently precise to distinguish between the different aerosol doses and the aerosol sizes likely to enter the trachea. There was no reason to believe that the same techniques could not be extended to review the data for other powder inhalers that are also used clinically by patients with variable MT geometries and breathing patterns. The biggest limitation of the present study was that the APSDs measured at the exit of the MT could not be compared directly with the regional lung deposition data from the clinical gamma scintigraphy study (Newman et al., 2000). Therefore, to explore the clinical importance of the results for APSD, an effort was made in Chapter 6 to predict regional drug deposition in the airways using computational fluid dynamic (CFD) simulations in combination with the *in vitro* testing techniques described in Chapter 5. It should be noted that the methods described in the present study are different from those used elsewhere (Chrystyn et al., 2015; Goodey et al., 2014; Nadarassan et al., 2010; Yakubu et al., 2013) and standardization of methods may be needed to facilitate application of realistic *in vitro* tests. Furthermore, some redesign of cascade impactors like NGI and/or their stages to

better enable aerosol characterization at high flow conditions may be required to enable other DPIs to be characterized across the range of realistic IPs.

The last study of this dissertation (Chapter 6) was designed to explore regional lung deposition and its variation for Budelin Novolizer under three inhalation conditions using a new hybrid *in vitro*–CFD approach. To facilitate coupling of the realistic *in vitro* test methods described in Chapter 5 to CFD simulations, a published airway model and the CFD methods described by (Tian et al., 2015a) was modified to allow the values for APSDs of Budelin's $TLD_{in\ vitro}$ and the associated IPs to be used as the initial conditions for CFD simulation at the tracheal opening. When comparing the regional deposition results produced using the hybrid *in vitro*–CFD approach with those from Tian et al. (2015a), small but finite differences were observed for the individual segments. This may be caused by differences in IPs between the two studies, as well as changes in particle injection time and particle trajectories at the tracheal inlet. Most likely however, the existence or absence of air turbulence introduced by the laryngeal jet, and differences in the APSDs of particles entering the trachea in both techniques appeared to produce differences in predicted regional deposition in the airways. The present study also showed that variations in IPs and the APSDs of $TLD_{in\ vitro}$ appeared to affect drug deposition in the airways of a model human adult respiratory tract; but regardless of the variations, most of the dose from Budelin that escaped the MT region appeared likely to reach beyond generation 15 into the lung periphery. The predicted regional deposition results using the *in vitro*–CFD approach were believed to be consistent with those reported in the gamma scintigraphy study (Newman et al., 2000), although our work demonstrated that a proportion of the counts usually attributed to deposition in the "central region" of the lung

should be shifted to the periphery to allow for the presence of significant numbers of small (peripheral) airways that overlay the “central regions” in two dimensional lung scintigraphs. It should be noted that the CFD model used by Tian et al. (2015a) and that used in the present study was designed to represent the “average” geometry of a healthy human adult. To further evaluate inter-subject variabilities in regional lung deposition, variations in airway geometries across a population may need to be incorporated. In addition, aerosol deposition patterns in the patient’s lung may be altered by changes in airway morphologies and physiologies (e.g. airway wall thickening, mucus hypersecretion, bronchoconstriction, etc.) caused by pulmonary diseases like asthma and COPD (Wang et al., 2014). An extensive study on the airway geometries of patients with different pulmonary diseases may be needed in future to generalize and select representative geometries for specific patient groups.

Overall, the realistic *in vitro* test methods described in this dissertation allow total and regional drug deposition in the lung of healthy human adults and their inter-subject variabilities to be predicted for DPIs. Such methods may benefit both product development scientists and regulators as it produces more meaningful *in vitro* data than standard compendial tests (U.S. Pharmacopeial Convention, 2013). While efforts have been made to standardize and improve the existing realistic *in vitro* test methods, how to incorporate these methods into bioequivalence studies and guidance documents, and ease the development process for generic inhalers, remains to be discussed. More study and discussion of this topic and collaboration between different research groups and regulators appears to be needed.

LIST OF REFERENCES

Anderson, P. J. (2005). History of aerosol therapy: liquid nebulization to MDIs to DPIs. *Respir Care, 50*(9), 1139-1150. Retrieved from http://rc.rcjournal.com/content/50/9/1139.full.pdf

Anderson, P. J., & Newman, S. P. (2009). Drugs for topical and systemic delivery by the pulmonary route. In S. P. Newman, P. Anderson, P. R. Byron, R. Dalby, & J. Peart (Eds.), *Respiratory drug delivery: essential theory and practice* (pp. 337-382). Richmond USA: RDD Online / Virginia Commonwealth University.

Andrews, L. C. (1992). *Special Functions of Mathematics for Engineers*. New York: McGraw-Hill.

Azouz, W., Chetcuti, P., Hosker, H., Saralaya, D., & Chrystyn, H. (2015a). Inhalation characteristics of asthma patients, COPD patients and healthy volunteers with the Spiromax(R) and Turbuhaler(R) devices: a randomised, cross-over study. *BMC Pulm Med, 15*, 47. doi:10.1186/s12890-015-0043-x

Azouz, W., Chetcuti, P., Hosker, H. S., Saralaya, D., Stephenson, J., & Chrystyn, H. (2015b). The inhalation characteristics of patients when they use different dry powder inhalers. *J Aerosol Med Pulm Drug Deliv, 28*(1), 35-42. doi:10.1089/jamp.2013.1119

Baba, K., Tanaka, H., Nishimura, M., Yokoe, N., Takahashi, D., Yagi, T., Yamaguchi, E., Maeda, Y., Muto, T., & Hasegawa, T. (2011). Age-dependent deterioration of peak inspiratory flow with two kinds of dry powder corticosteroid inhalers (Diskus and Turbuhaler) and relationships with asthma control. *J Aerosol Med Pulm Drug Deliv, 24*(6), 293-301. doi:10.1089/jamp.2010.0868

Below, A., Bickmann, D., & Breitkreutz, J. (2013). Assessing the performance of two dry powder inhalers in preschool children using an idealized pediatric upper airway model. *International Journal of Pharmaceutics, 444*(1–2), 169-174. doi:http://dx.doi.org/10.1016/j.ijpharm.2013.01.007

Borgstrom, L., Bondesson, E., Moren, F., Trofast, E., & Newman, S. P. (1994). Lung deposition of budesonide inhaled via Turbuhaler: a comparison with terbutaline sulphate in normal subjects. *Eur Respir J, 7*(1), 69-73. Retrieved from http://erj.ersjournals.com/content/7/1/69.full.pdf

Borgström, L., Olsson, B., & Thorsson, L. (2006). Degree of throat deposition can explain the variability in lung deposition of inhaled drugs. *J Aerosol Med, 19*(4), 473-483. doi:10.1089/jam.2006.19.473

Brindley, A., Sumby, B. S., & Smith, I. J. (1994). The characterisation of inhalation devices by an inhalation simulator: The Electronic Lung. *J Aerosol Med, 7*(2), 197-200.

Broeders, M. E., Molema, J., Hop, W. C., Vermue, N. A., & Folgering, H. T. (2004). The course of inhalation profiles during an exacerbation of obstructive lung disease. *Respir Med, 98*(12), 1173-1179. Retrieved from http://ac.els-cdn.com/S0954611104001799/1-s2.0-S0954611104001799-main.pdf?_tid=207a46f8-1084-11e5-bb34-00000aacb361&acdnat=1434059717_0ae69b3b3def00ec01080e27fd402003

Broeders, M. E., Sanchis, J., Levy, M. L., Crompton, G. K., & Dekhuijzen, P. N. (2009). The ADMIT series--issues in inhalation therapy. 2. Improving technique and

clinical effectiveness. *Prim Care Respir J, 18*(2), 76-82. doi:10.4104/pcrj.2009.00025

Burnell, P. K. P., Asking, L., Borgstrom, L., Nichols, S. C., Olsson, B., Prime, D., & Shrubb, I. (2007). Studies of the human oropharyngeal airspaces using magnetic resonance imaging IV--the oropharyngeal retention effect for four inhalation delivery systems. *J Aerosol Med, 20*(3), 269-281. doi:10.1089/jam.2007.0566

Burnell, P. K. P., Grant, A., Haywood, P., Prime, D., & Sumby, B. (1998a). Powder inhalers - exploring the limits of performance. In R. Dalby, P. R. Byron, & S. J. Farr (Eds.), *Respiratory Drug Delivery 1998* (Vol. 1, pp. 259-268). Richmond, VA: RDD Online.

Burnell, P. K. P., Malton, A., Reavill, K., & Ball, M. H. E. (1998b). Design, validation and initial testing of the Electronic LungTM device. *Journal of Aerosol Science, 29*(8), 1011-1025. doi:http://dx.doi.org/10.1016/S0021-8502(97)10039-8

Byron, P. R., Hindle, M., Lange, C. F., Longest, P. W., McRobbie, D., Oldham, M. J., Olsson, B., Thiel, C. G., Wachtel, H., & Finlay, W. H. (2010). In vivo-in vitro correlations: predicting pulmonary drug deposition from pharmaceutical aerosols. *J Aerosol Med Pulm Drug Deliv, 23 Suppl 2*, S59-69. doi:10.1089/jamp.2010.0846

Byron, P. R., Wei, X., Delvadia, R. R., & Longest, P. W. (2013). Standardizing in vitro test methods to support aerosol drug evaluation in the clinic. In R. Dalby, P. R. Byron, J. Peart, J. D. Suman, P. M. Young, & D. Traini (Eds.), *RDD Europe 2013* (Vol. 1, pp. 85-92). Richmond, VA: RDD Online.

Byron, P. R., Wei, X., Delvadia, R. R., Longest, P. W., & Venitz, J. (2014). Breath profiles for testing new DPI devices in development. In R. Dalby, P. R. Byron, J. Peart, S. J. Farr, J. D. Suman, P. M. Young, & D. Traini (Eds.), *Respiratory Drug Delivery 2014* (Vol. 1, pp. 295-302). Richmond, VA: RDD Online.

Carrigy, N. B., O'Reilly, C., Schmitt, J., Noga, M., & Finlay, W. H. (2014). Effect of facial material softness and applied force on face mask dead volume, face mask seal, and inhaled corticosteroid delivery through an idealized infant replica. *J Aerosol Med Pulm Drug Deliv, 27*(4), 290-298. doi:10.1089/jamp.2013.1087

Casaro, D., Brambilla, G., Pasquali, I., & Sisti, V. (2014). In vitro aerosol performances of NEXThaler® using representative inhalation profiles from asthmatic patients. In R. Dalby, P. R. Byron, J. Peart, S. J. Farr, J. D. Suman, P. M. Young, & D. Traini (Eds.), *Respiratory Drug Delivery 2014* (Vol. 2, pp. 375-380). Richmond, VA: RDD Online.

Chan, J. G., Wong, J., Zhou, Q. T., Leung, S. S., & Chan, H. K. (2014). Advances in device and formulation technologies for pulmonary drug delivery. *AAPS PharmSciTech, 15*(4), 882-897. doi:10.1208/s12249-014-0114-y

Chavan, V., & Dalby, R. (2002). Novel system to investigate the effects of inhaled volume and rates of rise in simulated inspiratory air flow on fine particle output from a dry powder inhaler. *AAPS PharmSci, 4*(2), E6. doi:10.1208/ps040206

Chrystyn, H. (2003). Is inhalation rate important for a dry powder inhaler? Using the In-Check Dial to identify these rates. *Respir Med, 97*(2), 181-187. Retrieved from http://www.resmedjournal.com/article/S0954-6111(03)91351-5/pdf

Chrystyn, H., Safioti, G., Keegstra, J. R., & Gopalan, G. (2015). Effect of inhalation profile and throat geometry on predicted lung deposition of budesonide and formoterol (BF) in COPD: An in-vitro comparison of Spiromax with Turbuhaler. *International Journal of Pharmaceutics, 491*(1–2), 268-276. doi:http://dx.doi.org/10.1016/j.ijpharm.2015.05.076

Clark, A. R., & Hollingworth, A. M. (1993). The relationship between powder inhaler resistance and peak inspiratory conditions in healthy volunteers — implications for in vitro testing. *J Aerosol Med, 6*(2), 99-110. doi:doi:10.1089/jam.1993.6.99

Coates, M. S., Chan, H. K., Fletcher, D. F., & Raper, J. A. (2005). Influence of air flow on the performance of a dry powder inhaler using computational and experimental analyses. *Pharm Res, 22*(9), 1445-1453. doi:10.1007/s11095-005-6155-x

Code of Federal Regulations, 21 C.F.R. § 320.1 (2015).

Daley-Yates, P. T., Mehta, R., Chan, R. H., Despa, S. X., & Louey, M. D. (2014). Pharmacokinetics and pharmacodynamics of fluticasone propionate and salmeterol delivered as a combination dry powder from a capsule-based inhaler and a multidose inhaler in asthma and COPD patients. *J Aerosol Med Pulm Drug Deliv, 27*(4), 279-289. doi:10.1089/jamp.2013.1040

Daley-Yates, P. T., Parkins, D. A., Thomas, M. J., Gillett, B., House, K. W., & Ortega, H. G. (2009). Pharmacokinetic, pharmacodynamic, efficacy, and safety data from two randomized, double-blind studies in patients with asthma and an in vitro study comparing two dry-powder inhalers delivering a combination of salmeterol 50 microg and fluticasone propionate 250 microg: implications for establishing

bioequivalence of inhaled products. *Clin Ther, 31*(2), 370-385. doi:10.1016/j.clinthera.2009.02.007

De Backer, W., Devolder, A., Poli, G., Acerbi, D., Monno, R., Herpich, C., Sommerer, K., Meyer, T., & Mariotti, F. (2010). Lung Deposition of BDP/Formoterol HFA pMDI in Healthy Volunteers, Asthmatic, and COPD Patients. *J Aerosol Med Pulm Drug Deliv, 23*(3), 137-148. doi:10.1089/jamp.2009.0772

de Boer, A. H., Bolhuis, G. K., Gjaltema, D., & Hagedoorn, P. (1997). Inhalation characteristics and their effects on in vitro drug delivery from dry powder inhalers: Part 3: the effect of flow increase rate (FIR) on the in vitro drug release from the Pulmicort 200 Turbuhaler. *International Journal of Pharmaceutics, 153*(1), 67-77. doi:http://dx.doi.org/10.1016/S0378-5173(97)00097-5

de Boer, A. H., Gjaltema, D., Hagedoorn, P., & Frijlink, H. W. (2004). Comparative in vitro performance evaluation of the Novopulmon 200 Novolizer and Budesonid-ratiopharm Jethaler: two novel budesonide dry powder inhalers. *Pharmazie, 59*(9), 692-699.

de Boer, A. H., Hagedoorn, P., Gjaltema, D., Goede, J., & Frijlink, H. W. (2003). Air classifier technology (ACT) in dry powder inhalation. Part 1. Introduction of a novel force distribution concept (FDC) explaining the performance of a basic air classifier on adhesive mixtures. *Int J Pharm, 260*(2), 187-200. Retrieved from http://www.sciencedirect.com/science/article/pii/S0378517303002503

http://ac.els-cdn.com/S0378517303002503/1-s2.0-S0378517303002503-main.pdf?_tid=3f3a65c2-2fa8-11e4-a326-00000aab0f27&acdnat=1409336219_8f87dd6b3334c1d5520a9d8bb60d1aff

de Boer, A. H., Hagedoorn, P., Gjaltema, D., Goede, J., & Frijlink, H. W. (2006). Air classifier technology (ACT) in dry powder inhalation. Part 4. Performance of air classifier technology in the Novolizer multi-dose dry powder inhaler. *Int J Pharm, 310*(1-2), 81-89. doi:10.1016/j.ijpharm.2005.11.029

Delvadia, R. R. (2012). *In vitro methods to predict aerosol drug deposition in normal adults.* (Doctoral Dissertation), Virginia Commonwealth University, Richmond, VA. Retrieved from http://scholarscompass.vcu.edu/etd/314

Delvadia, R. R., Hindle, M., Longest, P. W., & Byron, P. R. (2013a). In vitro tests for aerosol deposition. II: IVIVCs for different dry powder inhalers in normal adults. *J Aerosol Med Pulm Drug Deliv., 26*(3), 138 - 144. doi:10.1089/jamp.2012.0975

Delvadia, R. R., Longest, P. W., & Byron, P. R. (2012). In vitro tests for aerosol deposition. I: Scaling a physical model of the upper airways to predict drug deposition variation in normal humans. *J Aerosol Med Pulm Drug Deliv, 25*(1), 32-40. doi:10.1089/jamp.2011.0905

Delvadia, R. R., Longest, P. W., Hindle, M., & Byron, P. R. (2013b). In vitro tests for aerosol deposition. III: Effect of inhaler insertion angle on aerosol deposition. *J Aerosol Med Pulm Drug Deliv, 26*, 145 - 156. Retrieved from http://online.liebertpub.com/doi/pdfplus/10.1089/jamp.2012.0989

Farr, S. J., Rowe, A. M., Rubsamen, R., & Taylor, G. (1995). Aerosol deposition in the human lung following administration from a microprocessor controlled pressurised metered dose inhaler. *Thorax, 50*(6), 639-644. Retrieved from http://thorax.bmj.com/content/50/6/639.full.pdf

Fenton, C., Keating, G. M., & Plosker, G. L. (2003). Novolizer: a multidose dry powder inhaler. *Drugs, 63*(22), 2437-2445; discussion 2447-2438.

Finlay, W. H. (2013). ARLA Respiratory Deposition Calculator. Retrieved from http://www.mece.ualberta.ca/arla/deposition_calculator.html (Accessed on October 26, 2015)

Finlay, W. H., Golshahi, L., Noga, M., & Flores-Mir, C. (2010). Choosing 3-D mouth-throat dimensions: a rational merging of medical imaging and aerodynamics. In R. Dalby, P. R. Byron, J. Peart, S. J. Parr, J. D. Suman, & P. M. Young (Eds.), *Respiratory Drug Delivery 2010* (Vol. 1, pp. 185-194). Richmond, VA: RDD Online.

Gerrity, T. R. (1989). Pathophysiological and Disease Constraints on Aerosol Delivery. In P. R. Byron (Ed.), *Respiratory Drug Delivery* (pp. 1-38). Boca Raton, FL: CRC Press.

Goodey, A. P., Bupathi, B., Tat, H., Fang, X., George, M., & Li, Y. (2014). Probing dry powder inhaler performance robustness with an inhalation profile simulator. In R. Dalby, P. R. Byron, J. Peart, S. J. Farr, J. D. Suman, P. M. Young, & D. Traini (Eds.), *Respiratory Drug Delivery 2014* (Vol. 2, pp. 485-488). Richmond, VA: RDD Online.

Hankinson, J. L., Odencrantz, J. R., & Fedan, K. B. (1999). Spirometric reference values from a sample of the general U.S. population. *Am J Respir Crit Care Med, 159*(1), 179-187. doi:10.1164/ajrccm.159.1.9712108

Harris, D. (2015). Are inhaler testing methods stuck in the swinging sixties? [Web log post]. Retrieved from https://www.linkedin.com/pulse/inhaler-testing-methods-stuck-swinging-sixties-david-harris (Accessed on July 20, 2015)

Harris, D., & Willoughby, A. (2010). *How does airflow resistance affect inspiratory characteristics as a child grows into an adult?* Paper presented at the Drug Delivery to the Lungs 21, Edinburgh, UK.

Hindle, M., Byron, P. R., & Miller, N. C. (1996). Cascade impaction methods for dry powder inhalers using the high flowrate Marple-Miller impactor. *International Journal of Pharmaceutics, 134*(1–2), 137-146. doi:http://dx.doi.org/10.1016/0378-5173(95)04493-0

International Commission on Radiological Protection (ICRP). (1994). *ICRP publication 66: human respiratory tract model for radiological protection*. Washington, DC: SAGE Publications.

Kotian, R., Peart, J., Bryner, J., & Byron, P. R. (2009). Calibration of the modified Electrical Low-Pressure Impactor (ELPI) for use with pressurized pharmaceutical aerosols. *J Aerosol Med Pulm Drug Deliv, 22*(1), 55-65. doi:10.1089/jamp.2008.0683

Lavorini, F., Levy, M. L., Corrigan, C., & Crompton, G. (2010). The ADMIT series - issues in inhalation therapy. 6) Training tools for inhalation devices. *Prim Care Respir J, 19*(4), 335-341. doi:10.4104/pcrj.2010.00065

Lee, S. L., Adams, W. P., Li, B. V., Conner, D. P., Chowdhury, B. A., & Yu, L. X. (2009). In vitro considerations to support bioequivalence of locally acting drugs in dry

powder inhalers for lung diseases. *AAPS J, 11*(3), 414-423. doi:10.1208/s12248-009-9121-4

Longest, P. W. (2012). Virginia Commonwealth University mouth-throat (MT) geometries. Retrieved from http://www.rddonline.com/resources/tools/models.php (Accessed on February 16, 2015)

Longest, P. W., & Hindle, M. (2009). Evaluation of the Respimat Soft Mist Inhaler using a concurrent CFD and in vitro approach. *J Aerosol Med Pulm Drug Deliv, 22*(2), 99-112. doi:10.1089/jamp.2008.0708

Longest, P. W., & Holbrook, L. T. (2012). In silico models of aerosol delivery to the respiratory tract - development and applications. *Adv Drug Deliv Rev, 64*(4), 296-311. doi:10.1016/j.addr.2011.05.009

Longest, P. W., Tian, G., Delvadia, R., & Hindle, M. (2012a). Development of a Stochastic Individual Path (SIP) Model for Predicting the Deposition of Pharmaceutical Aerosols: Effects of Turbulence, Polydisperse Aerosol Size, and Evaluation of Multiple Lung Lobes. *Aerosol Science and Technology, 46*(12), 1271-1285. doi:10.1080/02786826.2012.708799

Longest, P. W., Tian, G., Walenga, R. L., & Hindle, M. (2012b). Comparing MDI and DPI aerosol deposition using in vitro experiments and a new stochastic individual path (SIP) model of the conducting airways. *Pharm Res, 29*(6), 1670-1688. doi:10.1007/s11095-012-0691-y

Malmberg, L. P., Rytila, P., Happonen, P., & Haahtela, T. (2010). Inspiratory flows through dry powder inhaler in chronic obstructive pulmonary disease: age and

gender rather than severity matters. *Int J Chron Obstruct Pulmon Dis, 5*, 257-262. Retrieved from http://www.dovepress.com/getfile.php?fileID=7182

Marion, M. S., Leonardson, G. R., Rhoades, E. R., Welty, T. K., & Enright, P. L. (2001). Spirometry reference values for American Indian adults: results from the Strong Heart Study. *Chest, 120*(2), 489-495. Retrieved from http://journal.publications.chestnet.org/data/Journals/CHEST/21965/489.pdf

Marple, V. A., Olson, B. A., Santhanakrishnan, K., Mitchell, J. P., Murray, S. C., & Hudson-Curtis, B. L. (2003a). Next generation pharmaceutical impactor (a new impactor for pharmaceutical inhaler testing). Part II: Archival calibration. *J Aerosol Med, 16*(3), 301-324. doi:10.1089/089426803769017668

Marple, V. A., Olson, B. A., Santhanakrishnan, K., Roberts, D. L., Mitchell, J. P., & Hudson-Curtis, B. L. (2004). Next generation pharmaceutical impactor: a new impactor for pharmaceutical inhaler testing. Part III. extension of archival calibration to 15 L/min. *J Aerosol Med, 17*(4), 335-343. doi:10.1089/jam.2004.17.335

Marple, V. A., Roberts, D. L., Romay, F. J., Miller, N. C., Truman, K. G., Van Oort, M., Olsson, B., Holroyd, M. J., Mitchell, J. P., & Hochrainer, D. (2003b). Next generation pharmaceutical impactor (a new impactor for pharmaceutical inhaler testing). Part I: Design. *J Aerosol Med, 16*(3), 283-299. doi:10.1089/089426803769017659

Miller, M. R., Hankinson, J., Brusasco, V., Burgos, F., Casaburi, R., Coates, A., Crapo, R., Enright, P., van der Grinten, C. P., Gustafsson, P., Jensen, R., Johnson, D. C., MacIntyre, N., McKay, R., Navajas, D., Pedersen, O. F., Pellegrino, R., Viegi,

G., & Wanger, J. (2005). Standardisation of spirometry. *Eur Respir J, 26*(2), 319-338. doi:10.1183/09031936.05.00034805

Miller, N. C. (1997). U.S. Patent No. 643,500,4. Washington, DC: U.S. Patent and Trademark Office.

Miller, N. C., Maniaci, M. J., Dwivedi, S. K., & Ward, G. H. (2000). Aerodynamic sizing with simulated inhalation profiles: total dose capture and measurement. In R. Dalby, P. R. Byron, S. J. Farr, & J. Peart (Eds.), *Respiratory Drug Delivery VII* (Vol. 1, pp. 191 - 196). Richmond, VA: RDD Online.

Mitchell, J. P. (2003). *Practices of coating collection surfaces of cascade impactors: a survey of members of the european pharmaceutical aerosol group (EPAG)*. Paper presented at the Drug Delivery to the Lungs 14, London, UK. Retrieved from http://www.epag.co.uk/Download2.asp?DID=841

Munzel, U., Marschall, K., Fyrnys, B., & Wedel, M. (2005). Variability of fine particle dose and lung deposition of budesonide delivered through two multidose dry powder inhalers. *Curr Med Res Opin, 21*(6), 827-833. doi:10.1185/030079905x46241

Nadarassan, D. K., Assi, K. H., & Chrystyn, H. (2010). Aerodynamic characteristics of a dry powder inhaler at low inhalation flows using a mixing inlet with an Andersen Cascade Impactor. *European Journal of Pharmaceutical Sciences, 39*(5), 348-354. doi:http://dx.doi.org/10.1016/j.ejps.2010.01.002

Newman, S. P., & Chan, H. K. (2008). In vitro/in vivo comparisons in pulmonary drug delivery. *J Aerosol Med Pulm Drug Deliv, 21*(1), 77-84. doi:10.1089/jamp.2007.0643

Newman, S. P., Clark, A. R., Talaee, N., & Clarke, S. W. (1989). Pressurised aerosol deposition in the human lung with and without an "open" spacer device. *Thorax, 44*(9), 706-710. Retrieved from http://thorax.bmj.com/content/44/9/706.full.pdf

Newman, S. P., Pitcairn, G. R., Hirst, P. H., Bacon, R. E., O'Keefe, E., Reiners, M., & Hermann, R. (2000). Scintigraphic comparison of budesonide deposition from two dry powder inhalers. *Eur Respir J, 16*(1), 178-183. Retrieved from http://erj.ersjournals.com/content/16/1/178.full.pdf

Olsson, B., Berg, E., & Svensson, M. (2010). Comparing aerosol size distributions that penetrate mouth-throat models under realistic inhalation conditions. In R. Dalby, P. R. Byron, J. Peart, J. D. Suman, S. J. Farr, & P. M. Young (Eds.), *Respiratory Drug Delivery 2010* (Vol. 1, pp. 225-234). River Grove, IL: DHI Publishing.

Olsson, B., Borgstrom, L., Asking, L., & Bondesson, E. (1996). Effect of inlet throat on the correlation between measured fine particle dose and lung deposition. In R. Dalby, P. R. Byron, & S. J. Farr (Eds.), *Respiratory Drug Delivery V* (Vol. 1, pp. 273-282). River Grove, IL: DHI Publishing.

Olsson, B., Borgstrom, L., Lundback, H., & Svensson, M. (2013). Validation of a general in vitro approach for prediction of total lung deposition in healthy adults for pharmaceutical inhalation products. *J Aerosol Med Pulm Drug Deliv, 26*(6), 355-369. doi:10.1089/jamp.2012.0986

Oropharyngeal Consortium. (2013). Oropharyngeal Consortium Mouth-Throat (MT) Geometries. Retrieved from http://www.isam.org/index.php?option=com_content&view=article&id=46&Itemid=183 (Accessed on August 7, 2015)

Pitcairn, G., Bogard, H., & Cooper, A. (2012). Inspiration and disease: a review of patient focused testing that impacts product design. In R. Dalby, P. R. Byron, J. Peart, J. D. Suman, S. J. Farr, & P. M. Young (Eds.), *Respiratory Drug Delivery 2012* (Vol. 1, pp. 337-346). Richmond, VA: RDD Online.

Reist, P. C. (1993). *Aerosol science and technology* (2nd ed.). Columbus, OH: McGraw-Hill.

Rosenthal, E. (2013). The soaring cost of a simple breath. *The New York Times*. Retrieved from http://www.nytimes.com/2013/10/13/us/the-soaring-cost-of-a-simple-breath.html?_r=0 (Accessed on July 27, 2015)

Rostami, A. A. (2009). Computational modeling of aerosol deposition in respiratory tract: a review. *Inhal Toxicol, 21*(4), 262-290. doi:10.1080/08958370802448987

Ruzycki, C. A., Golshahi, L., Vehring, R., & Finlay, W. H. (2014). Comparison of in vitro deposition of pharmaceutical aerosols in an idealized child throat with in vivo deposition in the upper respiratory tract of children. *Pharm Res, 31*(6), 1525-1535. doi:10.1007/s11095-013-1258-2

Saluja, B., Li, B. V., & Lee, S. L. (2014). Bioequivalence for orally inhaled and nasal drug products. In L. X. Yu & B. V. Li (Eds.), *FDA bioequivalence standards* (pp. 369-394). New York, NY: Springer

Sanders, M. (2007). Inhalation therapy: an historical review. *Prim Care Respir J, 16*(2), 71-81. doi:10.3132/pcrj.2007.00017

Sarinas, P. S., Robinson, T. E., Clark, A. R., Canfield, J., Jr., Chitkara, R. K., & Fick, R. B., Jr. (1998). Inspiratory flow rate and dynamic lung function in cystic fibrosis

and chronic obstructive lung diseases. *Chest, 114*(4), 988-992. Retrieved from http://journal.publications.chestnet.org/data/Journals/CHEST/21845/988.pdf

Schroeter, J. D., Pritchard, J. N., Hwang, D., & Martonen, T. B. (2005). Airway identification within planar gamma camera images using computer models of lung morphology. *Pharm Res, 22*(10), 1692-1699. doi:10.1007/s11095-005-6628-y

Smutney, C. C., Friedman, E. M., Polidoro, J. M., & Amin, N. (2009). Inspiratory efforts achieved in use of the Technosphere insulin inhalation system. *J Diabetes Sci Technol, 3*(5), 1175-1182. Retrieved from http://dst.sagepub.com/content/3/5/1175.full.pdf

Son, Y. J., & McConville, J. T. (2008). Advancements in dry powder delivery to the lung. *Drug Dev Ind Pharm, 34*(9), 948-959. doi:10.1080/03639040802235902

Stahlhofen, W., Rudolf, G., & James, A. C. (1989). Intercomparison of experimental regional aerosol deposition data. *J Aerosol Med, 2*(3), 285-308. Retrieved from http://online.liebertpub.com/doi/abs/10.1089/jam.1989.2.285

Stapleton, K. W., Guentsch, E., Hoskinson, M. K., & Finlay, W. H. (2000). On the suitability of k–ε turbulence modeling for aerosol deposition in the mouth and throat: a comparison with experiment. *Journal of Aerosol Science, 31*(6), 739-749. doi:http://dx.doi.org/10.1016/S0021-8502(99)00547-9

Swift, D. L. (1994). The oral airway - a conduit or collector for pharmaceutical aerosols? In P. R. Byron, R. Dalby, & S. J. Farr (Eds.), *Respiratory Drug Delivery IV* (Vol. 1, pp. 187-196). Richmond, VA: RDD Online.

Tarsin, W. Y., Pearson, S. B., Assi, K. H., & Chrystyn, H. (2006). Emitted dose estimates from Seretide® Diskus® and Symbicort® Turbuhaler® following inhalation by severe asthmatics. *International Journal of Pharmaceutics, 316*(1–2), 131-137. doi:http://dx.doi.org/10.1016/j.ijpharm.2006.02.040

Telko, M. J., & Hickey, A. J. (2005). Dry powder inhaler formulation. *Respir Care, 50*(9), 1209-1227. Retrieved from http://rc.rcjournal.com/content/50/9/1209.full.pdf

Tian, G. (2015). [Personal communication].

Tian, G., Hindle, M., Lee, S., & Longest, P. W. (2015a). Validating CFD Predictions of Pharmaceutical Aerosol Deposition with In Vivo Data. *Pharm Res, 32*(10), 3170-3187. doi:10.1007/s11095-015-1695-1

Tian, G., Longest, P. W., Su, G., Walenga, R. L., & Hindle, M. (2011). Development of a stochastic individual path (SIP) model for predicting the tracheobronchial deposition of pharmaceutical aerosols: Effects of transient inhalation and sampling the airways. *Journal of Aerosol Science, 42*(11), 781-799. doi:http://dx.doi.org/10.1016/j.jaerosci.2011.07.005

Tiddens, H. A., Geller, D. E., Challoner, P., Speirs, R. J., Kesser, K. C., Overbeek, S. E., Humble, D., Shrewsbury, S. B., & Standaert, T. A. (2006). Effect of dry powder inhaler resistance on the inspiratory flow rates and volumes of cystic fibrosis patients of six years and older. *J Aerosol Med, 19*(4), 456-465. doi:10.1089/jam.2006.19.456

U.S. Food and Drug Admiistration. (2013). *Product-specific recommendations for generic drug development: draft guidance on fluticasone propionate; salmeterol xinafoate*. Retrieved from

http://www.fda.gov/downloads/Drugs/GuidanceComplianceRegulatoryInformation/Guidances/UCM367643.pdf.

U.S. Food and Drug Administration. (2013). *Draft guidance for industry: bioequivalence studies with pharmacokinetic endpoints for drugs submitted under an ANDA*. Retrieved from http://www.fda.gov/downloads/drugs/guidancecomplianceregulatoryinformation/guidances/ucm377465.pdf.

U.S. Food and Drug Administration. (2015a). Drug treatments for asthma and chronic obstructive pulmonary disease that do not use chlorofluorocarbons. Retrieved from http://www.fda.gov/Drugs/DrugSafety/InformationbyDrugClass/ucm082370.htm (Accessed on June 15, 2015)

U.S. Food and Drug Administration. (2015b). *Orange book: approved drug products with therapeutic equivalence evaluations*. Retrieved from http://www.accessdata.fda.gov/scripts/cder/ob/default.cfm (Accessed on September 2, 2015).

U.S. Pharmacopeial Convention. (2013). General chapter <601> aerosols, nasal sprays, metered dose inhalers, and dry powder inhalers. *United states pharmacopeia and national formulary (USP 36-NF 31)* (Vol. 1, pp. 242-262). Rockville, MD: U.S. Pharmacopeial Convention.

Usmani, O. S. (2015). Small-airway disease in asthma: pharmacological considerations. *Curr Opin Pulm Med, 21*(1), 55-67. doi:10.1097/mcp.0000000000000115

Usmani, O. S., & Barnes, P. J. (2012). Assessing and treating small airways disease in asthma and chronic obstructive pulmonary disease. *Ann Med, 44*(2), 146-156. doi:10.3109/07853890.2011.585656

Usmani, O. S., Biddiscombe, M. F., & Barnes, P. J. (2005). Regional lung deposition and bronchodilator response as a function of beta2-agonist particle size. *Am J Respir Crit Care Med, 172*(12), 1497-1504. doi:10.1164/rccm.200410-1414OC

van Beerendonk, I., Mesters, I., Mudde, A. N., & Tan, T. D. (1998). Assessment of the inhalation technique in outpatients with asthma or chronic obstructive pulmonary disease using a metered-dose inhaler or dry powder device. *J Asthma, 35*(3), 273-279. doi:10.3109/02770909809068218

Virchow, J. C., Weuthen, T., Harmer, Q. J., & Jones, S. (2014). Identifying the features of an easy-to-use and intuitive dry powder inhaler for asthma and chronic obstructive pulmonary disease therapy: results from a 28-day device handling study, and an airflow resistance study. *Expert Opin Drug Deliv, 11*(12), 1849-1857. doi:10.1517/17425247.2014.949236

Wang, Y. B., Watts, A. B., Peters, J. I., & Williams, R. O., 3rd. (2014). The impact of pulmonary diseases on the fate of inhaled medicines--a review. *Int J Pharm, 461*(1-2), 112-128. doi:10.1016/j.ijpharm.2013.11.042

Weers, J. G., Clark, A. R., Rao, N., Ung, K., Haynes, A., Khindri, S. K., Perry, S. A., Machineni, S., & Colthorpe, P. (2014). In vitro-in vivo correlations observed with indacaterol-based formulations delivered with the Breezhaler. *J Aerosol Med Pulm Drug Deliv*. doi:10.1089/jamp.2014.1178

Weers, J. G., Ung, K., Le, J., Rao, N., Ament, B., Axford, G., Maltz, D., & Chan, L. (2013). Dose emission characteristics of placebo PulmoSphere(R) particles are unaffected by a subject's inhalation maneuver. *J Aerosol Med Pulm Drug Deliv, 26*(1), 56-68. doi:10.1089/jamp.2012.0973

Wei, X., Byron, P. R., & Longest, P. W. (2014). Predicting variations in lung dose with different mouth-throat models. In R. Dalby, P. R. Byron, J. Peart, S. J. Farr, J. D. Suman, P. M. Young, & D. Traini (Eds.), *Respiratory Drug Delivery 2014* (Vol. 3, pp. 773-776). Richmond, VA: RDD Online.

Wong, W., Fletcher, D. F., Traini, D., Chan, H. K., & Young, P. M. (2012). The use of computational approaches in inhaler development. *Adv Drug Deliv Rev, 64*(4), 312-322. doi:10.1016/j.addr.2011.10.004

Xi, J., & Longest, P. W. (2007). Transport and deposition of micro-aerosols in realistic and simplified models of the oral airway. *Ann Biomed Eng, 35*(4), 560-581. doi:10.1007/s10439-006-9245-y

Xi, J., Longest, P. W., & Martonen, T. B. (2008). Effects of the laryngeal jet on nano- and microparticle transport and deposition in an approximate model of the upper tracheobronchial airways. *J Appl Physiol (1985), 104*(6), 1761-1777. doi:10.1152/japplphysiol.01233.2007

Yakubu, S. I., Assi, K. H., & Chrystyn, H. (2013). Aerodynamic dose emission characteristics of dry powder inhalers using an Andersen Cascade Impactor with a mixing inlet: The influence of flow and volume. *International Journal of Pharmaceutics, 455*(1–2), 213-218. doi:http://dx.doi.org/10.1016/j.ijpharm.2013.07.036

Zhang, Y., Gilbertson, K., & Finlay, W. H. (2007). In vivo-in vitro comparison of deposition in three mouth-throat models with Qvar and Turbuhaler inhalers. *J Aerosol Med, 20*(3), 227-235. doi:10.1089/jam.2007.0584

Zhou, Q. T., Tang, P., Leung, S. S., Chan, J. G., & Chan, H. K. (2014). Emerging inhalation aerosol devices and strategies: where are we headed? *Adv Drug Deliv Rev, 75*, 3-17. doi:10.1016/j.addr.2014.03.006

APPENDIX I

REGIONAL DRUG DEPOSITION FROM POWDER INHALERS: LUNG SCINTIGRAPHY STUDIES IN HEALTHY HUMAN ADULTS

AI.1 INTRODUCTION

A literature review was performed to identify clinical studies of inhalers in humans that provided aerosol drug deposition data according to well-characterized inhalation maneuvers that could feasibly be mimicked *in vitro* using realistic or "bio-relevant" tests and models; whence to compare the results of such tests and create *in vitro–in vivo* correlations (IVIVCs). This thesis was focused on assessing the likely regional deposition of budesonide from Budelin® Novolizer® 200 mcg based on that inhaler's *in vitro* performance during realistic testing and subsequent computational fluid dynamics (CFD) modeling. Accordingly, the results were compared with the extensive work done by Newman et al. [1] on that inhaler using 2D gamma scintigraphy. This Appendix describes the process of selection and the merits of that study [1] from the broader aerosol drug deposition literature.

In vivo lung deposition studies for orally inhaled drug products are usually performed using gamma scintigraphy studies or pharmacokinetic (PK) studies in which a

charcoal block technique to prevent drug absorption from the gastrointestinal (GI) tract. Although both approaches allow total lung dose (TLD) to be evaluated, regional drug deposition can only be characterized using gamma scintigraphy. To select representative inhaler(s) that enable the *in vitro* measured TLD and CFD predicted regional drug deposition results to be compared with the *in vivo* data, a literature review was initially performed to retrieve and evaluate gamma scintigraphy studies for dry powder inhalers (DPI), metered dose inhalers (MDI) and soft mist inhalers (SMI). The results of this are shown for DPIs in this Appendix.

AI.2 METHODS

A literature search of peer reviewed journals and conference proceedings was performed using **Pubmed**, **Web of Science** and **RDDonline** with the following keyword combinations and total results (dated to March 26, 2015):

An “All Fields” search in **Pubmed** was performed for:

> (scintigraphy OR planar imaging OR 2D imaging OR two dimensional imaging OR lung imaging) AND (inhaler OR pulmonary drug OR inhalation drug OR respiratory drug OR aerosol OR lung deposition OR MDI OR DPI OR nebulizer) AND (human OR adult OR volunteer OR subject) AND healthy; a total of 387 references were found.

A “topic” search in **Web of Science** was performed for:

> (scintigraphy OR planar imaging OR 2D imaging OR two dimensional imaging OR lung imaging) AND (inhaler OR pulmonary drug OR inhalation drug OR respiratory

drug OR aerosol OR lung deposition OR MDI OR DPI OR nebulizer) AND (human OR adult OR volunteer OR subject) AND healthy; a total of 204 references were found.

A “keywords” and “title” search in **RDDonline** was performed for:

scintigraphy; 62 references were found for “keywords” search and 8 references were found for “title” search.

Initial screening of these articles was performed by reading all titles and abstracts, after which replicate references were discarded. 93 references were selected from the total and tabulated for individual reviews based on the possibility that they contained information where all of the following were reported: (a) lung deposition data in a group of healthy human adults following the use of radiolabeled formulations from inhalers described either within the reference itself or elsewhere, (b) inhalation profile (IP) variables used by the subjects in the study , and (c) pharmaceutical aerosol deposition. Many of the 93 references failed to provide aspects of this information and were rejected. However, 21 studies appeared to be promising for DPIs [1-21]. Data from those was tabulated and reviewed further.

AI.3 RESULTS AND DISCUSSION

Inhalers, drugs, inhalation profile parameters and related gamma scintigraphic deposition data in healthy volunteers from the 21 possible DPI studies are compiled in Table 1. These studies covered the publication period 1992 to 2009. Notably, over half of the studies included in Table AI.1 (14 out of 21) were performed by Newman and colleagues who generally used standardized techniques; other research groups employed their own (alternate) methods to perform and assess lung deposition results [e.g. different attenuation factors, definition of lung regions of interest (ROI), etc.]. This was not surprising because the studies in Table AI.2 were performed before efforts were made to standardize methods in 2012 [2] when it was noted that experimentaldifferences in gamma scintigraphic techniques should be carefully considered when selecting inhalers for realistic *in vitro* tests, as cross-study comparisons may be needed to assess an resulting IVIVCs.

Table AI.1. Summary of lung scintigraphy data from the literature for passive dry powder inhalers (DPIs) some of which are available commercially. References were published in the period 1992–2009 and were included if they contained descriptions of the IPs used by lung-normal subjects. Abbreviations are: PIFR = peak inhalation flow rate; TLD = total lung dose; P/C Ratio = %Peripheral/%Central.

Inhaler	Drug	PIFR (L/min)	Volume (L)	%TLD	%Central	%Intermediate	%Peripheral	P/C Ratio	Ref.
Clickhaler[a]	Budesonide	72.9±38.1 (35-200)	3.5±1.2 (1.6-6.4)	26.8±6.8				2.3±0.7 (sC/P)	[3]
Clickhaler[a]	Beclomethasone Dipropionate	Follow instructions in the manufacturers' info sheets		30.8±7.2				1.49±0.37 (sC/P)	[4]
Cyclohaler[b]	LAS 31025 (lactose)	98.8±24.8	3.5±1.0	19.1±7.6	7.4±3.2	6.4±3.0	5.2±1.9	0.8±0.4	[5]
		104.0±35.8	3.4±1.1	20.9±10.2	8.4±5.1	6.7±3.3	5.9±2.7	0.9±0.4	
		105.5±24.0	3.3±1.0	19.5±4.5	7.4±1.6	6.3±1.5	5.8±2.3	0.8±0.3	
		106.9±26.5	3.4±0.9	17.5±3.6	7.1±1.9	5.6±1.3	4.9±1.3	0.7±0.3	
Cyclohaler[b]	Budesonide (solid lipid microparticles, physical blend)	Subjects practiced breathing maneuver with an empty device. Breath holding for 5 sec.		62.8±4.9	18.6±2.6	22.1±2.4	22.0±3.9	1.2±0.4	[6]
	Budesonide (solid lipid microparticles, matricial)			49.9±3.7	15.6±2.3	16.9±2.0	17.4±2.6	1.1±0.3	
Diskhaler	Zanamivir (lactose)	84.0±16.5	2.77±1.02	13.2±4.0	5.1±2.2	4.2±1.3	3.9±1.0	0.9±0.4	[7]
Easyhaler[c]	Beclomethasone Dipropionate (lactose)	53±11	2.62±0.97	18.9±9.5	5.8±3.3	6.4±3.1	6.7±3.6	1.2±0.3	[8]
Elips	Budesonide (PulmoSphere)	44±5		57.7±7.8	17.9±4.1	20.0±2.6	19.7±6.1	1.2±0.6	[9]
		29±3		57.0±6.5	17.2±2.1	20.6±2.5	19.2±5.3	1.1±0.5	
Genuair[d]	Aclidinium Bromide	79.0±9.4	3.91±0.72	30.1±7.3	Lung was divided into 6 regions, with mean values of 9.9% and 2.6% for the innermost and outermost regions (data for 6 regions available)				[10]

Handihaler	Tiotropium Bromide	Inhale according to the description in the patient's info		18±5 (18-22)	Lung was divided into two rectangular regions: central (25% ROI) and peripheral (75% ROI)			0.73±0.22 (C/P)	[11]
Leiras	Salbutamol (lactose)	Inhale ASAP through the device and hold breath for 10 sec		23.9±1.4	7.1±0.5	8.7±0.6	8.1±0.5	1.2±0.1	[12]
MAGhaler	Salbutamol (lactose)	62.1 (46.0-73.0)	3.11 (1.6-4.1)	26.4±4.3	7.2±1.5	9.2±1.4	10.0±2.2	1.4±0.3	[13]
		36.3 (29.0-42.0)	3.31 (2.1-4.5)	21.1±5.1	5.6±1.7	7.2±1.9	8.3±2.3	1.5±0.6	
Monodose Miat Inhaler	Nacystelyn	Exhale, and then inhale with a nonmaximal inspiratory effort for ~4 sec, and hold breath for 5 sec		31.0±11.5	No specific definition of central, intermediate and peripheral regions			0.50±0.20	[14]
Novolizer[e]	Budesonide (lactose)	99±13	3.13±1.01	32.1 (9.4-41.0)	10.6 (3.0-13.4)	10.9 (3.8-15.9)	8.5 (2.5-13.4)	0.9 (0.6-1.3)	[1]
		65±3	2.96±0.83	25.0 (12.1-37.4)	7.8 (3.7-11.8)	8.9 (4.6-12.2)	7.8 (3.7-13.4)	1.0 (0.8-1.3)	
		54±7	2.77±0.97	19.9 (8.8-26.6)	6.3 (2.3-8.4)	6.7 (3.2-9.9)	6.5 (3.4-8.8)	1.0 (0.7-1.5)	
Pulvina[f]	Salbutamol (lactose)	46.0±4.4	3.11±0.67	14.1±3.2	4.9±1.3	4.3±1.0	4.9±1.1	1.0±0.2	[15]
		27.8±2.5	3.23±0.74	11.7±2.3	3.8±0.9	3.7±0.8	4.2±0.9	1.2±0.3	
Spinhaler	Sodium Cromoglycate	119.9 (107-130) (Tilted, BH)	2.78 (1.7-4.0)	13.1 (3.7-22.1)				1.7 (0.9-2.3)	[16]
		62.8 (58-71) (Tilted, BH)	2.94 (2.0-4.2)	5.5 (1.6-9.7)				1.37 (0.8-2.3)	
		120.4 (106-128) (Normal, BH)	2.86 (2.2-4.1)	17.1 (7.8-28.3)				1.49 (0.8-2.1)	
		117.9 (110-132) (Tilted)	2.59 (1.7-4.9)	12.3 (6.6-21.1)				1.27 (0.7-2.0)	
Turbuhaler[g]	Terbutaline Sulphate	57.8±5.6	2.54±0.87	21.4±6.1	5.5±1.5	7.1±2.0	8.8±2.9	1.62±0.39	[17]
Turbuhaler[g]	Terbutaline Sulphate	55±7	2.41±0.50	26.9±3.8	5.7±0.9	8.4±1.0	12.9±2.2	2.28±0.22	[18]
Turbuhaler[g]	Terbutaline Sulphate	57 (52-61)	2.95 (1.97-4.09)	27.0±7.7				2.03±0.48	[19]
Turbuhaler[g]	Budesonide	58 (53-64)	2.90 (2.07-4.97)	27.7±9.5				1.72±0.45	
		36 (32-38)	2.54 (1.36-3.72)	14.8±3.3				1.82±0.62	

Turbuhaler[g]	Budesonide	58±6	2.61±0.63	21.4 (4.7-29.2)	5.9 (1.7-10.0)	7.3 (3.2-11.0)	4.8 (2.5-9.1)	0.9 (0.5-1.6)	[1]
Turbuhaler[g]	Budesonide	73.3±31.2 (35-142)	3.4±0.9 (2.1-6.1)	15.8±6.6				1.9±0.7 (sC/P)	[3]
Turbospin	Tobramycin	Targeted PIFR of 60 L/min; Exhale, inhale rapidly to TLC, and hold breath for 5 sec		34.3±5.8	9.3±3.3	11.3±2.7	13.6±3.3	1.6±0.4	[20]
Ultrahaler	Nedocromil Sodium (lactose)	75.3±19.0	3.7±1.0	13.3±4.8	4.5±2.0	4.5±1.8	4.3±1.3	1.1±0.3	[21]
		42.5±8.6	4.0±1.2	9.8±3.5	3.2±1.3	3.1±1.2	3.5±1.4	1.2±0.4	
Ultrahaler	HMR 1031 (lactose)	Targeted PIFR 60 L/min		24.6±7.3	8.6±3.9	8.3±2.5	7.7±1.8	1.1±0.5	[22]

[a]Available as Asmabec Clickhaler (beclometasone dipropionate) (RPH Pharmaceuticals, U.K.)

[b]Available as Foradil Aerolizer (formoterol fumarate) (Novartis)

[c]Avialable as Easyhaler Salbutamol, Easyhaler Budesonide, Formoterol Easyhaler, Easyhaler Beclometasone (Orion Pharma, U.K.)

[d]Avialable as Eklira Genuair (aclidinium bromide) and Duaklir Genuair (formoterol fumarate dehydrate, aclidinium bromide) (Astrazeneca, U.K.)

[e]Avialable as Budelin Novolizer (budesonide) and Salbulin MDPI Novolizer (salbutamol sulfate) (Meda Pharmaceuticals, U.K.)

[f]Avialable as Pulvinal (salbutamol) and Pulvinal (beclometasone dipropionate) (Chiesi, Italy)

[g]Avialable as Bricanyl Turbohaler (terbutaline sulphate), Oxis Turbohaler 12 (formoterol fumarate dehydrate), Pulmicort Turbohaler (budesonide), Symbicort Turbohaler (budesonide, formoterol fumarate dehydrate) (Astrazeneca, U.K.)

A closer look at the 21 possible studies in Table AI.1 showed that many were unsuitable for use when attempting to construct IVIVCs. Not all inhalers (or inhaler-drug combinations) were commercially available, and a lack of well described inhalation maneuvers and regional lung deposition data in some studies limited our choices further. In order to test the *in vivo* predictability of our methods the following additional criteria were established to define acceptable studies for the purpose of IVIVC comparisons:

(a) Drug inhalers used in the gamma scintigraphy studies must be commercially available (to enable *in vitro* testing);

(b) Validation of the labeling procedure should be described. In short, a comparison between the radiolabel and the drug in a standardized testing situation should ensure a comparable aerodynamic size distribution between the drug (from the unlabeled inhaler) and the label (from the labeled version);

(c) Inhalation profile (IP) variables used by subjects in each study should be reported with statistics so that it is possible to simulate realistic IPs for *in vitro* testing. In short, values and statistics were required that described peak inspiratory flow rates (PIFR) and either total volume inhaled (V) or total inhalation time [before breath holding] (T).

(d) Regional deposition data should be reported to describe the % of each lung dose deposited in well-defined lung regions (e.g. central, intermediate and peripheral);

The references and data shown in Table AI.2 were selected for further consideration.

Table AI.2. Selected lung scintigraphy references for further discussion.

Inhaler	Drug	PIFR (L/min)	Volume (L)	%TLD	%Central	%Intermediate	%Peripheral	P/C Ratio	Ref.
Diskhaler	Zanamivir (lactose)	84.0±16.5	2.77±1.02	13.2±4.0	5.1±2.2	4.2±1.3	3.9±1.0	0.9±0.4	[7]
Easyhaler	Beclomethasone Dipropionate (lactose)	53±11	2.62±0.97	18.9±9.5	5.8±3.3	6.4±3.1	6.7±3.6	1.2±0.3	[8]
Genuair	Aclidinium Bromide (lactose)	79.0±9.4	3.91±0.72	30.1±7.3	Lung was divided into 6 regions, with mean values of 9.9% and 2.6% for the innermost and outermost regions (data for 6 regions available)				[10]
Novolizer	Budesonide (lactose)	99±13	3.13±1.01	32.1 (9.4-41.0)	10.6 (3.0-13.4)	10.9 (3.8-15.9)	8.5 (2.5-13.4)	0.9 (0.6-1.3)	[1]
		65±3	2.96±0.83	25.0 (12.1-37.4)	7.8 (3.7-11.8)	8.9 (4.6-12.2)	7.8 (3.7-13.4)	1.0 (0.8-1.3)	
		54±7	2.77±0.97	19.9 (8.8-26.6)	6.3 (2.3-8.4)	6.7 (3.2-9.9)	6.5 (3.4-8.8)	1.0 (0.7-1.5)	
Pulvina	Salbutamol (lactose)	46.0±4.4	3.11±0.67	14.1±3.2	4.9±1.3	4.3±1.0	4.9±1.1	1.0±0.2	[15]
		27.8±2.5	3.23±0.74	11.7±2.3	3.8±0.9	3.7±0.8	4.2±0.9	1.2±0.3	
Turbohaler	Terbutaline Sulphate	57.8±5.6	2.54±0.87	21.4±6.1	5.5±1.5	7.1±2.0	8.8±2.9	1.62±0.39	[17]
Turbohaler	Terbutaline Sulphate	55±7	2.41±0.50	26.9±3.8	5.7±0.9	8.4±1.0	12.9±2.2	2.28±0.22	[18]
Turbohaler	Budesonide	58±6	2.61±0.63	21.4 (4.7-29.2)	5.9 (1.7-10.0)	7.3 (3.2-11.0)	4.8 (2.5-9.1)	0.9 (0.5-1.6)	[1]

Selection of Budelin® Novolizer®

The ASTA Medica DPI Device and formulation tested clinically by Newman et al. [1] became Budelin Novolizer and was marketed by Meda Pharmaceuticals in the EU. This thesis is focused on that device primarily because reference [1] had the advantage that Budelin was labeled and tested using a cross-over deposition study in the clinic that clearly showed the dosing variations and reginal drug deposition results after asking each volunteer to inhale at three different peak inspiratory flow rates. We expected to be able to see differences in deposition *in vitro* that resulted from similar variations in the breath profiles simulated to mimic each of Newman et al.'s 3 clinical study cohorts [1]. In practice, and in the future, however, it may well prove possible to test the IVIVCs by employing the data in references [1, 7, 8, 10, 15, 17, 18] that describe the deposition of drug from Relenza™ Diskhaler™ (5 mg zanamivir, GlaxoSmithKline), Easyhaler® (200 mcg beclomethasone, Orion Pharma, U.K.), Eklira® Genuair® (322 mcg aclidinium, AstraZeneca, U.K.), Budelin® Novolizer® (200 mcg budesonide, Meda Pharmaceutics, U.K.), Pulvinal® (200 mcg salbutamol, Chiesi, Italy), Bricanyl® Turbohaler® (0.5 mg Terbutaline Sulphate, AstraZeneca, U.K.), and Pulmicort® Turbohaler® (100 mcg budesonide, AstraZeneca, U.K.) (Table IA.2).

AI.4 REFERENCES

1. Newman SP, Pitcairn GR, Hirst PH, Bacon RE, O'Keefe E, Reiners M, Hermann R: **Scintigraphic comparison of budesonide deposition from two dry powder inhalers.** *Eur Respir J* 2000, **16:**178-183.
2. Newman SP, Bennett WD, Biddiscombe M, Devadason SG, Dolovich MB, Fleming J, Haeussermann S, Kietzig C, Kuehl PJ, Laube BL, et al: **Standardization of techniques for using planar (2D) imaging for aerosol deposition assessment of orally inhaled products.** *J Aerosol Med Pulm Drug Deliv* 2012, **25 Suppl 1:**S10-28.
3. Warren S, Taylor G, Smith J, Buck H, Parry-Billings M: **Gamma scintigraphic evaluation of a novel budesonide dry powder inhaler using a validated radiolabeling technique.** *J Aerosol Med* 2002, **15:**15-25.
4. Warren SJ, Taylor G: **Effect of inhalation flow profiles on the deposition of radiolabelled BDP from a novel dry powder inhaler (DPI, Clickhaler(TM)), a conventional metered dose inhaler (MDI) and MDI plus spacer.** In *Respiratory Drug Delivery VI. Volume* I. Edited by Dalby R, Byron PR, Parr SJ. River Grove, IL: DHI Publishing; 1998: 453-456.
5. Newman SP, Rivero X, Luria X, Hooper G, Pitcairn GR: **A scintigraphic study to evaluate the deposition patterns of a novel anti-asthma drug inhaled from the Cyclohaler dry powder inhaler.** *Adv Drug Deliv Rev* 1997, **26:**59-67.
6. Sebti T, Pilcer G, Van Gansbeke B, Goldman S, Michils A, Vanderbist F, Amighi K: **Pharmacoscintigraphic evaluation of lipid dry powder budesonide formulations for inhalation.** *Eur J Pharm Biopharm* 2006, **64:**26-32.

7. Cass LM, Brown J, Pickford M, Fayinka S, Newman SP, Johansson CJ, Bye A: **Pharmacoscintigraphic evaluation of lung deposition of inhaled zanamivir in healthy volunteers.** *Clin Pharmacokinet* 1999, **36 Suppl 1:**21-31.

8. Newman SP, Pitcairn GR, Adkin DA, Vidgren MT, Silvasti M: **Comparison of beclomethasone dipropionate delivery by easyhaler dry powder inhaler and pMDI plus large volume spacer.** *J Aerosol Med* 2001, **14:**217-225.

9. Duddu SP, Sisk SA, Walter YH, Tarara TE, Trimble KR, Clark AR, Eldon MA, Elton RC, Pickford M, Hirst PH, et al: **Improved lung delivery from a passive dry powder inhaler using an Engineered PulmoSphere powder.** *Pharm Res* 2002, **19:**689-695.

10. Newman SP, Sutton DJ, Segarra R, Lamarca R, de Miquel G: **Lung deposition of aclidinium bromide from Genuair, a multidose dry powder inhaler.** *Respiration* 2009, **78:**322-328.

11. Brand P, Meyer T, Weuthen T, Timmer W, Berkel E, Wallenstein G, Scheuch G: **Lung deposition of radiolabeled tiotropium in healthy subjects and patients with chronic obstructive pulmonary disease.** *J Clin Pharmacol* 2007, **47:**1335-1341.

12. Pitcairn GR, Lankinen T, Valkila E, Newman SP: **Lung Deposition of Salbutamol from the Leiras Metered Dose Powder Inhaler.** *J Aerosol Med* 1995, **8:**307-311.

13. Newman SP, Malik S, Hirst R, Pitcairn G, Heide A, Pabst J, Dinkelaker A, Fleischer W: **Lung deposition of salbutamol in healthy human subjects from the MAGhaler dry powder inhaler.** *Respir Med* 2002, **96:**1026-1032.

14. Vanderbist F, Wery B, Baran D, Van Gansbeke B, Schoutens A, Moes AJ: **Deposition of nacystelyn from a dry powder inhaler in healthy volunteers and cystic fibrosis patients.** *Drug Dev Ind Pharm* 2001, **27:**205-212.

15. Pitcairn G, Lunghetti G, Ventura P, Newman S: **A comparison of the lung deposition of salbutamol inhaled from a new dry powder inhaler, at two inhaled flow rates.** *International Journal of Pharmaceutics* 1994, **102:**11-18.

16. Newman SP, Hollingworth A, Clark AR: **Effect of different modes of inhalation on drug delivery from a dry powder inhaler.** *International Journal of Pharmaceutics* 1994, **102:**127-132.

17. Borgström L, Newman S: **Total and regional lung deposition of terbutaline sulphate inhaled via a pressurised MDI or via Turbuhaler®.** *International Journal of Pharmaceutics* 1993, **97:**47-53.

18. Borgstrom L, Newman S, Weisz A, Moren F: **Pulmonary deposition of inhaled terbutaline: comparison of scanning gamma camera and urinary excretion methods.** *J Pharm Sci* 1992, **81:**753-755.

19. Borgstrom L, Bondesson E, Moren F, Trofast E, Newman SP: **Lung deposition of budesonide inhaled via Turbuhaler: a comparison with terbutaline sulphate in normal subjects.** *Eur Respir J* 1994, **7:**69-73.

20. Newhouse MT, Hirst PH, Duddu SP, Walter YH, Tarara TE, Clark AR, Weers JG: **Inhalation of a dry powder tobramycin PulmoSphere formulation in healthy volunteers.** *Chest* 2003, **124:**360-366.

21. Pitcairn GR, Lim J, Hollingworth A, Newman SP: **Scintigraphic assessment of drug delivery from the Ultrahaler dry powder inhaler.** *J Aerosol Med* 1997, **10:**295-306.

22. Rohatagi S, Chapel S, Kirkesseli S, Newman S, Zhang J, Paccaly D, Randall L, Wray H, Wellington S, Shah B, Jensen BK: **Pharmacoscintigraphic comparison of HMR 1031, a VLA-4 antagonist, in healthy volunteers following delivery via a nebulizer and a dry powder inhaler.** *Am J Ther* 2004, **11:**103-113.

APPENDIX II

GEOMETRY OF THE MODIFIED VCU MOUTH-THROAT MODELS

Three dimensional (3D) geometries of the original small, medium and large Virginia Commonwealth University (VCU) mouth-throat (MT) models are available at www.rddonline.com. These models were modified as shown below by adding a quick-fit adapter to allow an airtight connection between the MT and the Next Generation Pharmaceutical Impactor or NGI. Dimensions of the NGI quick-fit adapter were the same for all three MT models and the dimensions are shown in the figure below in mm. The exit of MT was centralized in the adapter in all cases.

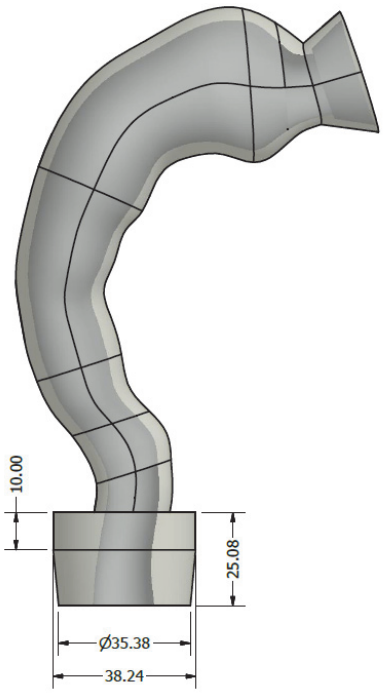

APPENDIX III

Pharm Res
DOI 10.1007/s11095-015-1695-1

RESEARCH PAPER

Validating CFD Predictions of Pharmaceutical Aerosol Deposition with *In Vivo* Data

Geng Tian [1] • Michael Hindle [2] • Sau Lee [3] • P. Worth Longest [1,2]

APPENDIX IV

CURVE FITTING METHODS FOR SIMULATING HUMAN INHALATION PROFILES

AIV.1 INTRODUCTION

Simulated inhalation profiles (IP) and equations described in Delvadia et al. [1-3] require the assignment of T_{hold}, an arbitrarily defined variable, or time to maintain the peak inhalation flow rate. Delvadia et al. [1] held the value of T_{hold} constant at 0.15 sec. In this thesis, a new process was proposed and published [4], which avoided the need to assign values to this variable. As a result, it was possible to advocate methods to simulate ranges of human IPs for DPI testing (Chapter 4) based solely on the clinical results from Delvadia [3] and a knowledge of the airflow resistance of the inhaler being tested. Essentially, the data presented in Delvadia [3] was reanalyzed in the present study in order to find optimal mathematical equations for IP simulation in the absence of T_{hold}.

AIV.2 METHODS

A variety of equations were assessed for their ability to describe the IPs presented in Delvadia [3]. Several different orders of polynomial equations and a combined exponential /sine equation $FR(t) = -A_0 e^{-k_1 t} + A_0 \cos\left(\frac{\pi}{2} \times \frac{t}{T}\right)$ were explored and rejected because their parameters (e.g. A_0, k_1) could not be directly assigned to the variables with physical meanings in a typical IP such as that shown in Figure 4.4. Therefore, the equations described in Delvadia et al. [1] were used as the basis for this study, and curve fitting analyses were performed to define values for T_{hold} in the hope that curve-fits would be no better in the case where $T_{hold} \rightarrow 0$. These equations are rewritten below (Equations AIV.1–AIV.3) as initially defined in Delvadia [3] and integrated using Mathematica 9.0.1 (Wolfram, Champaign, IL) to solve the relationship between T (total inhalation time) and T_{hold}:

$$FR(t) = PIFR \times \sin\left(\frac{\pi}{2} \frac{t}{T_{PIFR}}\right) \qquad 0 \le t < T_{PIFR} \qquad \text{Equation AIV.1}$$

$$FR(t) = PIFR \qquad T_{PIFR} \le t < \left(T_{PIFR} + T_{Hold}\right) \qquad \text{Equation AIV.2}$$

$$FR(t) = PIFR \times \cos\left(\frac{\pi}{2} \frac{\left(t - \left(T_{PIFR} + T_{Hold}\right)\right)}{\left(T - \left(T_{PIFR} + T_{Hold}\right)\right)}\right) \quad \left(T_{PIFR} + T_{Hold}\right) \le t \le T \qquad \text{Equation AIV.3}$$

Inhaled volume [V; area under the flow rate (FR) *vs.* time curve from t = 0 to t = T) can be described as a function of the peak inhalation flow rate (PIFR), time to achieve PIFR (T_{PIFR}), time to maintain PIFR (T_{hold}), and the total inhalation time (T) from:

$$V = \int_{0}^{T_{PIFR}} FR(t) + \int_{T_{PIFR}}^{T_{PIFR}+T_{Hold}} FR(t) + \int_{T_{PIFR}+T_{Hold}}^{T} FR(t)$$
$$= \frac{PIFR \times T_{PIFR}}{30\pi} + \frac{PIFR \times T_{Hold}}{60} + \frac{PIFR \times (T - T_{PIFR} - T_{Hold})}{30\pi} \quad \text{Equation AIV.4}$$

$$V = \frac{PIFR \times [\frac{2}{\pi}(T - T_{Hold}) + T_{Hold}]}{60} \quad \text{Equation AIV.5}$$

Or:

$$T = \frac{\pi}{2}(\frac{60V}{PIFR} - T_{Hold}) + T_{Hold} \quad \text{Equation AIV.6}$$

The real data in 10, 50, and 90 percentile FR *vs.* time profiles for all six resistances (red inhalation profiles in Figure 4.5 of Chapter 4) were used for curve fitting, and a total of 18 Text files [defined as an input format in MATLAB® R2012b (MathWorks, Natick, MA); 3 profiles for each resistance, 6 resistances in total) were created to store the FR *vs.* time data. In practice, each curve contained > 300 individual data points with a time interval of 0.005 sec. For each profile, values for PIFR were selected using the MAX function across all flow rates in Microsoft Excel 2013 (Microsoft Corporation, Redmond, WA), and the values for V under each IP were obtained by calculating the area under each curve trapezoidally. To facilitate curve fitting, values for T_{PIFR} were fixed at three selected values: 0.276 sec, 0.493 sec, and 0.885 sec that corresponded to the 10, 50 and 90 percentile values of the 240 T_{PIFR} values from the trial population (Figure 4.5 of Chapter 4). Non-linear least-squares curve fitting was then used with T_{hold} floating in Equations AIV.1–AIV.3 to assess the goodness of fit for each data set. Combinations of PIFR, V and T_{PIFR} that were employed at summarized in Table 1. All analyses were performed in MATLAB® R2012b. Examples of MATLAB scripts are shown in Figures AIV.1 and AIV.2.

Table AIV.1. Combinations of PIFR, V and T_{PIFR} used to curve fit the 10, 50 and 90 percentile IPs across six resistances. Each of the 18 inhalation profile data sets was analyzed for all three T_{PIFR} conditions to determine the best estimate for the T_{hold}.

Resistance ($kPa^{0.5}$ L^{-1} min)	Profile	PIFR (L/min)	V (L)
0.0462 (Tube 1)	10 Percentile	45.781	1.352
	50 Percentile	58.297	2.557
	90 Percentile	74.456	4.432
0.0432 (Tube 2)	10 Percentile	52.556	1.389
	50 Percentile	65.564	2.694
	90 Percentile	78.977	4.369
0.0344 (Tube 3)	10 Percentile	60.773	1.466
	50 Percentile	73.085	2.575
	90 Percentile	93.259	4.428
0.0241 (Tube 4)	10 Percentile	76.887	1.43
	50 Percentile	98.160	2.723
	90 Percentile	126.241	4.64
0.0200 (Tube 5)	10 Percentile	92.543	1.469
	50 Percentile	110.811	2.7
	90 Percentile	147.181	4.862
0.0179 (Tube 6)	10 Percentile	95.286	1.435
	50 Percentile	122.947	2.733
	90 Percentile	162.254	4.773

```
function F=sinfun(Thold,t)

   % Assign values for known parameters
   PIFR=98.1601;
   V=2.723;
   Tpifr=0.493;

   % Creat an array for flow rate
   Y=zeros(1,length(t));
   F=Y.';

   % Convert T to Thold
   T=pi/2*(60*V/PIFR-Thold)+Thold;

   % Creat functions
   for i=1:length(t)
       if(t(i)>=0 && t(i)<Tpifr)
          F(i)=PIFR*sin(pi/2*t(i)/Tpifr);
       end
       if(t(i)>=Tpifr && t(i)<Tpifr+Thold)
          F(i)=PIFR;
       end;
       if(t(i)>=Tpifr+Thold && t(i)<=T)
          F(i)=PIFR*cos(pi/2*(t(i)-(Tpifr+Thold))/(T-(Tpifr+Thold)));
       end
   end
```

Figure AIV.1. MATLAB scripts for defining functions used for curve fitting. The above example was shown for the 50 percentile profiles from Tube 4. Values for PIFR, V and T_{PIFR} were assigned and T_{Hold} was defined as the unknown (floating) parameter in each case.

```
% Fix PIFR, V and Tpifr, fit Thold/T

% Import data as a matrix (t, time; Q, flow rate)
t=data(:,1);
Q=data(:,2);

% Use least square curve fit method to fit data
F=@(Thold,t)sinfun(Thold,t);
Thold0=[0];
[Thold,resnorm,residual,exitflag,output,lambda,jacobian]=lsqcurvefit(F,Thold0,t,Q,0);

% Calculate curve fitting parameters
n=length(t);
p=1;
ci = nlparci(Thold,residual,'jacobian',jacobian,'alpha',0.05)
Rsq = 1 - sum(residual.^2) / sum((Q - mean(Q)).^2);
Rsq_adj = 1 - (1-Rsq) * (n-1) / (n-p-1);
RMSE=sqrt(mean((F(Thold,t)-Q).^2));

% Report curve fitting parameters
fprintf('Thold = %.3f\n\n',Thold)
fprintf('CI = [%.3f,%.3f]\n\n',ci)
fprintf('RMSE = %.3f\n\n', RMSE);
fprintf('Rsq = %.3f\n\n',Rsq);
fprintf('Rsq_adj = %.3f\n\n',Rsq_adj);

% Plot original data and fitted curve
y=plot(t,Q,'r',t,F(Thold,t),'k','linewidth',2);
title('Tube 4 (50th Percentile)');
xlabel('Time (s)');
ylabel('Flow Rate (L/min)');
axis([0 6 0 160])
legend('Experimental','Fitted');
```

Figure AIV.2. MATLAB scripts for curve fitting of T_{hold} using non-linear least-squares approach. The above example was shown for the 50 percentile profiles of Tube 4. Data were imported as a matrix where “t” refers to inhalation time and “Q” refers to flow rate. “lsqcurvefit” function was used to perform non-linear least-squares curve fitting.

AIV.3 RESULTS

Best estimates for T_{hold} and the statistical parameters resulting from each of the profiles are summarized for the three tested T_{PIFR} conditions in Tables AIV.2–AIV.4. The results showed that the best estimate for T_{hold} was zero in 52 out of 54 cases. Only in two of 54 cases (10 percentile profile for Tube 1 in Tables AIV.2–AIV.3) was a small positive value for T_{hold} seen to be a better estimate value than zero. Based on these analyses, the finite variable choice of Delvadia [3] for T_{hold} = 0.15 sec eliminated from Equations AIV.1–AIV.3 and the Equations AIV.7–AIV.8 shown below used for simulating human inhalation profiles in this thesis.

$$FR(t) = PIFR \times \sin\left(\frac{\pi}{2}\frac{t}{T_{PIFR}}\right) \qquad 0 \le t < T_{PIFR} \qquad \text{Equation AIV.7}$$

$$FR(t) = PIFR \times \cos\left(\frac{\pi}{2}\frac{\left(t - T_{PIFR}\right)}{\left(T - T_{PIFR}\right)}\right) \qquad T_{PIFR} \le t \le T \qquad \text{Equation AIV.8}$$

Equations AIV.7–AIV.8 are the same as those presented in the simulation in Chapter 4 (Equations 4.7–4.8) and reference [4].

Table AIV.2. Best estimates for T_{hold} and statistical parameters from curve fitting the 10, 50 and 90 percentile profiles across six resistances (T_{PIFR} = 0.276 sec; 10 percentile value in the total population). RMSE = root mean square error (used to measure the difference between predicted value and observed value); r^2 = coefficient of determination (used to assess how well the data fit a model).

Resistance ($kPa^{0.5}$ L^{-1} min)	T_{hold} (Best Estimate; sec)	95% CI (Lower, Upper)		RMSE	r^2
0.0462 (Tube 1)	0.067	-0.029	0.163	6.79	0.751
	0.000	-0.076	0.076	4.84	0.880
	0.000	-0.084	0.084	7.33	0.857
0.0432 (Tube 2)	0.000	-0.109	0.109	9.58	0.600
	0.000	-0.066	0.066	5.48	0.902
	0.000	-0.049	0.049	4.72	0.954
0.0344 (Tube 3)	0.000	-0.090	0.090	9.33	0.669
	0.000	-0.052	0.052	5.57	0.932
	0.000	-0.067	0.067	8.31	0.888
0.0241 (Tube 4)	0.000	-0.092	0.092	15.65	0.548
	0.000	-0.049	0.049	8.50	0.918
	0.000	-0.053	0.053	10.22	0.928
0.0200 (Tube 5)	0.000	-0.129	0.129	29.24	0.047
	0.000	-0.053	0.053	11.13	0.897
	0.000	-0.040	0.040	9.57	0.958
0.0179 (Tube 6)	0.000	-0.113	0.113	26.99	0.198
	0.000	-0.054	0.054	13.48	0.878
	0.000	-0.051	0.051	14.29	0.917

Table AIV.3. Best estimates for T_{hold} and statistical parameters from curve fitting the 10, 50 and 90 percentile profiles across six resistances (T_{PIFR} = 0.493 sec; 10 percentile value in the total population). RMSE = root mean square error (used to measure the difference between predicted value and observed value); r^2 = coefficient of determination (used to assess how well the data fit a model).

Resistance ($kPa^{0.5}$ L^{-1} min)	T_{hold} (Best Estimate; sec)	95% CI (Lower, Upper)		RMSE	r^2
0.0462 (Tube 1)	0.025	-0.020	0.071	3.22	0.944
	0.000	-0.050	0.050	3.24	0.946
	0.000	-0.087	0.087	7.78	0.839
0.0432 (Tube 2)	0.000	-0.059	0.059	5.42	0.872
	0.000	-0.031	0.031	2.65	0.977
	0.000	-0.055	0.055	5.40	0.940
0.0344 (Tube 3)	0.000	-0.046	0.046	5.01	0.905
	0.000	-0.021	0.021	2.35	0.988
	0.000	-0.064	0.064	8.05	0.894
0.0241 (Tube 4)	0.000	-0.043	0.043	7.96	0.883
	0.000	-0.027	0.027	4.85	0.973
	0.000	-0.053	0.053	10.56	0.923
0.0200 (Tube 5)	0.000	-0.079	0.079	19.75	0.565
	0.000	-0.019	0.019	4.33	0.984
	0.000	-0.036	0.036	8.76	0.965
0.0179 (Tube 6)	0.000	-0.062	0.062	16.40	0.704
	0.000	-0.020	0.020	5.15	0.982
	0.000	-0.057	0.057	16.70	0.887

Table AIV.4. Best estimates for T_{hold} and statistical parameters from curve fitting the 10, 50 and 90 percentile profiles across six resistances (T_{PIFR} = 0.885 sec; 10 percentile value in the total population). RMSE = root mean square error (used to measure the difference between predicted value and observed value); r^2 = coefficient of determination (used to assess how well the data fit a model).

Resistance ($kPa^{0.5}$ L^{-1} min)	T_{hold} (Best Estimate; sec)	95% CI (Lower, Upper)		RMSE	r^2
0.0462 (Tube 1)	0.000	-0.070	0.070	5.11	0.859
	0.000	-0.102	0.102	6.76	0.765
	0.000	-0.116	0.116	10.79	0.690
0.0432 (Tube 2)	0.000	-0.053	0.053	5.31	0.877
	0.000	-0.077	0.077	6.91	0.844
	0.000	-0.097	0.097	9.97	0.795
0.0344 (Tube 3)	0.000	-0.072	0.072	8.57	0.721
	0.000	-0.077	0.077	9.09	0.818
	0.000	-0.093	0.093	12.33	0.753
0.0241 (Tube 4)	0.000	-0.041	0.041	9.14	0.846
	0.000	-0.074	0.074	14.82	0.750
	0.000	-0.088	0.088	18.80	0.756
0.0200 (Tube 5)	0.000	-0.040	0.040	12.72	0.820
	0.000	-0.068	0.068	17.08	0.758
	0.000	-0.075	0.075	20.12	0.816
0.0179 (Tube 6)	0.000	-0.034	0.034	11.78	0.847
	0.000	-0.065	0.065	19.88	0.735
	0.000	-0.093	0.093	29.63	0.644

AIV.4 REFERENCES

1. Delvadia RR, Longest PW, Byron PR: **In vitro tests for aerosol deposition. I: Scaling a physical model of the upper airways to predict drug deposition variation in normal humans.** *J Aerosol Med Pulm Drug Deliv* 2012, **25:**32-40.
2. Delvadia RR, Hindle M, Longest PW, Byron PR: **In vitro tests for aerosol deposition. II: IVIVCs for different dry powder inhalers in normal adults.** *J Aerosol Med Pulm Drug Deliv* 2013, **26:**138 - 144.
3. Delvadia RR: **In vitro methods to predict aerosol drug deposition in normal adults.** *Doctoral Dissertation.* Virginia Commonwealth University, Pharmaceutical Sciences; 2012.
4. Delvadia RR, Wei X, Longest PW, Venitz J, Byron PR: **In vitro tests for aerosol deposition. IV: Simulating variations in human breath profiles for realistic DPI testing.** *J Aerosol Med Pulm Drug Deliv* 2015.

VITA

XIANGYIN WEI

VCU School of Pharmacy (804) 683-0688

410 N 12th St, Richmond, VA 23298-0533 xiangyinwei@gmail.com

I. EDUCATION

2011-present	Ph.D. student at Aerosol Research Group, Department of Pharmaceutics, Virginia Commonwealth University Major advisor: Dr. Peter R. Byron
2008-2011	M.S., Pharmaceutics, Shanghai Institute of Pharmaceutical Industry, China Thesis title: Development and evaluation of an injectable formulation of salvianolic acid B
2004-2008	B.S.E., Pharmaceutical Engineering, Yangzhou University, China Thesis title: A new synthetic method for the preparation of cyclopropyl bromide

II. PUBLICATIONS

a. Articles of Original Research

1. Delvadia RR, **Wei X,** Longest PW, Venitz J, Byron PR: In Vitro Tests for Aerosol Deposition. IV: Simulating Variations in Human Breath Profiles for Realistic DPI Testing. *J Aerosol Med Pulm Drug Deliv* on July 22, 2015. [Epub ahead of print]. doi: 10.1089/jamp.2015.1215
2. Byron PR, **Wei X**, Delvadia RR, Longest PW, Venitz J: Breath profiles for testing new DPI devices in development. In *Respiratory Drug Delivery 2014*. *Volume I*. Edited by Dalby R, Byron PR, Peart J, Farr SJ, Suman JD, Young PM, Traini D. River Grove, IL: DHI Publishing; 2014: 295-302. Available at www.rddonline.org

3. Byron PR, **Wei X**, Delvadia RR, Longest PW: Standardizing in vitro test methods to support aerosol drug evaluation in the clinic. In *Respiratory Drug Delivery 2013*. *Volume I*. Edited by Dalby R, Byron PR, Peart J, Parr SJ, Suman JD. River Grove, IL: DHI Publishing; 2013: 85-92. Available at www.rddonline.org

b. Abstracts of Original Research (National and International Meetings)

1. **Wei X**, Bormann K, Byron PR: Predicting variations in aerodynamic particle size distribution of the lung dose from Budelin Novolizer. In *Respiratory Drug Delivery 2015*. *Volume II*. Edited by Dalby R, Byron PR, Peart J, Suman JD, Young PM, Traini D. River Grove, IL: DHI Publishing; 2015: 533-536. Available at www.rddonline.org
2. **Wei X**, Byron PR, Longest PW: Predicting variations in lung dose with different mouth-throat models. In *Respiratory Drug Delivery 2014*. *Volume III*. Edited by Dalby R, Byron PR, Peart J, Farr SJ, Suman JD, Young PM, Traini D. River Grove, IL: DHI Publishing; 2014: 773-776. Available at www.rddonline.org
3. **Wei X** and Byron PR: Predicting total lung dose in vitro ($TLD_{in\ vitro}$) with different mouth-throat (MT) models". Poster presentation at the 2013 AAPS Annual Meeting and Exposition, San Antonio, TX, November 10-14, 2013, Poster R6184. Available at http://abstracts.aaps.org/published/ContentInfo.aspx?conID=43425

c. Translated Articles and Book Chapters

1. Li M, Yu X: Intellectual property protection and enforcement for pharmaceuticals in China: status and trends. In *Respiratory Drug Delivery 2015*. *Volume I*. Edited by Dalby R, Byron PR, Peart J, Farr SJ, Suman JD, Young PM, Traini D. River Grove, IL: DHI Publishing; 2015: In Publication. Available at www.rddonline.org (Chinese to English)
2. Li M: Regulatory Requirements for Inhalers in China. In *Respiratory Drug Delivery 2012*. *Volume I*. Edited by Dalby R, Byron PR, Peart J, Suman JD, Farr SJ, Young PM. River Grove, IL: DHI Publishing; 2012: 119-136. Available at www.rddonline.org (Chinese to English)
3. Zhou D, R. Porter W, G.Z. Zhang G: Chapter 5 - Drug stability and degradation studies. In *Developing Solid Oral Dosage Forms: Pharmaceutical Theory and Practice*. Edited by Qiu Y, Chen Y, Zhang G, Liu L, and Porter W. San Diego: Academic Press; 2009: 87-124. (English to Chinese, Chinese version published in 2013)
4. Porter WR: Chapter 10 - Applied statistics in product development. In *Developing Solid Oral Dosage Forms: Pharmaceutical Theory and Practice*. Edited by Qiu Y, Chen Y, Zhang G, Liu L, and Porter W. San Diego: Academic Press; 2009: 87-124. (English to Chinese, Chinese version published in 2013)

5. Yang Y, Yu LX: Chapter 12 - Oral drug absorption, evaluation, and prediction. In *Developing Solid Oral Dosage Forms: Pharmaceutical Theory and Practice*. Edited by Qiu Y, Chen Y, Zhang G, Liu L, and Porter W. San Diego: Academic Press; 2009: 87-124. (English to Chinese, Chinese version published in 2013)
6. Qiu Y: Chapter 17 - In vitro–in vivo correlations: fundamentals, development considerations, and applications. In *Developing Solid Oral Dosage Forms: Pharmaceutical Theory and Practice*. Edited by Qiu Y, Chen Y, Zhang G, Liu L, and Porter W. San Diego: Academic Press; 2009: 87-124. (English to Chinese, Chinese version published in 2013)
7. Newman S: Chapter 1 - The background to pulmonary drug delivery in man. In *Respiratory Drug Delivery: Essential Theory and Practice*, Newman, S, Anderson, P, Byron PR, Dalby, R, and Peart, J, Richmond USA: RDD Online / Virginia Commonwealth University, 2009: 1-28. (English to Chinese, Chinese version published in 2011)
8. Newman S: Chapter 2 - Aerosol properties and deposition principles. In *Respiratory Drug Delivery: Essential Theory and Practice*, Newman, S, Anderson, P, Byron PR, Dalby, R, and Peart, J, Richmond USA: RDD Online / Virginia Commonwealth University, 2009: 29-58. (English to Chinese, Chinese version published in 2011)

d. Patent Application

1. China Patent Application. Xi Q, **Wei X**, Chen L, Li J, Jin F. An injectable drug composition and preparation methods. Application #CN201010230586.2. Withdrawn on March 11, 2015.

III. AWARDS

2015 2015 Graduate Training /Travel Fund. Received at the 18th Annual Pharmaceutical Sciences Graduate Program Student Awards luncheon, May 22, 2015. Virginia Commonwealth University, Richmond VA.

2013 Joseph Schwartz Graduate Student Travel Award. Received on School of Pharmacy 16th Annual Pharmaceutical Sciences Research and Career Day, November 8, 2013. Virginia Commonwealth University, Richmond VA.